Hexaarylbiimidazole-based Dynamic Materials and their Utilization

by

Dowon Ahn

A dissertation submitted in partial fulfillment
of the requirements for the degree of
Doctor of Philosophy
(Macromolecular Science and Engineering)
in the University of Michigan
2017

Doctoral Committee:
Assistant Professor Timothy F. Scott, Chair
Professor Jinsang Kim
Professor Brian J. Love
Professor Anne J. McNeil

Dowon Ahn

ahndowon@umich.edu

ORCID ID: 0000-0003-4837-0038

Dedication

This dissertation is dedicated to

Mom, Dad and my brother Taewon

For their love and endless support

Acknowledgements

I want to thank my PhD advisor Prof. Timothy F. Scott for all of his guidance, support and encouragement throughout my doctoral studies at the University of Michigan. I would also like to thank my dissertation committee members, Prof. Jinsang Kim, Prof. Brian J. Love, and Prof. Anne J. McNeil, for all of their advice and feedback.

I was fortunate to have met wonderful lab mates including Dr. Scott Zavada, Prof. Joseph Furgal, Dr. Jae Hwan Jung, Dr. Tao Wei, Megan Dunn, Harry van der Laan, Max Ma, Samuel Leguizamon, Abdulla Alqubati, Austin Bingham, Dr. Junting Li, Sameer Sathe, and Dan Li. I would like to thank them for all of their help and assistant throughout my PhD.

I should mention how lucky I am to be a graduate student at the University of Michigan, and particularly in the Macro program. I would like to thank Prof. Rick Lane, Prof. Mark Banaszak Holl, Nonna Hamilton, and Adam Mael for building the family atmosphere of Macro as well all the help and assistance I received from them.

I am eternally thankful for the love and support of my parents and brother. I especially want to mention my Mom, Youngsook for being a constant source of inspiration and support. Thanks for being a role model throughout my life. I will do my best to repay your kindness and devotion for the rest of my life.

Table of Contents

List of Figures

List of Tables

List of Schemes

Abstract

Free radicals, atomic or molecular species with an unpaired valence electron, are common reactive species in many chemical reactions. Indeed, radicals often participate in many naturally-occurring biological processes as well as in polymerization reactions as the active propagating centers in both chain- and step-growth polymerizations. One particularly interesting class of radical-generating compounds consists of hexaarylbiimidazoles (HABIs) which have been the focus of significant research activity owing to their photo-, piezo-, and thermo-chromic nature. Upon irradiation, HABIs undergo homolytic cleavage to yield two strongly colored, 2,4,5-triarylimidazolyl radicals that are relatively unreactive with oxygen and show slow recombination rates, attributable to steric hindrance and electron delocalization, and thermally recombine to reproduce the HABI dimer. Because of their unique attributes, HABIs have found industrial utility as proofing papers, photoresists, and radical polymerization initiators.

This dissertation details the design and synthesis of novel HABI derivatives to 1) address the deficiencies of conventional HABI photoinitiators, including their poor visible light absorption and low solubility, 2) elucidate the recombination mechanism of lophyl radicals and resolve the apparent disagreement between reported reaction orders, and 3) explore their utilization as a novel class of dynamic covalent bonds to effect the photo-mediated healing of cross-linked polymer networks.

A novel, bis(hydroxyhexyl)-functionalized HABI was synthesized and employed as an efficient, visible light-active photoinitiator for thiol–ene resin formulations in the absence of any accompanying photosensitizer. Owing to the high reactivity of thiol functional groups with HABI-derived lophyl radical, in conjunction with the necessarily high thiol concentration in thiol–ene formulations, this HABI photoinitiator effectively initiated thiol–ene polymerizations upon visible light irradiation and exhibited improved visible light absorption and solubility in both organic solvents and resins relative to a commercial HABI photoinitiator. Additionally, the photo-mediated dissociation of HABIs and subsequent dark recombination of lophyl radicals were examined, where analysis of lophyl radical concentration curves revealed that the recombination reactions were well described as 3/2- and second-order reactions for the two respective parent HABIs. Finally, HABI-based functional groups were utilized as a new class of dynamic covalent bonds to demonstrate the photo-mediated healing of cross-linked polymer networks. Novel di- and tetra-functional, polymerizable HABI-based monomers were synthesized and subsequently incorporated into cross-linked polymer networks. The resultant HABI-incorporating cross-linked polymer networks were able to undergo photo-mediated backbone cleavage, temporarily affording reduced cross-link densities and dynamic connectivity rearrangement while under irradiation, then reverting back to stable, static networks upon irradiation cessation. This network stability in the dark, combined with a highly dynamic nature under irradiation, enabled rapid healing rates while precluding the creep that often accompanies the dynamic connectivity of intrinsically-healable polymer networks. Moreover, the cross-link density reduction upon irradiation and long half-life of the photo-generated lophyl radicals tethered to network

strands provided sufficient time for effective, successful healing within HABI-incorporating, vitrified, cross-linked polymer networks.

The findings described herein open up possibilities in the design and synthesis of novel, intrinsically-healable cross-linked polymer networks, and suggest the suitability of HABIs in advanced, responsive materials applications, including in stress-indicating and self-reinforcing materials.

Chapter 1

Introduction

1.1 Background and research overview

The ability to spontaneously heal injury is a key feature of biological materials, significantly increasing the life span of plants and animals. In contrast, the longevity of synthetic materials is curtailed by the occurrence of macroscopic damage or microcracking and fatigue that severely decrease mechanical performance, eventually leading to structural failure. Consequently, a new research area focused on synthetic, 'self-healing' polymeric materials, mimicking natural healing process, has emerged that aims to extend material service life spans, improve safety, and ensure sustainability.[1-3] One approach to achieve self-healing in polymeric materials employs embedded, liquid-filled microcapsules[1] or vascular networks[3,4] throughout the material that, upon catastrophic failure, release monomer which polymerizes to form a healed 'scar'. A potential drawback of this approach is that, should a repeat-fracture occur, the material is unable to re-heal as the healing agent has already been consumed during repair of the initial break. To address this shortcoming, new approaches involving 'intrinsically-healable' materials have been developed. In these approaches, the bulk polymer contains covalent cross-links which are designed to undergo well-defined and fully-reversible bond breaking and bond forming reactions (i.e., dynamic rearrangement of the network connectivity) during healing.[2] As a result, the self-healing process can undergo multiple

cycles even upon repeated damage at the same sites and the material within the healed zone can be chemically identical to that of the bulk polymer.

Dynamic covalent chemistry refers to a class of covalent bond-forming reactions whose products can be rearranged or reverted back to the constituent reactants under specific reaction conditions. Over the last few decades, introducing these chemical dynamics into synthetic, covalently cross-linked polymeric materials has drawn much attention in efforts to fabricate adaptable, healable networks.[5-7] Although all bimolecular addition reactions are, to some extent, reversible as dictated by the equilibrium constant temperature dependence, most reactions can essentially be considered irreversible as several temperature constraints exclude the majority of these reactions from being thermally-reversible dynamic covalent building blocks, including consideration of a practical temperature range, high temperature-induced side reactions, and chemical decomposition temperatures.

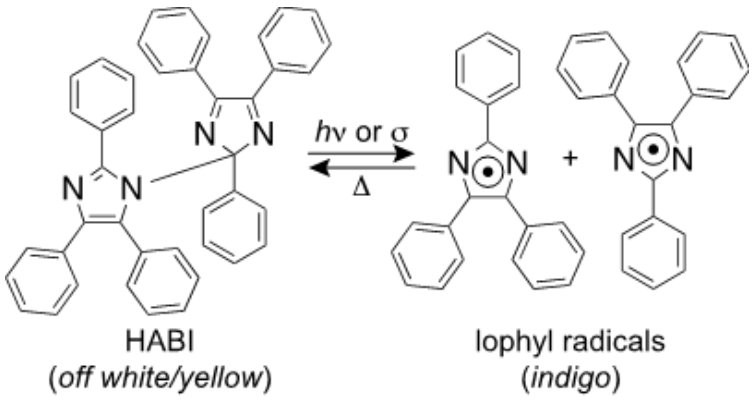

Figure 1.1. *Reversible photo-mediated homolysis of HABIs into lophyl radicals. The spontaneous recombination reaction proceeds over tens of seconds to minutes in solution.*

Hexaarylbiimidazoles (HABIs) are well known as thermo- and photo-chromic materials and photoinitiators that are widely used in proofing papers, photoimaging and photoresists.[8,9] They efficiently produce lophyl radicals upon light irradiation and can thermally recombine to reproduce the dimer (see Figure 1.1). The photochromic behavior of HABI derivatives can be attributed to the homolytic, reversible cleavage of the carbon-nitrogen (C-N) bond between the imidazole rings. Owing to the extraordinary stability of lophyl radicals and concomitant reversibility, we hypothesize that the HABI functional group can be used as a new class of dynamic covalent bonds within the polymer network. We aim to utilize the sluggish lophyl radical recombination reaction rates to yield a significant, although temporary, reduction in cross-link density, decreasing the T_g to sub-ambient temperatures upon application of light and dramatically increasing chain mobility, enabling photo-induced crack healing in cross-linked polymers.

Herein, we have modified HABI moieties to afford a novel visible light-active, single component photoinitiator with improved optical and chemical properties, and studied the kinetic behavior of HABIs depending on their chemical structures and surrounding environment. Also, we have synthesized new HABI monomers and utilized them as a new class of dynamic covalent bonds to demonstrate the photo-mediated healable materials.

1.2 Self-healing polymers

Polymeric materials underpin almost every aspect of everyday life with employing a very wide range of organic macromolecules; however, repeated exposure of these polymers to environmental stresses such as chemical attack, radiation, mechanical abrasion, impact, and fluctuating temperature can result in degradation of the material's physical properties and lead to irreversible failure. It has been proposed[10] that this process starts at the microscopic level with the formation of microvoids, which then expand to generate microcracks and ultimately lead to formation of macroscopic cracks. The resulting loss of structural integrity leads to weakening of mechanical properties and ultimately to failure of the polymeric component. Incorporating an ability to repair physical damage and cracks can effectively prevent catastrophic failure, thus extending the lifespan of materials. Consequently, the development of self-healing materials, defined as "materials where damage automates a healing response", has recently attracted significant attention.[11,12]

Numerous strategies have been reported to afford self-healing polymers. Based on the nature of self-healing and external triggers applied, they can be classified into non-autonomous and autonomous systems. Non-autonomous self-healing polymers require external triggers such as light, temperature, and pH change, whereas autonomous self-healing materials do not need any triggers to initiate the self-healing process. Alternatively, a number of strategies can be classified as intrinsic and extrinsic.[13] Extrinsic self-healing involves the encapsulation of external healing agents, in the form of microcapsules or fibers, impregnated deliberately in the polymer matrix.[14,15] When cracks or damages occur, the contents encapsulated in these containers are released to fill

the disrupted parts, which then begin self-repairing either by polymerization or chemical reactions. In contrast to extrinsic self-healing occurring in a single event, intrinsic self-healing is repeatable and occurs in multiple events. Intrinsic self-healing materials are designed with reversible cross-links, and self-healing is accomplished by bonding upon external stimuli to the system.[16,17] When the damage is below the critical limit, the damaged portion can be rejoined with the aid of either chemical cross-linking through dynamic covalent bond formation[18] or physical cross-linking through supramolecular (non-covalent) interactions.[19]

1.2.1 Extrinsic healing methods

In 2001, White and co-workers first reported self-healing concept based on the polymeric materials incorporating microencapsulated healing agent.[1] Microcapsules incorporated in these materials contain the healing agent while the catalyst for the healing polymerization reaction is dispersed in the polymer matrix. When a crack forms, the capsules are broken and the healing agent is released, pulled into the crack by capillary forces, and exposed to the catalyst, leading to polymerization and crack repair (see Figure 1.2). Although this seminal report initiated the entire field of self-healing materials and this microcapsule approach shows great promise for extending the lifetime of thermoset materials, it is still far away from the sophistication of natural healing as, owing to the loss of capsules upon healing, the repair is a one-time healing process rather than a continuous regeneration of the material properties. In addition, microcapsules can only efficiently repair microcracks since insufficient healing agent is available for larger defects. Inspired by healing process in biological systems, White et al. have proposed the

use of vascular channels with healing agent to overcome these limitations.[3] A cut in the skin triggers blood flow from the capillary network in the skin to wound site rapidly forming a clot. After the model of this healing process in nature, they prepared an epoxy coating contains a pervasive three-dimensional microvascular network. Solid catalyst particles are incorporated within the coating and the network is filled with a liquid healing agent. After damage occurs in the coating, healing agent wicks from the microchannels into the crack through capillary action. Once in the crack plane, the healing agent interacts with the catalyst particles in the coating to initiate polymerization, re-bonding the crack faces autonomically. Although above-mentioned mechanisms do achieve self-healing behavior, questions remain concerning the long-term stability of the catalyst and the ability of the materials to heal injury multiple times. Moreover, this approach necessarily reduces the strength and modulus of the virgin materials as the liquid-filled inclusions do not provide any load-bearing contribution.[20] Nevertheless, this approach does contribute to the development of self-healing materials and provides tremendous inspiration and momentum for other researchers in the field.[21-24]

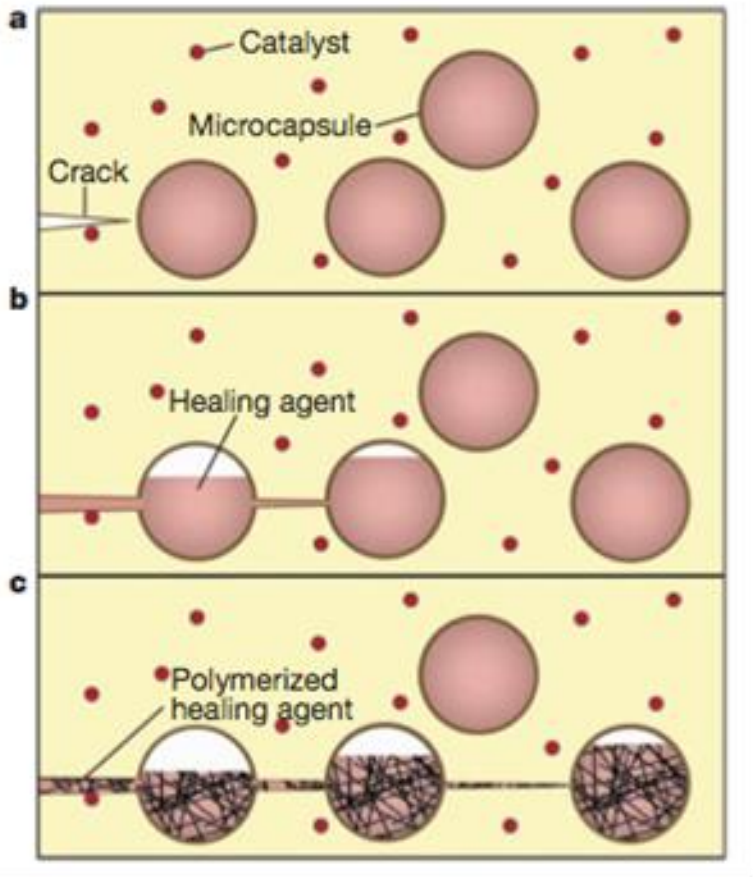

Figure 1.2. *The autonomic healing concept. A microencapsulated healing agent is embedded in a structural composite matrix containing a catalyst capable of polymerizing the healing agent.*

1.2.2 Intrinsic healing methods

The design of these materials involves the incorporation of dynamic covalent bonds as cross-linkers in self-healable networks. These reversible linkages are later utilized through the reformation of covalent bonds to reattach materials fractured by mechanical forces. Unlike physical cross-linking methods based on supramolecular interactions, chemical cross-linking methods utilizing reversible covalent bond formation

provide higher mechanical strength and dimensional stability. These features can be advantageous in the development of tough self-healable materials.

1.2.2.1 Thermally-reversible dynamic covalent bonds

Several thermally-reversible reaction mechanisms have been used to fabricate adaptable networks (Figure 1.3). Nucleophilic addition reactions are well-suited as thermoreversible reactions; however, the nucleophile must also be a good leaving group in order for the reaction to revert over a reasonable temperature range. Although the reaction of isocyanates with imidazoles has been successfully employed for a thermoreversible network under inert conditions (Figure 1.3a),[25] the intolerance of isocyanates to moisture significantly limits its implementation. Carbene dimerization, another candidate thermoreversible reaction (Figure 1.3b), has been used to fabricate dynamic, thermally-responsive polymers[26,27] and, given its capacity to yield electrically conductive polymers, has been proposed as a path to yield materials that self-heal by ohmic heating, where the electrical resistance of the material dramatically increases upon fracture.[28] Unfortunately, carbenes tend to highly reactive species where, for example, exposure of the carbene species shown in Figure 1.2b to oxygen results in the formation of a cyclic urea.[26]

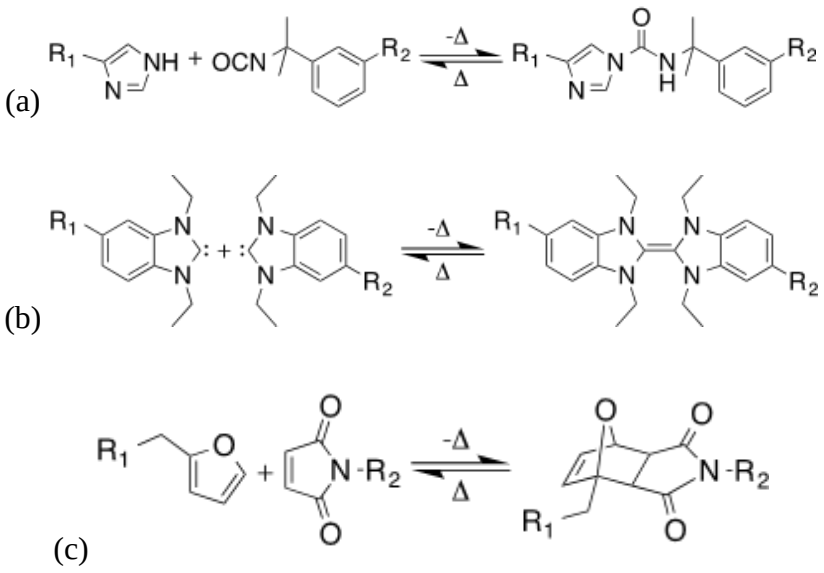

Figure 1.3. *Temperature-mediated dynamic covalent chemistries. Thermoreversible (a) nucleophilic addition between isocyanate and imidazole, (b) carbene dimerization, and (c) Diels–Alder cycloaddition between furan and maleimide.*

While these reactions have their own particular advantages, the cyclical reversion potential of the [4+2] cycloaddition between a conjugated diene and, typically, an electronically-activated double bond (i.e., a dienophile), known as Diels–Alder (DA) reaction, is prevalent in thermoreversible polymer networks. DA reactions exhibit reasonable tolerance of typical environmental species such as water and oxygen, and can be turned to respond over a wide range of temperatures. In particular, furan and maleimide functional groups have been the predominant species used to fabricate the thermoreversible networks owing to their synthetic accessibility and the convenient temperature range over which the reaction shifts from products to reactants.[10] In 1969, Craven first described the cross-linking of linear polymers having pendant furan moieties with bis- and tris-maleimide moieties *via* a DA reaction to afford a material that was reshapeable upon heating but formed an insoluble network upon cooling. Several

researchers have adopted this strategy; however, the common use of functionalized linear chains, which essentially act as prepolymers with a high degree of functionality, significantly reduces the gel's ability to undergo a gel-to-sol transition. Thus, other researchers have employed low molecular weight, low functionality diene and dienophile monomers to raise the gel-point conversion and significantly improve the ability of these systems to revert to liquids at reasonable temperatures.[2,29,30] Unfortunately, many networks that utilize diene and dienophile pairs require excessive heating to undergo the retro-DA reaction, which can also trigger irreversible side reactions.[31]

In order to decrease the working temperature for dynamic covalent bond rupture and re-forming reaction, urea bonds bearing a bulky group on the nitrogen have been developed.[32] They can dissociate into the corresponding isocyanate and amine; they then reversibly form the urea bonds. This dynamic hindered urea chemistry has been exploited in the development of catalyst-free, low-temperature self-healing of poly(urethane-urea) containing hindered urea bonds (HUBs). The HUBs in cuts were involved in the reverse process of typical urea bond formation, leading to the occurrence of autonomous repairing for 12 hours at 37°C.[33] This chemistry has been further explored to synthesize hydrolysable polyureas bearing HUBs.[34]

1.2.2.2 Photochemically-reversible dynamic covalent bonds

Although temperature-mediated reactions have proved capable of effecting network connectivity rearrangement and healing, they suffer from inherent poor spatial and temporal reaction confinement. Unlike thermoreversible networks, photoreversible networks only undergo bond rearrangement upon irradiation, otherwise exhibiting little to

no creep or adaptation in the absence of irradiation. Furthermore, photochemical approaches enable three-dimensional spatial control of the reaction reversion as well as the ability to remotely trigger a process on and off. Several distinct approaches to photochemically-triggered rearrangeable polymer networks have been developed, including photoinduced cyclization reactions and photochemical radical-mediated addition-fragmentation approaches. The cyclization reactions exhibit limited relative response rates, as at most a single cross-link is reversibly broken for each absorbed photon, afford relatively low quantum yields,[35,36] and necessitate short wavelength irradiation.[37] Conversely, the addition-fragmentation reactions undergo a network rearrangement cascade, where multiple reversible bond breaking and re-forming reactions occur for each absorbed photon.[38] However, the addition-fragmentation reactions are limited by never having a large fraction of the bonds cleaved at a given time,[38,39] thus restricting such materials from any applications where a gel-to-sol transition is required.

Photoinduced cyclization reactions, commonly known as photodimerizations, occur when two functionalities incorporating carbon-carbon double bonds undergo a photo-induced cycloaddition reaction. The corresponding photo-scission reaction is achieved simply by exposure of the sample to a different irradiating wavelength. This process, with its associated ability to effect spatially patterning, has been utilized extensively for reversible polymer network connectivity rearrangement.[40] Several functionalities, including coumarins,[40-42] cinnamates,[37,43] anthracenes,[44-46] and thymines,[47] have been investigated for polymer network rearrangement. With the exception of anthracenes, which undergo a [4+4] cycloaddition (Figure 1.4a), photodimerization typically proceeds *via* a [2+2] cycloaddition of ethylenic bonds

(Figure 1.4b). Near-ultraviolet irradiation of materials incorporating photodimerizable functionalities induces the forward, cycloaddition reaction while irradiation at shorter wavelengths favors the reverse, scission reaction.[37] Thus, these reactions are analogous to the thermally controlled DA forward and retro reactions where the light intensity, controlling the rates of the forward and reverse reactions, and the wavelength, controlling the equilibrium extent of the cyclization and scission reactions, are analogous to the temperature control exerted over DA and other thermoreversible systems. Additionally, photoinduced cyclization systems are, with sufficient light exposure at the appropriate wavelength, capable of reverting to a liquid state, providing the assorted benefits of crack-healing and mending available to materials in that state.[44]

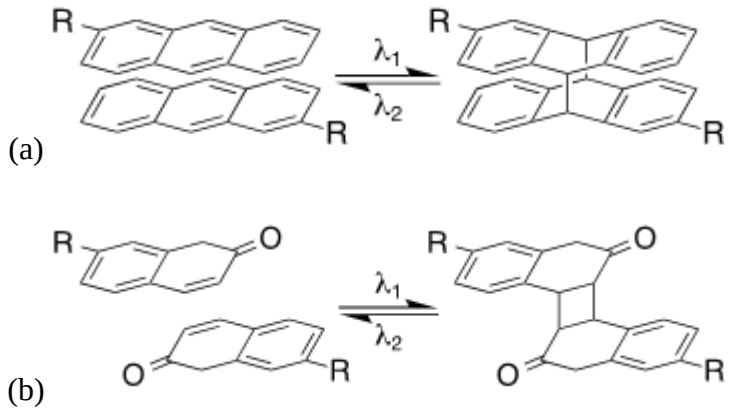

Figure 1.4. *Photo-mediated dynamic covalent cyclization chemistries. Photoinduced (a) [4+4] cyclization of anthracenes and (b) [2+2] cyclization of coumarins affords dimerized products. Near-ultraviolet irradiation of materials incorporating photodimerizable functionalities effects the forward, cycloaddition reaction while irradiation at shorter wavelengths favors the reverse reaction.*

A unique, photoinduced, non-destructive scission approach was recently developed for rearranging network connectivity by utilizing addition/fragmentation chain

transfer functionalities incorporated in the backbone of cross-linked polymers.[38,39] This technique exhibits all the advantages of photoinduced reactions whereby the network exists in a permanent, nonadaptable state in the absence of light, the network adaptation response is photo-patternable, and the adaptation process can be commenced and ceased on demand. When first described by Scott et al., these polymer networks were fabricated such that a significant residual amount of a radical generating photoinitiator remained after polymerization.[38,39] Thus, upon irradiation of polymerized films, cleavage of the residual photoinitiator introduces radicals into these materials, initiating the addition-fragmentation chain transfer reaction (shown in Figure 1.5) and ultimately effecting network adaptation. In post-polymerization studies, allyl sulfide-containing networks demonstrated the utility of this phenomenon *via* photoinduced creep, stress relaxation, and photoinduced actuation.[38,39] Irradiating these samples while a tensile stress is applied, network rearrangement due to the reversible addition-fragmentation chain transfer process allows for either stress relaxation or creep, depending on the mode of the applied stress, and the equilibrium shape and state of the material are altered (i.e., permanent set[48]). Unlike its photodimerization/scission counterpart, this approach does not effect a concomitant variation in the cross-link density since, although individual bonds are being broken and re-formed, the overall cross-link density remains essentially constant throughout irradiation. However, although photomediated addition/fragmentation chain transfer has been used to effect self-healing in cross-linked elastomeric and organogel materials, the processes are sluggish and typically proceed over several hours.[49,50]

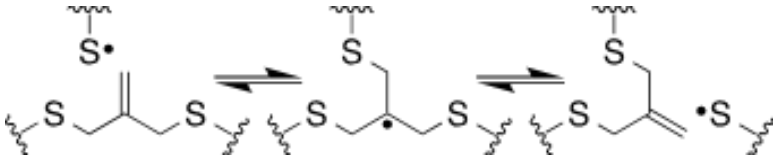

Figure 1.5. *Stress relaxation in cross-linked polymers. Radical-mediated addition-fragmentation chain transfer (AFCT) allows for rearrangement of polymer connectivity.*

1.2.2.3 Other dynamic covalent bonds

Disulfide linkages are cleaved to the corresponding thiols either under a reducing condition in the presence of reducing agents such as phosphines or through thiol-disulfide exchange reactions in the presence of thiols.[51,52] They can also be cleaved to the corresponding thiyl radicals under conditions such as thermal scission,[53] mechanical load,[54] or light irradiation.[55] Reversibly, the formed thiols or thiyl radicals are utilized to reform disulfide bonds by several reactions: oxidation of thiols, thiol-disulfide exchange reaction, and recombination of thiyl radicals. More, disulfide linkages can be exchanged through disulfide metathesis (or disulfide rearrangement) catalyzed by phosphine,[56] tertiary amine,[57,58] or photo-irradiation.[59] These unique redox chemistries have been utilized in the design and construction of disulfide-containing self-healing materials.[60-66]

Figure 1.6. *Reversible disulfide linkage.*

1.2.2.4 Dynamic non-covalent bonds

Another type of intrinsic healing method utilizes non-covalent interactions, typically hydrogen bonding, metal complexation, π- π, ionic, and host-guest interactions. The formed physical cross-links within polymer networks are easily disrupted in response to external stimuli such as heat, light, pH change, and mechanical stress. Such physical disruptions are restored to their original interactions owing to the typically ready reversibility of these relatively weak, transient cross-links.

The utilization of hydrogen bonds for the development of self-healable, supramolecular networks requires the incorporation of hydrogen bonding moieties as donors and acceptors into polymer strands as pendant groups, within arms, or at chain ends. Widely explored hydrogen bonding motifs include 2-ureido-4-pyrimidinone[67] and secondary amide groups. Thymine/2,6-diaminotriazine,[68] urea moieties,[69] and carboxylic acids[70,71] have also been used. These functional groups enable the formation of reversible supramolecular cross-linking networks through their intermolecular hydrogen bonding. Upon mechanical stresses, the non-covalent cross-links are disrupted; however, they can be reformed because of their unique reversibility; however, most self-healable materials utilizing hydrogen bonding interactions exhibit weak mechanical strength owing to the use of soft polymers as self-healable matrices for these systems.

Self-healing through dynamic π- π stacking utilizes aromatic units, mostly pyrene moieties as π-electron-rich residues and diimide units as π-electron-deficient residues which form complexes adopting chain-folded conformation through π- π stacking interactions. These supramolecular interactions can be disrupted and reformed upon external stimuli, a consequence of which is the healing of physical damage.

Besides the interactions described above, various other non-covalent interactions have been used to effect self-healable supramolecular networks, including metallo-supramolecular interactions, ionic interactions, and host-guest interactions. For approaches utilizing metal-ligand interactions, these materials are designed to have ligand motifs that bind to metal ions at the chain ends or in the side chains. Upon the incorporation of metal ions, such as Zn, Fe, Co, and Ni, linear supramolecular polymers or supramolecular cross-linked networks can be formed through specific metal-ligand interactions. These interactions can be disrupted physically, thermally, or upon UV irradiation. Subsequent restoration of such interactions can induce self-healing behavior of the materials. Ionic interactions have also been commonly employed for the development of self-healable, supramolecular networks. This method utilizes ionic cross-linking between anionic polymers and cationic species as metal ions, small molecules, or macromolecules. The formed ionic cross-linking networks can be broken when physically disrupted and subsequently restored in response to change in stimuli under ambient conditions.[72] Specific interlocking host-guest interactions are reversibly disassembled in response to stimuli such as redox potential, pH, and temperature. Such reversibility has been explored in the design of self-healing polymeric materials in the form of supramolecular hydrogels, nanofibers, and organo-gels.[73]

1.3 Hexaarylbiimidazoles

Free radicals, atomic or molecular species with an unpaired valence electron, are common reactive species in many chemical reactions. Indeed, radicals participate in many naturally-occurring biological processes[74-76] as well as in polymerization reactions

as the active propagating centers in both chain- and step-growth polymerizations.[77] One particularly interesting class of radical-generating compounds is that of hexaarylbiimidazoles (HABIs). HABIs, 2,4,5-triaryl-substituted imidazole dimers that were first synthesized by Hayashi and Maeda in 1960,[78] are well known thermo- and photo-chromic materials and photoinitiators that have been widely used in proofing paper, photoimaging, and photoresist applications.[79,80] Upon irradiation, HABIs undergo reversible, homolytic cleavage of the carbon-nitrogen (C-N) bond between the imidazole rings to efficiently afford two colored 2,4,5-triarylimidazolyl (i.e., lophyl) radicals (see Figure 1.7) which thermally recombine to reproduce the imidazole dimer.[81] With some notable exceptions (e.g., nitroxides), organic radicals are typically highly reactive species that recombine at diffusion-controlled rates; in contrast, the lophyl radicals generated by HABI homolysis are insensitive to atmospheric oxygen and show extraordinary slow recombination rates,[82] attributable to their unique chemical structure affording stabilization by steric hindrance and electron delocalization.[83] Indeed, HABI photoinitiators show no initiation activity in (meth)acrylate formulations without the presence of a hydrogen-donating coinitiator such as a thiol,[84] where hydrogen abstraction by the HABI-derived lophyl radicals yields initiating thiyl radicals (Figure 1.7). HABIs also exhibit mechanochromic behavior owing to the low bond energy of the inter-imidazole C-N bond, where the homolytic cleavage of this bond can be effected by application of a threshold pressure through, for example, grinding.

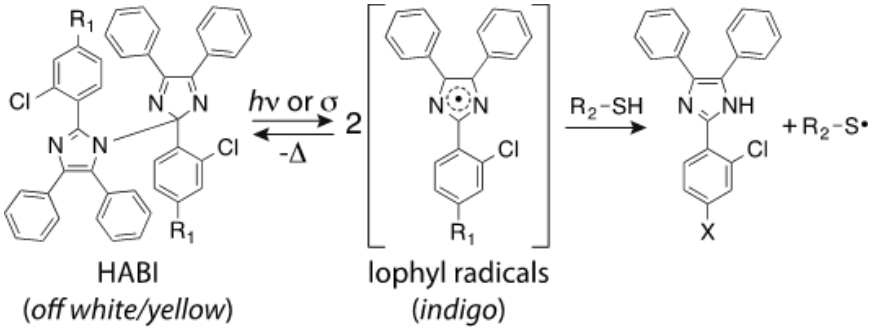

Figure 1.7. *Reversible photo- or mechano-mediated homolysis of HABIs into lophyl radicals. The spontaneous recombination reaction proceeds over tens of seconds to minutes in solution. In the presence of thiol, a lophyl radical can abstract a thiol hydrogen, generating a thiyl radical capable of initiating polymerization.*

The ready synthetic accessibility of HABIs enables their facile modification to afford particular properties. For example, the solubility of these typically solid materials can be dramatically increased by affixing alkyl substituents,[80,85] the lophyl radical recombination rate can be decreased, with a corresponding bathochromic shift in its absorption spectrum, by incorporating extended π-conjugated moieties,[86] or dramatically increased by attaching both units of the imidazole dimer to a rigid bridge.[87] Notably, this synthetic adaptability has even been utilized to synthesize linear polymers bearing 2,4,5-triaryl-substituted imidazole pendant groups which generated polymer networks incorporating HABI-based cross-links upon subsequent oxidation,[88,89] an approach that, as described above, limits the gel-to-sol transition ability owing to the high degree of functionality of the precursor polymer.

Given the low inter-imidazole bond energy and the low reactivity and long lifetime of the lophyl radicals originating from HABI cleavage, cross-linked polymers composed of HABI-incorporating network strands offer extraordinary properties

otherwise unattainable in conventional thermoset materials. For example, the relatively poor reactivity of HABI-derived lophyl radicals yields an inherent reversibility where the cleaved covalent bond spontaneously reforms without participating in parasitic side reactions, imparting autonomous healing characteristics. Owing to their longevity, these lophyl radicals can countervail the reduced chain mobility within glassy resins and provide sufficient time for effective healing. Moreover, HABI-based functionalities can act as mechanophores within the network strands of cross-linked polymer networks, where application of a mechanical stress selectively breaks the incorporated HABI groups, generating indigo-colored lophyl radicals. Additionally, the capacity for thiol hydrogen abstraction by mechanically-generated lophyl radicals suggests the potential for initiating self-reinforcing polymerization exclusively at a damage site.

As noted above, the thermodynamic and kinetic elements of dynamic covalent reactions must coincide with the application-dependent characteristic time scale. Consequently, by incorporating HABI moieties as dynamic covalent functional groups in the network strands of cross-linked polymers, we aim to utilize the sluggish lophyl radical recombination reaction rates to yield a significant, although temporary, reduction in cross-link density, decreasing the T_g to sub-ambient temperatures upon application of light or a threshold mechanical stress and dramatically increasing chain mobility, enabling photo-induced crack healing and pressure-mediated cold welding in cross-linked polymers.

1.4 Overview of subsequent chapters

The remaining chapters of this dissertation are organized as follows:

Chapter 2 details the design and synthesis of a new HABI photoinitiator that efficiently generates lophyl radicals upon visible light irradiation and initiates thiol–ene polymerization. Owing to the reactivity of lophyl radicals with thiols and the necessarily high concentration of thiol in thiol–ene formulations, HABIs can be used as single-component, visible light-active initiator for thiol–ene photopolymerizations. Chapter 2 also provides a comparison of this novel HABI photoinitiator with contemporary photoinitiators, highlighting its advantageous attributes.

In Chapter 3, the photo-mediated dissociation and recombination kinetics of HABIs were examined. The recombination kinetics of lophyl radicals have been previously studied; however, there remains an apparent disagreement between reported reaction orders. Analysis of radical concentration curves revealed that the recombination reactions were well fit as 3/2- and second-order reactions for the two respective parent HABI compounds.

Chapter 4 describes the utilization of HABI functional groups as new class of dynamic covalent bonds to demonstrate photo-mediated healing of HABI-containing polymeric gels, which undergo photo-mediated backbone cleavage, temporarily affording reduced cross-link density and dynamic connectivity rearrangement, and revert back to stable, static networks upon irradiation cessation. This network stability in the dark, combined with its highly dynamic nature under irradiation, enables rapid healing rates

while precluding the creep that often accompanies the dynamic connectivity of intrinsically-healable polymer networks.

Chapter 5 details the design and synthesis of a new HABI-based monomer and its utilization to demonstrate vitrified, photo-mediated, healable cross-linked polymer network. Given the dependence of glass transition temperature on cross-link density, the reduced cross-link density that accompanies the photo-mediated backbone cleavage exhibited by these HABI-incorporating networks provides a route to achieve sub-glass transition temperature healing of vitrified thermoset polymers.

Chapter 6 provides an overall summary and conclusions of this work followed by a discussion of future work.

1.5 References

(1) White, S. R.; Sottos, N. R.; Geubelle, P. H.; Moore, J. S.; Kessler, M. R.; Sriram, S. R.; Brown, E. N.; Viswanathan, S. Autonomic healing of polymer composites. *Nature* **2001**, *409*, 794-797.

(2) Chen, X.; Dam, M. A.; Ono, K.; Mal, A.; Shen, H.; Nutt, S. R.; Sheran, K.; Wudl, F. A thermally re-mendable cross-linked polymeric material. *Science* **2002**, *295*, 1698-1702.

(3) Toohey, K. S.; Sottos, N. R.; Lewis, J. A.; Moore, J. S.; White, S. R. Self-healing materials with microvascular networks. *Nat. Mater.* **2007**, *6*, 581-585.

(4) White, S. R.; Moore, J. S.; Sottos, N. R.; Krull, B. P.; Santa Cruz, W. A.; Gergely, R. C. R. Restoration of large damage volumes in polymers. *Science* **2014**, *344*, 620-623.

(5) Kloxin, C. J.; Scott, T. F.; Adzima, B. J.; Bowman, C. N. Covalent adaptable networks (CANs): A unique paradigm in cross-linked polymers. *Macromolecules* **2010**, *43*, 2643-2653.

(6) Wojtecki, R. J.; Meador, M. A.; Rowan, S. J. Using the dynamic bond to access macroscopically responsive structurally dynamic polymers. *Nat. Mater.* **2011**, *10*, 14-27.

(7) Brandt, J.; Oehlenschlaeger, K. K.; Schmidt, F. G.; Barner-Kowollik, C.; Lederer, A. State-of-the-art analytical methods for assessing dynamic bonding soft matter materials. *Advanced Materials* **2014**, *26*, 5758-5785.

(8) Qin, X. Z.; Liu, A.; Trifunac, A. D.; Krongauz, V. V. Photodissociation of hexaarylbiimidazole. 1. Triplet-state formation. *Journal of Physical Chemistry* **1991**, *95*, 5822-5826.

(9) Liu, A. D.; Trifunac, A. D.; Krongauz, V. V. Photodissociation of hexaarylbiimidazole. 2. Direct and sensitized dissociation. *Journal of Physical Chemistry* **1992**, *96*, 207-211.

(10) Bergman, S. D.; Wudl, F. Mendable polymers. *J. Mater. Chem.* **2008**, *18*, 41-62.

(11) Blaiszik, B. J.; Kramer, S. L. B.; Olugebefola, S. C.; Moore, J. S.; Sottos, N. R.; White, S. R.: Self-healing polymers and composites. In *Annual Review of Materials Research*, 2010; Vol. 40; pp 179-211.

(12) Burattini, S.; Greenland, B. W.; Chappell, D.; Colquhoun, H. M.; Hayes, W. Healable polymeric materials: A tutorial review. *Chemical Society Reviews* **2010**, *39*, 1973-1985.

(13) Billiet, S.; Hillewaere, X. K. D.; Teixeira, R. F. A.; Du Prez, F. E. Chemistry of crosslinking processes for self-healing polymers. *Macromol. Rapid Commun.* **2013**, *34*, 290-309.

(14) Shchukin, D. G. Container-based multifunctional self-healing polymer coatings. *Polym. Chem.* **2013**, *4*, 4871-4877.

(15) Zhao, Z.; Arruda, E. M. An internal cure for damaged polymers. *Science* **2014**, *344*, 591-592.

(16) Garcia, S. J. Effect of polymer architecture on the intrinsic self-healing character of polymers. *European Polymer Journal* **2014**, *53*, 118-125.

(17) Wei, Z.; Yang, J. H.; Zhou, J.; Xu, F.; Zrínyi, M.; Dussault, P. H.; Osada, Y.; Chen, Y. M. Self-healing gels based on constitutional dynamic chemistry and their potential applications. *Chemical Society Reviews* **2014**, *43*, 8114-8131.

(18) Zhang, M. Q.; Rong, M. Z. Intrinsic self-healing of covalent polymers through bond reconnection towards strength restoration. *Polym. Chem.* **2013**, *4*, 4878-4884.

(19) Hart, L. R.; Harries, J. L.; Greenland, B. W.; Colquhoun, H. M.; Hayes, W. Healable supramolecular polymers. *Polym. Chem.* **2013**, *4*, 4860-4870.

(20) Tian, W.; Wang, X.; Pan, Q.; Mao, Z. Microcapsule used for self-healing polymer material. *Huagong Xuebao/Journal of Chemical Industry and Engineering (China)* **2005**, *56*, 1138-1140.

(21) Cho, S. H.; Andersson, H. M.; White, S. R.; Sottos, N. R.; Braun, P. V. Polydiniethylsiloxane-based self-healing materials. *Advanced Materials* **2006**, *18*, 997-1000.

(22) Trask, R. S.; Williams, G. J.; Bond, I. P. Bioinspired self-healing of advanced composite structures using hollow glass fibres. *Journal of the Royal Society Interface* **2007**, *4*, 363-371.

(23) Yin, T.; Rong, M. Z.; Zhang, M. Q.; Yang, G. C. Self-healing epoxy composites - Preparation and effect of the healant consisting of microencapsulated epoxy and latent curing agent. *Composites Science and Technology* **2007**, *67*, 201-212.

(24) Hansen, C. J.; Wu, W.; Toohey, K. S.; Sottos, N. R.; White, S. R.; Lewis, J. A. Self-healing materials with interpenetrating microvascular networks. *Advanced Materials* **2009**, *21*, 4143-4147.

(25) Chang, J. Y.; Do, S. K.; Han, M. J. A sol-gel reaction of vinyl polymers based on thermally reversible urea linkages. *Polymer* **2001**, *42*, 7589-7594.

(26) Kamplain, J. W.; Bielawski, C. W. Dynamic covalent polymers based upon carbene dimerization. *Chemical Communications* **2006**, 1727-1729.

(27) Neilson, B. M.; Tennyson, A. G.; Bielawski, C. W. Advances in bis(N-heterocyclic carbene) chemistry: New classes of structurally dynamic materials. *Journal of Physical Organic Chemistry* **2012**, *25*, 531-543.

(28) Williams, K. A.; Boydston, A. J.; Bielawski, C. W. Towards electrically conductive, self-healing materials. *Journal of the Royal Society Interface* **2007**, *4*, 359-362.

(29) Chen, X.; Wudl, F.; Mal, A. K.; Shen, H.; Nutt, S. R. New thermally remendable highly cross-linked polymeric materials. *Macromolecules* **2003**, *36*, 1802-1807.

(30) Adzima, B. J.; Kloxin, C. J.; Bowman, C. N. Externally triggered healing of a thermoreversible covalent network via self-limited hysteresis heating. *Advanced Materials* **2010**, *22*, 2784-2787.

(31) Adzima, B. J.; Aguirre, H. A.; Kloxin, C. J.; Scott, T. F.; Bowman, C. N. Rheological and chemical analysis of reverse gelation in a covalently cross-linked diels-alder polymer network. *Macromolecules* **2008**, *41*, 9112-9117.

(32) Hutchby, M.; Houlden, C. E.; Gair Ford, J.; Tyler, S. N. G.; Gagné, M. R.; Lloyd-Jones, G. C.; Booker-Milburn, K. I. Hindered ureas as masked isocyanates: Facile carbamoylation of nucleophiles under neutral conditions. *Angewandte Chemie - International Edition* **2009**, *48*, 8721-8724.

(33) Ying, H.; Zhang, Y.; Cheng, J. Dynamic urea bond for the design of reversible and self-healing polymers. *Nat. Commun.* **2014**, *5*.

(34) Ying, H.; Cheng, J. Hydrolyzable polyureas bearing hindered urea bonds. *Journal of the American Chemical Society* **2014**, *136*, 16974-16977.

(35) Coqueret, X. Photoreactivity of polymers with dimerizable side-groups: Kinetic analysis for probing morphology and molecular organization. *Macromolecular Chemistry and Physics* **1999**, *200*, 1567-1579.

(36) Schreier, W. J.; Schrader, T. E.; Koller, F. O.; Gilch, P.; Crespo-Hernández, C. E.; Swaminathan, V. N.; Carell, T.; Zinth, W.; Kohler, B. Thymine dimerization in DNA is an ultrafast photoreaction. *Science* **2007**, *315*, 625-629.

(37) Lendlein, A.; Jiang, H.; Jünger, O.; Langer, R. Light-induced shape-memory polymers. *Nature* **2005**, *434*, 879-882.

(38) Scott, T. F.; Draughon, R. B.; Bowman, C. N. Actuation in crosslinked polymers via photoinduced stress relaxation. *Advanced Materials* **2006**, *18*, 2128-2132.

(39) Scott, T. F.; Schneider, A. D.; Cook, W. D.; Bowman, C. N. Chemistry: Photoinduced plasticity in cross-linked polymers. *Science* **2005**, *308*, 1615-1617.

(40) Trenor, S. R.; Shultz, A. R.; Love, B. J.; Long, T. E. Coumarins in polymers: From light harvesting to photo-cross-linkable tissue scaffolds. *Chemical Reviews* **2004**, *104*, 3059-3077.

(41) Fu, Q.; Cheng, L.; Zhang, Y.; Shi, W. Preparation and reversible photo-crosslinking/photo-cleavage behavior of 4-methylcoumarin functionalized hyperbranched polyester. *Polymer* **2008**, *49*, 4981-4988.

(42) He, J.; Tong, X.; Zhao, Y. Photoresponsive nanogels based on photocontrollable cross-links. *Macromolecules* **2009**, *42*, 4845-4852.

(43) Oya, N.; Sukarsaatmadja, P.; Ishida, K.; Yoshie, N. Photoinduced mendable network polymer from poly(butylene adipate) end-functionalized with cinnamoyl groups. *Polym. J.* **2012**, *44*, 724-729.

(44) Froimowicz, P.; Frey, H.; Landfester, K. Towards the generation of self-healing materials by means of a reversible photo-induced approach. *Macromol. Rapid Commun.* **2011**, *32*, 468-473.

(45) Wells, L. A.; Brook, M. A.; Sheardown, H. Generic, anthracene-based hydrogel crosslinkers for photo-controllable drug delivery. *Macromol. Biosci.* **2011**, *11*, 988-998.

(46) Xu, J. F.; Chen, Y. Z.; Wu, L. Z.; Tung, C. H.; Yang, Q. Z. Dynamic covalent bond based on reversible photo [4 + 4] cycloaddition of anthracene for construction of double-dynamic polymers. *Organic Letters* **2013**, *15*, 6148-6151.

(47) Imai, Y.; Ogoshi, T.; Naka, K.; Chujo, Y. Formation of IPN organic-inorganic polymer hybrids utilizing the photodimerization of thymine. *Polymer Bulletin* **2000**, *45*, 9-16.

(48) Bowman, C. N.; Kloxin, C. J. Toward an enhanced understanding and implementation of photopolymerization reactions. *AIChE Journal* **2008**, *54*, 275-2795.

(49) Amamoto, Y.; Kamada, J.; Otsuka, H.; Takahara, A.; Matyjaszewski, K. Repeatable photoinduced self-healing of covalently cross-linked polymers through

reshuffling of trithiocarbonate units. *Angewandte Chemie - International Edition* **2011**, *50*, 1660-1663.

(50) Amamoto, Y.; Otsuka, H.; Takahara, A.; Matyjaszewski, K. Self-healing of covalently cross-linked polymers by reshuffling thiuram disulfide moieties in air under visible light. *Advanced Materials* **2012**, *24*, 3975-3980.

(51) Chujo, Y.; Sada, K.; Nomura, R.; Naka, A.; Saegusa, T. Photogelation and Redox Properties of Anthracene-Disulfide-Modified Polyoxazolines. *Macromolecules* **1993**, *26*, 5611-5614.

(52) Tsarevsky, N. V.; Matyjaszewski, K. Reversible redox cleavage/coupling of polystyrene with disulfide or thiol groups prepared by atom transfer radical polymerization. *Macromolecules* **2002**, *35*, 9009-9014.

(53) Rajan, V. V.; Dierkes, W. K.; Joseph, R.; Noordermeer, J. W. M. Science and technology of rubber reclamation with special attention to NR-based waste latex products. *Progress in Polymer Science (Oxford)* **2006**, *31*, 811-834.

(54) Wiita, A. P.; Ainavarapu, S. R. K.; Huang, H. H.; Fernandez, J. M. Force-dependent chemical kinetics of disulfide bond reduction observed with single-molecule techniques. *Proceedings of the National Academy of Sciences of the United States of America* **2006**, *103*, 7222-7227.

(55) Fairbanks, B. D.; Singh, S. P.; Bowman, C. N.; Anseth, K. S. Photodegradable, photoadaptable hydrogels via radical-mediated disulfide fragmentation reaction. *Macromolecules* **2011**, *44*, 2444-2450.

(56) Caraballo, R.; Rahm, M.; Vongvilai, P.; Brinck, T.; Ramström, O. Phosphine-catalyzed disulfide metathesis. *Chemical Communications* **2008**, 6603-6605.

(57) Martin, R.; Rekondo, A.; Ruiz De Luzuriaga, A.; Cabañero, G.; Grande, H. J.; Odriozola, I. The processability of a poly(urea-urethane) elastomer reversibly crosslinked with aromatic disulfide bridges. *J. Mater. Chem. A* **2014**, *2*, 5710-5715.

(58) Rekondo, A.; Martin, R.; Ruiz De Luzuriaga, A.; Cabañero, G.; Grande, H. J.; Odriozola, I. Catalyst-free room-temperature self-healing elastomers based on aromatic disulfide metathesis. *Materials Horizons* **2014**, *1*, 237-240.

(59) Otsuka, H.; Nagano, S.; Kobashi, Y.; Maeda, T.; Takahara, A. A dynamic covalent polymer driven by disulfide metathesis under photoirradiation. *Chemical Communications* **2010**, *46*, 1150-1152.

(60) Canadell, J.; Goossens, H.; Klumperman, B. Self-healing materials based on disulfide links. *Macromolecules* **2011**, *44*, 2536-2541.

(61) Lafont, U.; Van Zeijl, H.; Van Der Zwaag, S. Influence of cross-linkers on the cohesive and adhesive self-healing ability of polysulfide-based thermosets. *ACS Applied Materials and Interfaces* **2012**, *4*, 6280-6288.

(62) Yoon, J. A.; Kamada, J.; Koynov, K.; Mohin, J.; Nicolaÿ, R.; Zhang, Y.; Balazs, A. C.; Kowalewski, T.; Matyjaszewski, K. Self-healing polymer films based on thiol-disulfide exchange reactions and self-healing kinetics measured using atomic force microscopy. *Macromolecules* **2012**, *45*, 142-149.

(63) Pepels, M.; Filot, I.; Klumperman, B.; Goossens, H. Self-healing systems based on disulfide-thiol exchange reactions. *Polym. Chem.* **2013**, *4*, 4955-4965.

(64) Abdolahzadeh, M.; C. Esteves, A. C.; Van Der Zwaag, S.; Garcia, S. J. Healable dual organic-inorganic crosslinked sol-gel based polymers: Crosslinking density and tetrasulfide content effect. *Journal of Polymer Science, Part A: Polymer Chemistry* **2014**, *52*, 1953-1961.

(65) Lei, Z. Q.; Xiang, H. P.; Yuan, Y. J.; Rong, M. Z.; Zhang, M. Q. Room-temperature self-healable and remoldable cross-linked polymer based on the dynamic exchange of disulfide bonds. *Chem. Mater.* **2014**, *26*, 2038-2046.

(66) Barcan, G. A.; Zhang, X.; Waymouth, R. M. Structurally dynamic hydrogels derived from 1,2-dithiolanes. *Journal of the American Chemical Society* **2015**, *137*, 5650-5653.

(67) Van Gemert, G. M. L.; Peeters, J. W.; Söntjens, S. H. M.; Janssen, H. M.; Bosman, A. W. Self-healing supramolecular polymers in action. *Macromolecular Chemistry and Physics* **2012**, *213*, 234-242.

(68) Herbst, F.; Schröter, K.; Gunkel, I.; Gröger, S.; Thurn-Albrecht, T.; Balbach, J.; Binder, W. H. Aggregation and chain dynamics in supramolecular polymers by dynamic rheology: Cluster formation and self-Aggregation. *Macromolecules* **2010**, *43*, 10006-10016.

(69) Cordier, P.; Tournilhac, F.; Soulié-Ziakovic, C.; Leibler, L. Self-healing and thermoreversible rubber from supramolecular assembly. *Nature* **2008**, *451*, 977-980.

(70) Wilson, G. O.; Caruso, M. M.; Schelkopf, S. R.; Sottos, N. R.; White, S. R.; Moore, J. S. Adhesion promotion via noncovalent interactions in self-healing polymers. *ACS Applied Materials and Interfaces* **2011**, *3*, 3072-3077.

(71) Phadke, A.; Zhang, C.; Arman, B.; Hsu, C. C.; Mashelkar, R. A.; Lele, A. K.; Tauber, M. J.; Arya, G.; Varghese, S. Rapid self-healing hydrogels. *Proceedings of the National Academy of Sciences of the United States of America* **2012**, *109*, 4383-4388.

(72) Zhong, M.; Liu, Y.-T.; Xie, X.-M. Self-healable, super tough graphene oxide-poly(acrylic acid) nanocomposite hydrogels facilitated by dual cross-linking effects through dynamic ionic interactions. *Journal of Materials Chemistry B* **2015**, *3*, 4001-4008.

(73) Yang, X.; Yu, H.; Wang, L.; Tong, R.; Akram, M.; Chen, Y.; Zhai, X. Self-healing polymer materials constructed by macrocycle-based host-guest interactions. *Soft Matter* **2015**, *11*, 1242-1252.

(74) Dröge, W. Free radicals in the physiological control of cell function. *Physiological Reviews* **2002**, *82*, 47-95.

(75) Halliwell, B.; Whiteman, M. Measuring reactive species and oxidative damage in vivo and in cell culture: How should you do it and what do the results mean? *British Journal of Pharmacology* **2004**, *142*, 231-255.

(76) Valko, M.; Leibfritz, D.; Moncol, J.; Cronin, M. T. D.; Mazur, M.; Telser, J. Free radicals and antioxidants in normal physiological functions and human disease. *International Journal of Biochemistry and Cell Biology* **2007**, *39*, 44-84.

(77) Braunecker, W. A.; Matyjaszewski, K. Controlled/living radical polymerization: Features, developments, and perspectives. *Progress in Polymer Science (Oxford)* **2007**, *32*, 93-146.

(78) Hayashi, T.; Maeda, K. Preparation of a new phototropic substance. *Bull. Chem. Soc. Jpn.* **1960**, *33*.

(79) Monroe, B. M.; Weed, G. C. Photoinitiators for Free-Radical-Initiated Photoimaging Systems. *Chemical Reviews* **1993**, *93*, 435-448.

(80) Shi, Y.; Yin, J.; Kaji, M.; Yori, H. Synthesis of a novel hexaarylbiimidazole with ether groups and characterization of its photoinitiation properties for acrylate derivatives. *Polymer Engineering and Science* **2006**, *46*, 474-479.

(81) Caspar, J. V.; Khudyakov, I. V.; Turro, N. J.; Weed, G. C. ESR Study of Lophyl Free Radicals in Dry Films. *Macromolecules* **1995**, *28*, 636-641.

(82) Berdzinski, S.; Horst, J.; Straßburg, P.; Strehmel, V. Recombination of lophyl radicals in pyrrolidinium-based ionic liquids. *ChemPhysChem* **2013**, *14*, 1899-1908.

(83) Kawano, M.; Sano, T.; Abe, J.; Ohashi, Y. The first in situ direct observation of the light-induced radical pair from a hexaarylbiimidazolyl derivative by x-ray crystallography [2]. *Journal of the American Chemical Society* **1999**, *121*, 8106-8107.

(84) Berdzinski, S.; Strehmel, N.; Lindauer, H.; Strehmel, V.; Strehmel, B. Extended mechanistic aspects on photoinitiated polymerization of 1,6-hexanediol diacrylate by hexaarylbisimidazoles and heterocyclic mercapto compounds. *Photochemical and Photobiological Sciences* **2014**, *13*, 789-798.

(85) Shi, Y.; Yin, J.; Kaji, M.; Yori, H. Photopolymerization of acrylate derivatives initiated by hexaarylbiimidazole with ether groups. *Polymer International* **2006**, *55*, 330-339.

(86) Kikuchi, A.; Iyoda, T.; Abe, J. Electronic structure of light-induced lophyl radical derived from a novel hexaarylbiimidazole with π-conjugated chromophore. *Chemical Communications* **2002**, 1484-1485.

(87) Kishimoto, Y.; Abe, J. A fast photochromic molecule that colors only under UV light. *Journal of the American Chemical Society* **2009**, *131*, 4227-4229.

(88) Iwamura, T.; Sakaguchi, M. A novel de-cross-linking system from cross-linked polymer to linear polymer utilizing pressure or visible light irradiation. *Macromolecules* **2008**, *41*, 8995-8999.

(89) Iwamura, T.; Nakamura, S. Synthesis and properties of de-cross-linkable acrylate polymers based on hexaarylbiimidazole. *Polymer (United Kingdom)* **2013**, *54*, 4161-4170.

Chapter 2

Hexaarylbiimidazoles as visible light thiol–ene photoinitiators

2.1 Abstract

The aim of this study is to determine if hexaarylbiimidazoles (HABIs) are efficient, visible light-active photoinitiators for thiol–ene systems. I hypothesize that, owing to the reactivity of lophyl radicals with thiols and the necessarily high concentration of thiol in thiol–ene formulations, HABIs will efficiently initiate thiol–ene polymerization upon visible light irradiation. UV-vis absorption spectra of photoinitiator solutions were obtained using UV-vis spectroscopy, while EPR spectroscopy was used to confirm radical species generation upon HABI photolysis. Functional group conversion during photopolymerization were monitored using FTIR spectroscopy, and thermomechanical properties were determined using dynamic mechanical analysis.

As a result, the HABI derivatives investigated exhibit less absorptivity than camphorquinone at 469 nm; however, they afford increased sensitivity at this wavelength when compared with bis(2,4,6-trimethylbenzoyl)-phenylphosphineoxide. Photolysis of the investigated HABIs affords lophyl radicals. Affixing hydroxyhexyl functional groups to the HABI core significantly improved solubility. Thiol–ene resins formulated with HABI photoinitiators polymerized rapidly upon irradiation with 469 nm. The glass transition temperatures of the thiol–ene resin formulated with a bis(hydroxyhexyl)-functionalized HABI and photopolymerized at room and body temperature were

49.5±0.5°C and 52.2±0.1°C, respectively, values that increased to 82.0±0.2°C and 81.0±0.1°C, respectively, upon a second temperature ramp.

Although thiol–enes show promise as the continuous polymeric phase for composite dental restorative materials, they show poor reactivity with the conventional camphorquinone/tertiary amine photoinitiation system. Conversely, despite their relatively low visible light absorptivity, HABI photoinitiators afford rapid thiol–ene photopolymerization rates. Moreover, minor structural modifications suggest facile pathways for improved HABI solubility and visible light absorption.

2.2 Introduction

Resin formulations primarily composed of dimethacrylate-based monomers, including bisphenol A diglycidyl ether dimethacrylate (bisGMA), triethyleneglycol dimethacrylate (TEGDMA), and urethane dimethacrylate (UDMA), have been commonly utilized as the continuous polymeric phase in composite dental restorative materials for several decades.[1,2] The long-standing success of these materials is attributable to several factors, including their high modulus and glass transition temperature upon polymerization, and adequate hydrophobicity and concomitant low water sorption. Unfortunately, the radical-mediated polymerization of these dimethacrylates is strongly inhibited by oxygen,[3,4] yielding tacky surfaces owing to incomplete surface polymerization. Additionally, as the molecular weight evolution of these polymerizations proceeds *via* chain-growth,[5,6] large amounts of unreacted, extractable monomer often remain after polymerization has ceased, potentially leading to acute toxicity or sensitization.[7,8] Moreover, as this chain-growth mechanism yields a low gel point

conversion, frustration of the shrinkage accompanying polymerization occurs early in the reaction, resulting in the development of high shrinkage stress levels in the polymerized material.[1,9,10] Attempts to mitigate high shrinkage stress, the clinical consequences of which include marginal discoloration and debonding, enamel and dentin crack formation, and secondary caries,[9,11,12] by limiting the conversion *via* the utilization of resin formulations that vitrify early during their polymerization in turn affords materials with undesirably high residual methacrylate monomer concentrations.[13,14]

In recent years, several polymerization mechanisms have emerged as potential alternatives to the prevalent dimethacrylate polymerization for composite dental restorative materials, including the cation-mediated ring-opening of oxiranes,[15,16] copper(I)-catalyzed azide–alkyne cycloadditions,[17] and radical-mediated thiol–ene additions.[13,18-20] The utilization of thiol–ene polymerizations for dental restorative materials is particularly promising owing to their potential as toxicologically safer alternatives to acrylics[13] and their unique and desirable combination of characteristics relative to other radical polymerization systems.[14,19,20] In contrast to the chain-growth mechanism typically associated with (meth)acrylate systems, thiol–ene polymerizations proceed *via* a radical-mediated step growth mechanism between multifunctional thiol and non-homopolymerizable vinyl monomers,[21] where a thiyl radical adds to a vinyl, which subsequently abstracts a hydrogen from a thiol, generating a thioether moiety and regenerating a thiyl radical (see Figure 2.1a). These thiol–ene systems demonstrate nearly all of the advantages of typical radical-mediated polymerizations in that they polymerize rapidly, do not require solvents for processing, are optically clear, and provide an excellent range of mechanical properties.[22] Additionally, owing to their step-

growth polymerization mechanism, thiol–ene polymerizations display delayed gelation, form homogeneous polymer networks with very narrow glass transitions,[13] and exhibit less shrinkage per mole of double bonds reacted (12-15 $cm^3 \cdot mol^{-1}$ for thiol–enes versus 22.5 $cm^3 \cdot mol^{-1}$ for methacrylates),[13,23] leading to reduced polymerization shrinkage stress and improved substrate adhesion. Furthermore, thiol–ene polymerizations demonstrate extraordinary resistance to oxygen inhibition,[21] attributable to facile hydrogen abstraction by peroxy radicals from the ubiquitous thiol.

Composite dental restorative materials are typically cured *via* photopolymerization where, upon placement of the restorative material at the defect site, visible light irradiation, used in preference to ultraviolet light for clinical acceptability, initiates the polymerization reaction and hardens the material *in situ*. This processing approach necessitates the incorporation of a visible light-absorbing photoinitiator in the resin formulation. The most commonly employed visible light-active photoinitiator for dimethacrylate-based formulations is camphorquinone (CQ) which, in order to afford sufficient radical-generation activity, is used in combination with a tertiary amine.[24] Thus, CQ is a 'Type II' photoinitiator (i.e., H-abstraction) where, upon photoexcitation, it abstracts a hydrogen from the tertiary amine H-donor to yield a reactive, initiating radical centered on the amine and a relatively unreactive camphorquinone-centered radical.[25] As hydrogen abstraction only proceeds while the Type II photoinitiator remains in its excited state, the lifetime of which is often short,[26] the radical generation quantum yield for these compounds can be low. In contrast, 'Type I' photointiators undergo direct homolysis upon irradiation to yield two polymerization-initiating radicals at typically high radical generation efficiencies.[26] Moreover, the necessity for Type II photoinitiators to be

formulated with a co-initiator can lead to potentially deleterious consequences such as co-initiator discoloration and toxicity.[27]

Although the CQ/tertiary amine photoinitiation system is employed extensively in dimethacrylate dental formulations, it displays poor reactivity in thiol–ene-based resins.[28,29] Conversely, direct-cleavage-type photoinitiators have been shown to efficiently initiate thiol–ene formulations upon irradiation.[13,29,30] Notably, whereas the absorbance peak of CQ is centered at approximately 470 nm,[31,32] only a very few single component photoinitiators, such as benzoyl phosphine oxides,[33] titanocenes,[34,35] and benzoyl germanes,[27] absorb well into the visible spectral region. HABIs, a class of photoinitiators first synthesized by Hayashi and Maeda in 1960,[36] are presented here as promising direct cleavage, visible light-active photoinitiators specifically for thiol–ene systems. Upon irradiation, HABIs undergo homolytic cleavage to yield two lophyl radicals (Figure 2.1b) that are unreactive with oxygen and show slow recombination rates,[37] attributable to steric hindrance and electron delocalization,[38] indeed, HABI photoinitiators show no initiation activity in (meth)acrylate formulations without the presence of a hydrogen-donating coinitiator.[39] Thiols are commonly used as coinitiators in conjunction with HABIs,[39] where hydrogen abstraction by the HABI-derived lophyl radicals yields initiating thiyl radicals (Figure 2.1b), suggesting a particular suitability for HABI photoinitiators in thiol–ene formulations. Unfortunately, commercial HABIs often exhibit poor absorption in the visible spectrum, sometimes requiring a photosensitizer, and low solubility in common resins and organic solvents.[40,41] Here, we examine the hypothesis that HABIs will effectively initiate thiol–ene polymerization upon visible light irradiation by describing the synthesis of a novel, dihydroxy-functionalized HABI with

enhanced solubility and visible light absorptivity, and investigating its utilization as a photoinitiator in thiol–ene formulations, focusing on its influence on the polymerization kinetics and thermomechanical properties of the resultant polymers.

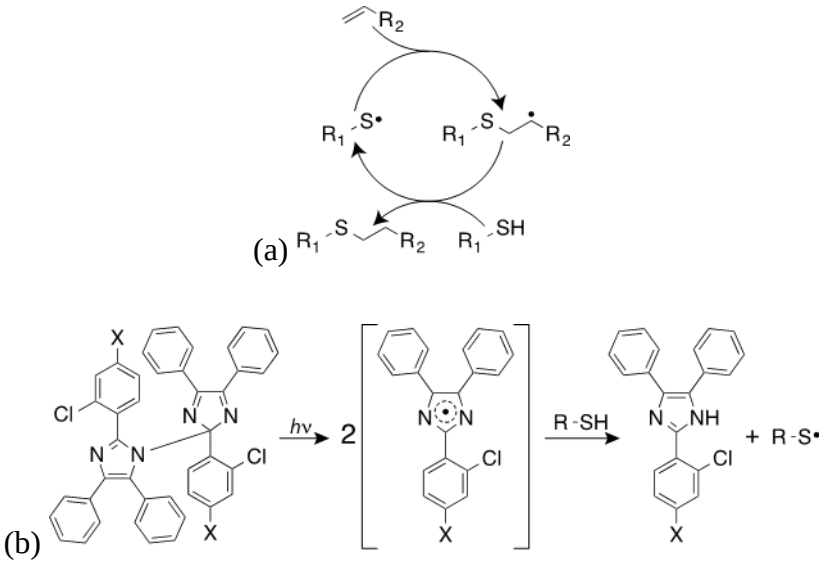

Figure 2.1. *(a) The radical-mediated thiol–ene polymerization mechanism proceeds via alternating propagation and chain transfer events, where a thiyl radical initially propagates to a vinyl group, yielding a thioether and carbon-centered radical reaction product. This radical subsequently abstracts a hydrogen from a thiol, regenerating a thiyl radical. (b) Upon irradiation, the inter-imidazole HABI bond undergoes homolytic cleavage, generating two relatively stable, long-lived lophyl radicals which then abstract a hydrogen from thiol to produce thiyl radicals.*

2.3 Experimental

2.3.1 Materials

The monomers bisphenol A bis(2-hydroxy-3-methacryloxypropyl) ether (bisGMA, Esstech Inc., Essington, PA, USA) and triethylene glycol dimethacrylate (TEGDMA, Esstech) were formulated as a mixture consisting of 70 wt% bisGMA and 30

wt% TEGDMA and used as a model dimethacrylate-based resin. The monomers pentaerythritol tetra-3-mercaptopropionate (PETMP, Evans Chemetics, Teaneck, NJ, USA) and 1,3,5,-triallyl-1,3,5-triazine-2,4,6(1H,3H,5H)-trione (TATATO, Sigma-Aldrich, St. Louis, MO, USA) were similarly formulated as a mixture, such that the thiol (i.e., mercapto) and ene (i.e., allyl) functional groups were present at a 1:1 stoichiometric ratio, and used as a model thiol–ene resin. Prior to thiol and ene component mixing, 0.01 wt% tris(*N*-nitroso-*N*-phenylhydroxylaminato)aluminum (Q1301, Wako Chemicals, Richmond, VA, USA) was added to the PETMP as a radical polymerization inhibitor to preclude premature thiol–ene polymerization. Camphorquinone (CQ, Esstech), ethyl 4-dimethylaminobenzoate (EDAB, Esstech), bis(2,4,6-trimethylbenzoyl)-phenylphosphineoxide (Irgacure 819, BASF, Florham Park, NJ, USA), 2,2′-bis(2-chlorophenyl)-4,4′,5,5′-tetraphenyl-1,2′-biimidazole (*o*-Cl-HABI, TCI America, Portland, OR, USA), and 2,2′-bis(2-chloro-4-hexan-1-ol-phenoxy)-4,4′,5,5′-tetraphenyl-1,2′-biimidazole (*p*-HOH-HABI) were used as visible light-active photoinitiating systems. CQ was used in conjunction with EDAB as a co-initiator (1 wt% CQ:0.5 wt% EDAB), whereas Irgacure 819, *o*-Cl-HABI, and *p*-HOH-HABI were used at the concentrations as indicated in the text. All commercial monomers and photoinitiators were used without further purification, the synthesis of *p*-HOH-HABI is described below, and their structures are shown in Figure 2.2. The solubility of the HABI photoinitiators was determined by addition of a photoinitiator to a liquid monomer or organic solvent (by weight ratio) and heating the combined materials in an oven (50–60°C) while mixing. Samples were then kept at room temperature for 30 minutes and, if no recrystallization occurred, the photoinitiator loading was recorded as soluble. Photoinitiator increments of

0.1 wt% or 5 wt% were employed in this study for systems where the solubility was found to be <1 wt% or >10 wt%, respectively. For example, the solubility of *o*-Cl-HABI in dimethylformamide (DMF) is <20 wt%, which means that its solubility in DMF is above 15 wt% but below 20 wt%.

2.3.2 *p*-HOH-HABI synthesis

2.3.2.1 Synthesis of 2-Chloro-4-((6-hydroxyhexyl)oxy)benzaldehyde (2).

2-Chloro-4-hydroxybenzaldehyde (10.0 g, 63.9 mmol) and potassium carbonate (26.5 g, 192 mmol) were added to 150 mL of DMF and the mixture stirred. 6-Chlorohexanol (11.1 mL, 83.0 mmol) was then added and the mixture heated at 120°C for 16 hours under nitrogen. After cooling to room temperature, the mixture was filtered to remove potassium carbonate, DMF was evaporated under reduced pressure, and the residue was carefully distilled, removing the excess 6-chlorohexanol, yielding 15.0 g of **2** (91.6% yield). ^{1}H NMR (400 MHz, DMSO-d_6), δ: 1.31-1.45 (m, 6H), 1.69-1.75 (m, 2H), 3.35-3.41 (q, 2H), 4.08-4.12 (t, 2H), 4.34-4.37 (t, 1H), 7.05-7.08 (q, 1H), 7.16-7.17 (d, 1H), 7.80-7.82 (d, 1H), 10.18 (s, 1H).

2.3.2.2 Synthesis of 6-(3-Chloro-4-(4,5-diphenyl-1H-imidazol-2-yl)phenoxy)hexyl-acetate (3).

A mixture of **2** (10.0 g, 39.0 mmol), benzil (8.19 g, 39.0 mmol), ammonium acetate (25.4 g, 330 mmol), and acetic acid (150 mL) was refluxed for 16 hours under nitrogen. After cooling to room temperature, the solvent was partially removed under

reduced pressure and poured into 10-fold water. The generated brown-yellow precipitate was filtered, washed with water, and dried. The precipitate was recrystallized in ethanol/water, yielding 11.2 g of **3** (58.7% yield). ^{1}H NMR (400 MHz, DMSO-d_6), δ: 1.35-1.47 (m, 4H), 1.57-1.63 (m, 2H), 1.71-1.78 (m, 2H), 2.00 (s, 3H), 4.00-4.02 (t, 2H), 4.04-4.08 (t, 2H), 7.03-7.05 (q, 1H), 7.15-7.16 (d, 1H), 7.22-7.23 (d, 1H), 7.24-7.32 (t, 2H), 7.35-7.36 (d, 1H), 7.40-7.43 (t, 2H), 7.47-7.49 (d, 2H), 7.52-7.54 (d, 2H), 7.68-7.70 (d, 1H), 12.49 (s, 1H).

2.3.2.3 6-(3-Chloro-4-(4,5-diphenyl-1H-imidazol-2-yl)phenoxy)hexan-1-ol) (4).

A solution of **3** (3.00 g, 6.13 mmol) in tetrahydrofuran (THF) (10 mL) was mixed with 3 M NaOH aqueous solution (100 mL) and refluxed at 75°C for 12 hours. After cooling to room temperature, solvent was partially removed under reduced pressure and extracted with dichloromethane. The organic layer was collected, washed with brine, and dried over anhydrous magnesium sulfate. The organic solvents were removed under reduced pressure to afford a yellow powder, yielding 2.50 g of **4** (91.2% yield). ^{1}H NMR (400 MHz, DMSO-d_6), δ: 1.35-1.47 (m, 4H), 1.57-1.63 (m, 2H), 1.71-1.78 (m, 2H), 4.00-4.02 (t, 2H), 4.04-4.08 (t, 2H), 7.03-7.05 (q, 1H), 7.15-7.16 (d, 1H), 7.22-7.23 (d, 1H), 7.24-7.32 (t, 2H), 7.35-7.36 (d, 1H), 7.40-7.43 (t, 2H), 7.47-7.49 (d, 2H), 7.52-7.54 (d, 2H), 7.68-7.70 (d, 1H), 12.49 (s, 1H).

2.3.2.4 2,2'-bis(2-Chloro-4-hexan-1-ol-phenoxy)-4,4',5,5'-tetraphenyl-1,2'-biimidazole (p-HOH-HABI).

To a vigorously stirred solution of potassium ferricyanide (3.29 g, 10.0 mmol) and potassium hydroxide (12.0 g, 214 mmol) in water (100 mL), a solution of **4** (1.00 g, 2.24 mmol) in dichloromethane (50 mL) was added dropwise under nitrogen. The mixture was refluxed at 45°C for 16 hours. After cooling to room temperature, the organic layer was collected, washed with water, dried over anhydrous magnesium sulfate, filtered, and the solvent removed under reduced pressure. The residue was recrystallized in diethyl ether/hexane, yielding 0.810 g of *p*-HOH-HABI (81.1% yield). ^{1}H NMR (400 MHz, DMSO-d_6), δ: 1.30-1.50 (m, 12H), 1.59-1.70 (m, 4H), 3.36-3.45 (m, 4H), 3.73-3.87 (m, 4H), 4.33-4.40 (t, 2H), 6.17-7.64 (m, 26H).

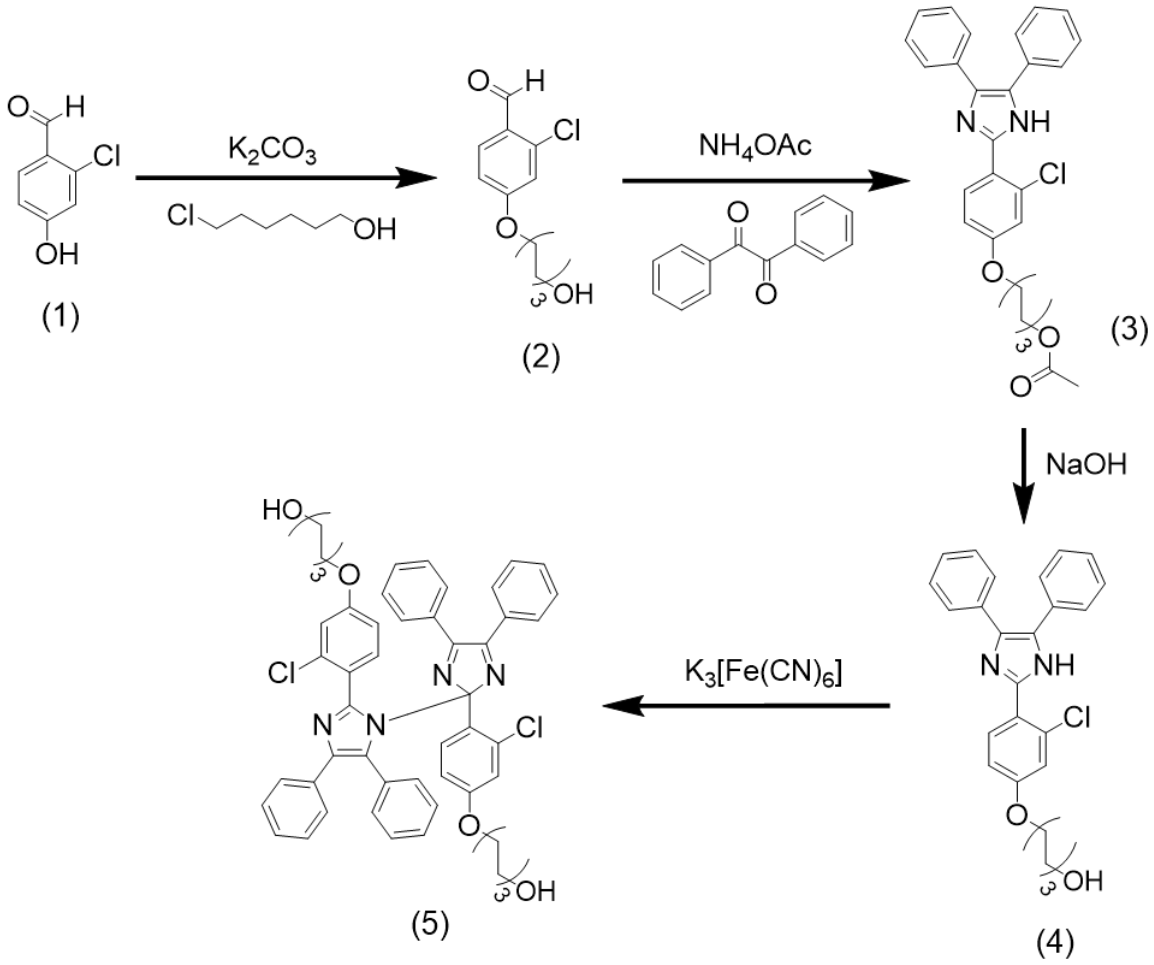

Scheme 2.1. *Synthetic route of p-HOH-HABI.*

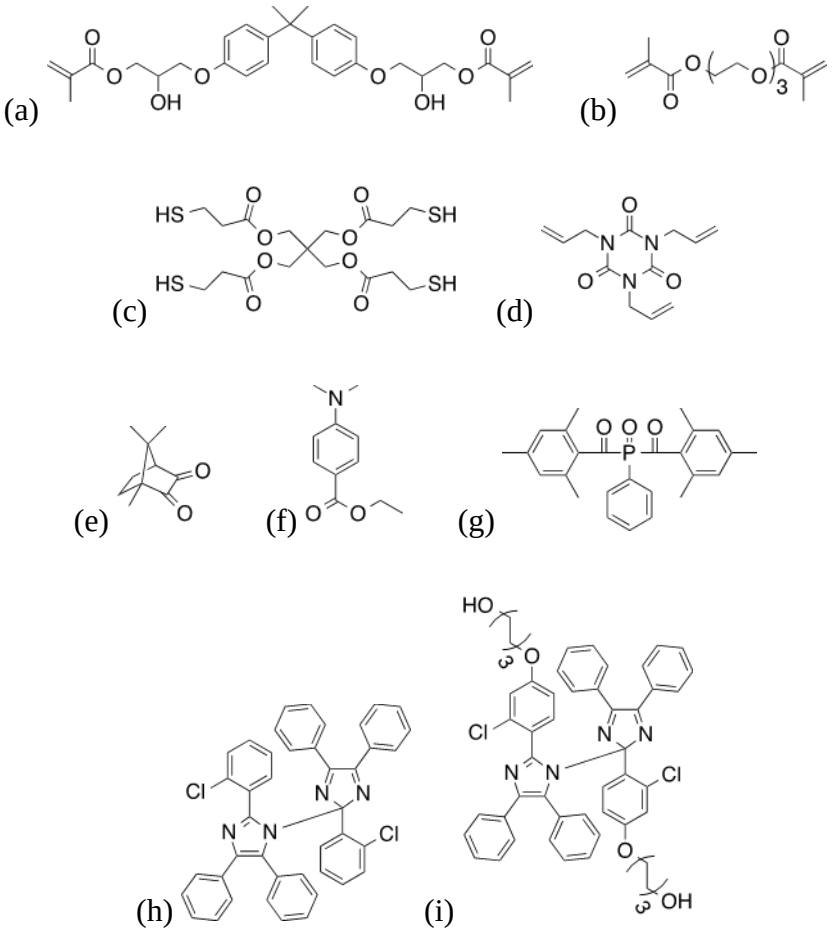

Figure 2.2. *Materials used in this study: (a) bisGMA, (b) TEGDMA, (c) PETMP, (d) TATATO, (e) CQ, (f) EDAB, (g) Irgacure 819, (h) o-Cl-HABI, and (i) p-HOH-HABI.*

2.3.3 Methods

2.3.3.1 Light source and intensity measurement

Blue light was provided by an LED-based dental lamp (G-Light, GC America) equipped with a longpass filter (435 nm cut-on wavelength) yielding a single emittance curve peak centered at 469 nm (full width at half maximum (FWHM) 29 nm), while violet light was provided by a collimated, LED-based illumination source (Thorlabs M405L2-C) with an emittance centered at 405 nm (FWHM 13 nm), used in combination with a current-adjustable LED driver (Thorlabs LEDD1B) for intensity control. UV light

was provided by a high pressure mercury vapor lamp (EXFO Acticure 4000) equipped with a filter to isolate the 365 nm spectral line (FWHM 10 nm). Irradiation intensities were measured with an International Light IL1400A radiometer equipped with a broadband silicon detector (model SEL033), a 10× attenuation neutral density filter (model QNDS1), and a quartz diffuser (model W).

2.3.3.2 UV-vis Spectrophotometry

UV-visible spectrophotometry was performed on 1 wt% samples of photoinitiator in toluene using an Agilent Technologies Cary 60 UV-Vis spectrophotometer. Spectra were collected from 200 to 800 nm on solutions using a 1 mm pathlength quartz cuvette both in the dark and under irradiation once the radical concentration reached equilibrium. HABI photodissociation and subsequent recombination was examined by monitoring 554 nm and 598 nm for *o*-Cl-HABI and *p*-HOH-HABI, respectively, the wavelengths where the visible light absorbance by the generated lophyl radicals was greatest (i.e., λ_{max}), while the sample solutions in the cuvette were irradiated with 405 nm for 9.5 minutes to ensure radical concentration equilibration, then for a further 10 minutes after the light was turned off.

2.3.3.3 EPR Spectroscopy

Electron paramagnetic resonance (EPR) spectroscopy was performed on 1 wt% samples of HABI photoinitiators in toluene using a Bruker EMX spectrometer. A TE_{102} cavity (ER4102ST, Bruker), 100 kHz modulation frequency, and 1 G_{pp} modulation

amplitude were used for all experiments. Optical access within the cavity was afforded by a 10 mm × 23 mm grid providing 50% light transmittance to the sample. All sample solutions were held in a 3.2 mm inner diameter quartz EPR sample tube which was inserted into the spectrometer cavity for analysis. The sample solutions were irradiated *in situ* with 405 nm light at 10 $mW \cdot cm^{-2}$ and spectra were collected once the radical concentration reached steady state. All experiments were performed at room temperature.

2.3.3.4 FTIR Spectroscopy

Resin formulations were introduced between glass microscope slides separated by spacers (250 μm thick for bisGMA/TEGDMA and 50 μm thick for PETMP/TATATO) to maintain constant sample thickness during polymerization. Each sample was placed in a Thermo Scientific Nicolet 6700 FTIR spectrometer equipped with a horizontal transmission accessory, as described elsewhere,[42] and spectra were collected from 2000 to 7000 cm^{-1} at a rate of 3 every 2 seconds. The functional group conversion upon irradiation was determined by monitoring the disappearance of the peak area centered at 2571 cm^{-1} corresponding to the thiol group stretch, 3083 cm^{-1} corresponding to the allylic vinyl group stretch, and 6164 cm^{-1} corresponding to the methacrylate group stretch. All experiments were performed in triplicate.

2.3.3.5 Dynamic Mechanical Analysis

Cross-linked polymer films were prepared from PETMP/TATATO formulations containing 1 wt% *p*-HOH-HABI which were polymerized between glass microscope slides separated by 250 μm thick spacers for 20 minutes at either 23°C (room temperature) or 37°C (body temperature) under 469 nm irradiation at 10 $mW \cdot cm^{-2}$. Samples of approximately 15 mm × 5 mm × 0.25 mm were cut from the cured films and mounted in a TA Instruments Q800 dynamic mechanical analyzer equipped with a film tension clamp. Experiments were performed at a strain and frequency of 0.1% and 1 Hz, respectively, scanning the temperature from −20°C to 200°C twice at $1°C \cdot min^{-1}$, and the elastic moduli (E′) and tan δ curves were recorded; the repeated temperature scan was used to determine the influence of dark polymerization at temperatures greater than the glass transition temperature (T_g). The T_g was assigned as the temperature at the tan δ curve peak.

2.4 Results

2.4.1 HABI absorbance and photolysis

The UV-vis absorption spectra presented in Figure 2.3 show the absorption by 1 wt% (a) *o*-Cl-HABI and (b) *p*-HOH-HABI in toluene (black), and the absorbance and molar absorptivity of the four photoinitiating systems examined in this study at three wavelengths tabulated in Table 2.1. Both HABIs display extended absorption tails well into the visible spectral region; however, whereas *o*-Cl-HABI displays higher absorbance at shorter wavelengths, the absorbance tail of *p*-HOH-HABI extends further into the visible and hence affords higher absorbance in the blue region of the spectrum (i.e., 469

nm). In contrast, CQ exhibits good absorptivity at 469 nm but absorbs poorly at 405 nm and 365 nm. Finally, Irgacure 819 demonstrates negligible absorbance at 469 nm but relatively strong absorbance at 405 nm and 365 nm.

Table 2.1. *Absorbance of 1 wt% photoinitiator in toluene solutions and molar absorptivities at various wavelengths.*

Absorbance of photoinitiator and molar absorptivities at various wavelengths						
Photoinitiator	λ = 469 nm		λ = 405 nm		λ = 365 nm	
	Absorbance	Molar absorptivity ($M^{-1}\cdot cm^{-1}$)	Absorbance	Molar absorptivity ($M^{-1}\cdot cm^{-1}$)	Absorbance	Molar absorptivity ($M^{-1}\cdot cm^{-1}$)
CQ/Amine	0.268	51.4	0.035	6.80	0.011	2.05
Irgacure 819	0.003	1.39	1.44	696	2.07	1002
o-Cl-HABI	0.007	5.69	0.287	219	0.494	376
p-HOH-HABI	0.014	14.7	0.096	99.0	0.390	401

The solubilities of *o*-Cl-HABI and *p*-HOH-HABI in the triallyl monomer TATATO and two common, polar organic solvents are tabulated in Table 2.2. Although *o*-Cl-HABI is reasonably soluble in the solvents examined, it exhibits limited solubility in the allylic monomer. Conversely, p-HOH-HABI is freely soluble in the monomer and both solvents.

Table 2.2. Solubility of HABI photoinitiators in monomer and polar organic solvents.

Solubility of HABI photoinitiators in monomer and polar organic solvents.			
Photoinitiator	Solvent		
	TATATO	Dimethylformamide	Tetrahydrofuran
o-Cl-HABI	<0.2 wt%	<20 wt%	<40 wt%
p-HOH-HABI	<35 wt%	<40 wt%	<65 wt%

The absorption spectra of 1 wt% *o*-Cl-HABI and *p*-HOH-HABI in toluene under irradiation with 405 nm (red) are also presented in Figure 2.3a and 3b. During irradiation, these photoinitiator solutions turn indigo, absorbing strongly throughout the visible spectrum with absorbance peaks at 554 and 598 nm for *o*-Cl-HABI and *p*-HOH-HABI, respectively. EPR spectra (Figure 2.3a and 3b, inset) indicate an absence of radicals in the as-formulated HABI solutions but confirm significant radical formation upon irradiation, establishing the indigo color generation as attributable to HABI-derived lophyl radical formation (see Figure 2.1b).[37,43] As shown in Figure 2.4, the photo-generated lophyl radicals are uncommonly stable in the absence of hydrogen abstraction source where the HABI photolysis is completely reversible and lophyl radical recombination proceeds over several minutes.

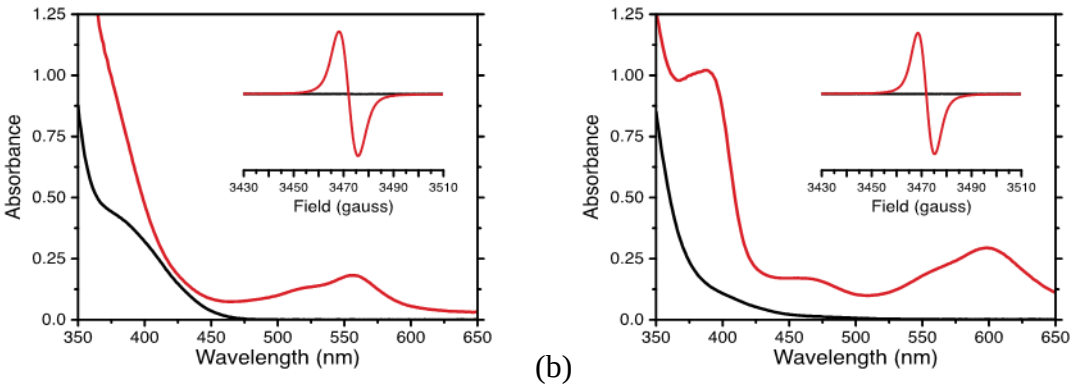

Figure 2.3. *UV-vis absorbance spectra and EPR spectra (inset) for (a) o-Cl-HABI and (b) p-HOH-HABI prior to (black) and during (red) irradiation with 405 nm at 10 mW·cm^{-2}.*

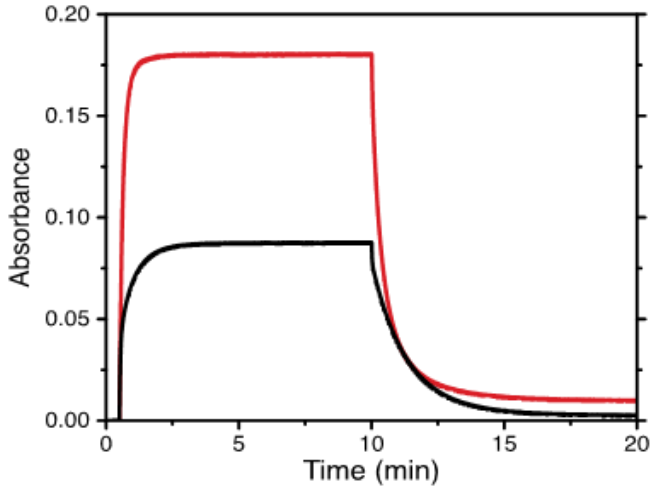

Figure 2.4. *Absorbance at λ_{max} versus time for o-Cl-HABI (black) and p-HOH-HABI (red), irradiated with 405 nm at 1 mW·cm^{-2} from 0.5 – 10 minutes.*

2.4.2 Photopolymerization kinetics – Influence of photoinitiator

BisGMA/TEGDMA formulations were prepared with four different photoinitiation systems – CQ/EDAB, Irgacure 819, *o*-Cl-HABI and *p*-HOH-HABI – at 1 wt% and their photopolymerization kinetics were examined using FTIR spectroscopy

(see Figure 2.5). The photopolymerization of these dimethacrylate-based resins was initiated upon exposure to blue light at 469 nm, a wavelength commonly emitted by contemporary LED dental curing units,[44,45] and matching the CQ visible absorbance peak,[31,32] and at several irradiation intensities. Increased incident irradiation intensities afforded correspondingly faster methacrylate polymerization rates and, after the 4 minute irradiation period, raised methacrylate conversions (Figure 2.5a). A short polymerization induction period upon irradiation was observed for all CQ/EDAB-containing methacrylate formulations, monotonically decreasing from 12 seconds to 2 seconds with raised intensity from 1 $mW \cdot cm^{-2}$ to 20 $mW \cdot cm^{-2}$. Conversely, methacrylate polymerization only proceeded upon irradiation of the bisGMA/TEGDMA formulated with Irgacure 819 at the highest intensity (i.e., 20 $mW \cdot cm^{-2}$) after a 1.5 minute induction period (see Figure 2.5b), and the resultant polymerization rate was markedly slower than that for the CQ/EDAB-formulated system under 1 $mW \cdot cm^{-2}$ irradiation. The bisGMA/TEGDMA formulation containing HABI photoinitiators did not exhibit observable polymerization under any of the applied irradiation conditions.

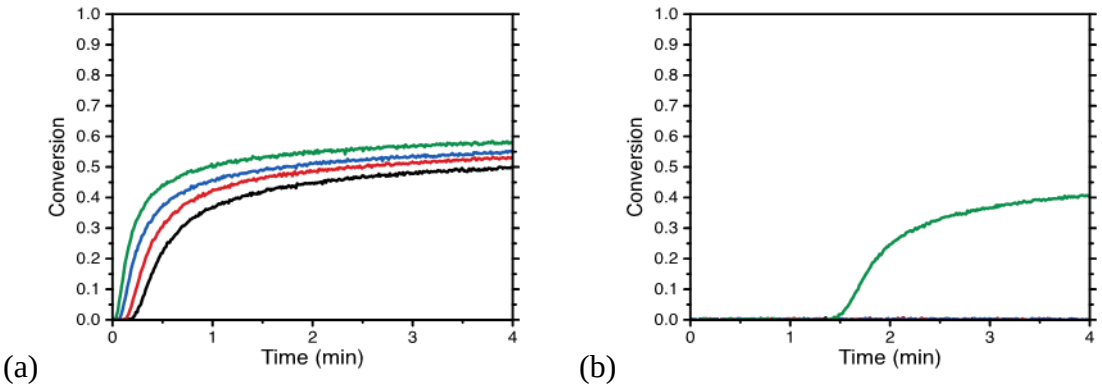

Figure 2.5. *Conversion versus time for the photopolymerization of bisGMA/TEGDMA irradiated with 469 nm light at intensities of 1 (black), 3 (red), 10 (blue), and 20 (green) mW·cm^{-2} and formulated with 1 wt% (a) CQ/EDAB and (b) Irgacure 819. No photopolymerization was observed for bisGMA/TEGDMA formulations containing 1 wt% o-Cl-HABI or p-HOH-HABI under these irradiation conditions.*

PETMP/TATATO formulations were similarly prepared with each photoinitiator at 1 wt% and their photopolymerization kinetics when exposed to 469 nm light were examined using FTIR spectroscopy (Figure 2.6). All of the examined formulations displayed increased thiol–ene polymerization rates as the incident irradiation intensity was raised. Moreover, although the resins were formulated with an initial 1:1 thiol to allyl functional group stoichiometry, allyl consumption consistently proceeded faster than that of thiol; this allyl and thiol conversion deviation increased throughout the polymerization. Additionally, no distinct polymerization induction period was observed for any system even at the lowest irradiation intensity. The photopolymerization rates for CQ/EDAB- and Irgacure 819-containing formulations were similar, both yielding allyl and thiol conversions of 50% and 44%, respectively, after 4 minutes of irradiation at an intensity of 20 mW·cm^{-2} (Figure 2.6a and 6b). In contrast, the HABI-containing thiol–ene formulations displayed markedly faster photopolymerization rates than either the

CQ/EDAB- or Irgacure 819-containing formulations, with the *p*-HOH-HABI affording approximately twice the polymerization rate of the *o*-Cl-HABI system. After 4 minutes of irradiation at 20 $mW \cdot cm^{-2}$, the *o*-Cl-HABI-containing formulation yielded allyl and thiol conversions of 76.4±0.8% and 70.7±0.9%, respectively (Figure 2.6c), while the *p*-HOH-HABI-containing formulation yielded allyl and thiol conversions of 81.3±0.8% and 74.5±0.3%, respectively (Figure 2.6d). Furthermore, whereas the maximum polymerization rate (R_{p_max}) for the Irgacure 819-containing formulation occurs at the onset of polymerization, R_{p_max} occurs at 21.0±0.6% and 41.8±0.4% for the CQ/EDAB- and both HABI-containing formulations, respectively, irrespective of the incident irradiation intensity (Figure 2.6c and 6d).

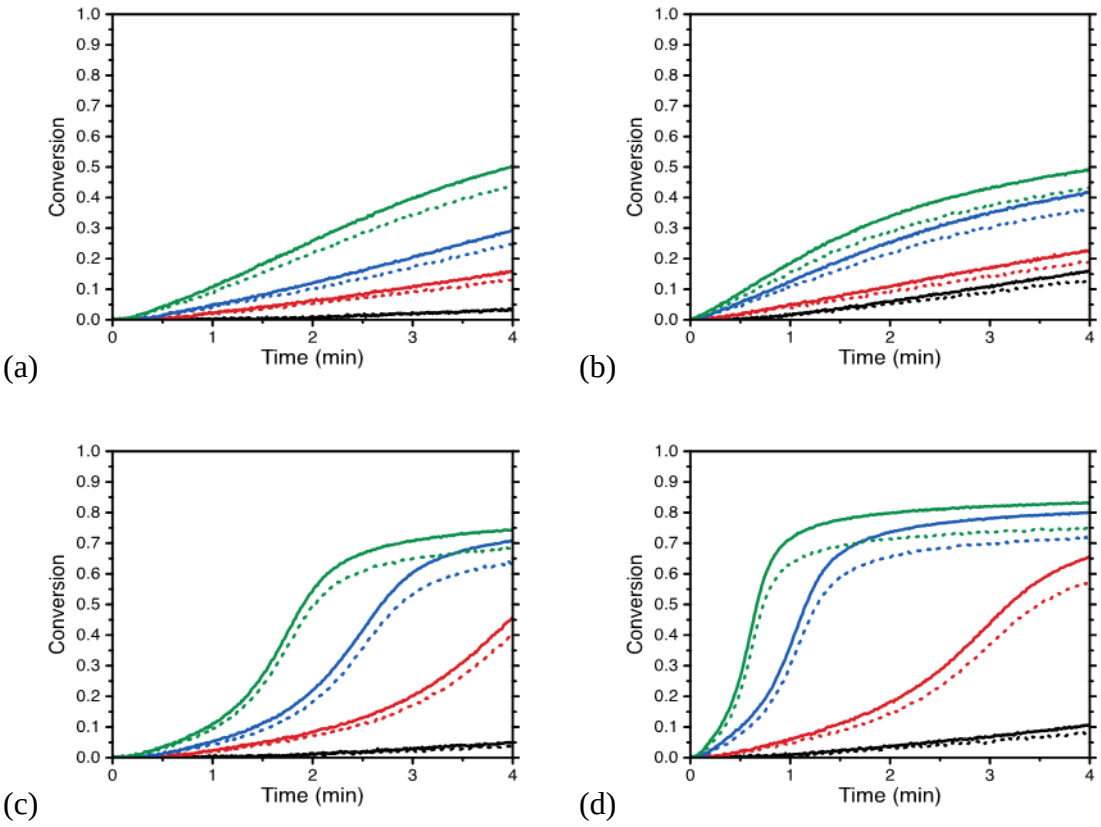

Figure 2.6. *Conversion versus time for the photopolymerization of PETMP/TATATO irradiated with 469 nm light at intensities of 1 (black), 3 (red), 10 (blue), and 20 (green) mW·cm^{-2} and formulated with 1 wt% (a) CQ/EDAB, (b) Irgacure 819, (c) o-Cl-HABI, and (d) p-HOH-HABI. Vinyl conversions are indicated by solid lines, whereas thiol conversions are indicated by dashed lines.*

To ascertain the ultimate conversions of both bisGMA/TEGDMA and PETMP/TATATO upon vitrification for isothermal photopolymerizations at room temperature, the conversion trajectories of resins formulated with 1 wt% photoinitiator were monitored during irradiation with 469 nm light at 10 mW·cm^{-2} for extended periods, as presented in Figure 2.7. Photopolymerization of the methacrylate-based resin formulated with CQ/EDAB proceeded rapidly and vitrified at 61.9±1.1% conversion while, under the same irradiation conditions, the Irgacure 819-containing methacrylate

formulation exhibited a long, ~12 minute induction period prior to polymerization and did not approach vitrification after over 19 minutes of irradiation, having attained only attained 33% conversion (single run) after the elapsed irradiation time (Figure 2.7a). Notably, neither HABI-containing methacrylate formulation demonstrated any observable photopolymerization, even over this extended irradiation. In contrast, photopolymerization proceeded upon irradiation with no observable induction period for all examined PETMP/TATATO formulations (Figure 2.7b). Although the conversion for the CQ/EDAB- and Irgacure 819-containing formulations was still increasing after 20 minutes of irradiation, the *p*-HOH-HABI-containing thiol–ene formulation had vitrified with allyl and thiol conversions of 83.7±1.2% and 76.1±0.7%, respectively, while the *o*-Cl-HABI-containing thiol–ene resin had slightly lower allyl and thiol conversions of 82.6±0.1% and 74.5±0.3%, respectively, after 20 minutes irradiation.

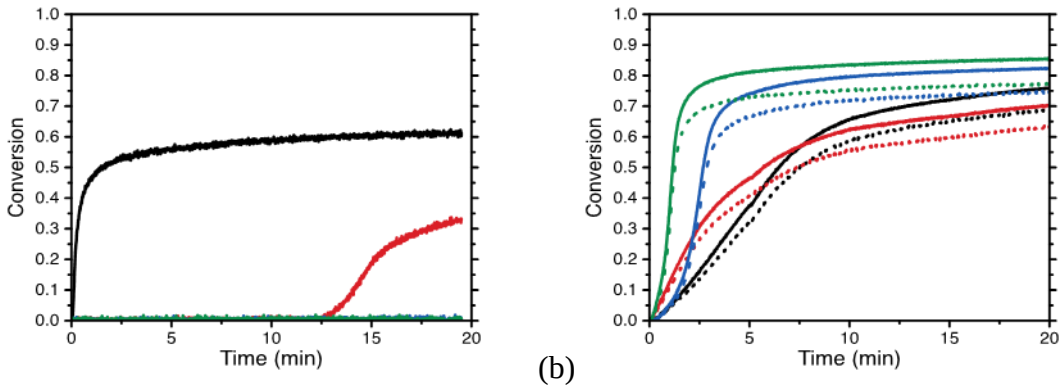

(a) (b)

Figure 2.7. *Conversion versus time for the photopolymerization of (a) bisGMA/TEGDMA, and (b) PETMP/TATATO, formulated with 1 wt% CQ/EDAB (black), Irgacure 819 (red), o-Cl-HABI (blue), and p-HOH-HABI (green) and irradiated with 469 nm light at 10 mW·cm^{-2}. Vinyl conversions are indicated by solid lines, whereas thiol conversions are indicated by dashed lines.*

2.4.3 Photopolymerization kinetics – Influence of irradiation wavelength

As contemporary dental lamps can emit a variety of wavelengths,[45-47] the influence of the incident irradiation wavelength on photopolymerization kinetics was examined by subjecting the methacrylate systems to three different irradiation wavelengths, including 469 nm (blue), 405 nm (violet), and 365 nm (near UV), at an intensity of 1 $mW \cdot cm^{-2}$. For the CQ/EDAB-containing bisGMA/TEGDMA formulation, the induction time increased and photopolymerization rate decreased for progressively shorter incident irradiation wavelengths, whereas the Irgacure 819-containing methacrylate resin did not polymerize after 4 minutes of 469 nm irradiation but exhibited very similar induction times and polymerization rates under 405 and 365 nm irradiation (Figure 2.8a and 8b). Again, no conversion was observed for either HABI-containing methacrylate resin.

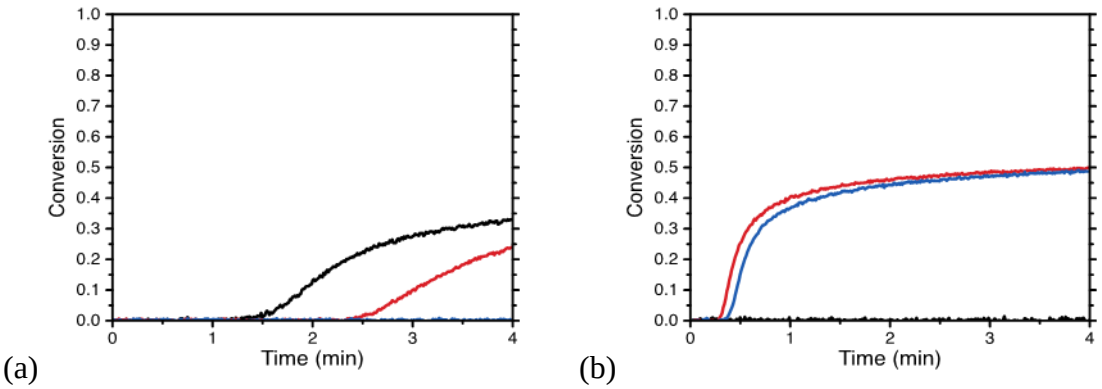

(a) (b)

Figure 2.8. *Conversion versus time for the photopolymerization of bisGMA/TEGDMA irradiated at 1 $mW \cdot cm^{-2}$ with 469 (black), 405 (red), and 365 (blue) nm light and formulated with 0.1 wt% (a) CQ/EDAB and (b) Irgacure 819. No photopolymerization was observed for bisGMA/TEGDMA formulations containing 0.1 wt% o-Cl-HABI or p-HOH-HABI under these irradiation conditions.*

Equivalent experiments examining the irradiation wavelength on PETMP/TATATO photopolymerization were also performed. For the CQ/EDAB-containing thiol–ene formulation, the photopolymerization rate was very low, yielding conversions of <3% after 4 minutes irradiation, irrespective of wavelength. In contrast, although the Irgacure 819-containing resin also polymerized very slowly under 469 nm irradiation, 405 nm and 365 nm irradiation both afforded rapid thiol–ene photopolymerization with that photoinitiator at near-identical rates throughout the 4 minute irradiation period. HABI-containing PETMP/TATATO resins similarly exhibited very low photopolymerization rates under these reaction conditions at 469 nm irradiation; however, thiol–ene polymerization proceeded rapidly under 405 nm and even more rapidly under 365 nm irradiation for both HABI photoinitiators. Notably, the thiol–ene resin formulated with *o*-Cl-HABI polymerized more rapidly that that formulated with *p*-HOH-HABI at both 405 and 365 nm. Nevertheless, the *p*-HOH-HABI-containing thiol–ene resin achieved allyl and thiol conversions of 81.9±0.5% and 74.4±0.9% after 4 minutes irradiation at 365 nm, slightly higher than the equivalent *o*-Cl-HABI system that attained allyl and thiol conversions of 79.6±0.4% and 71.7±0.2%, respectively, under the same irradiation conditions.

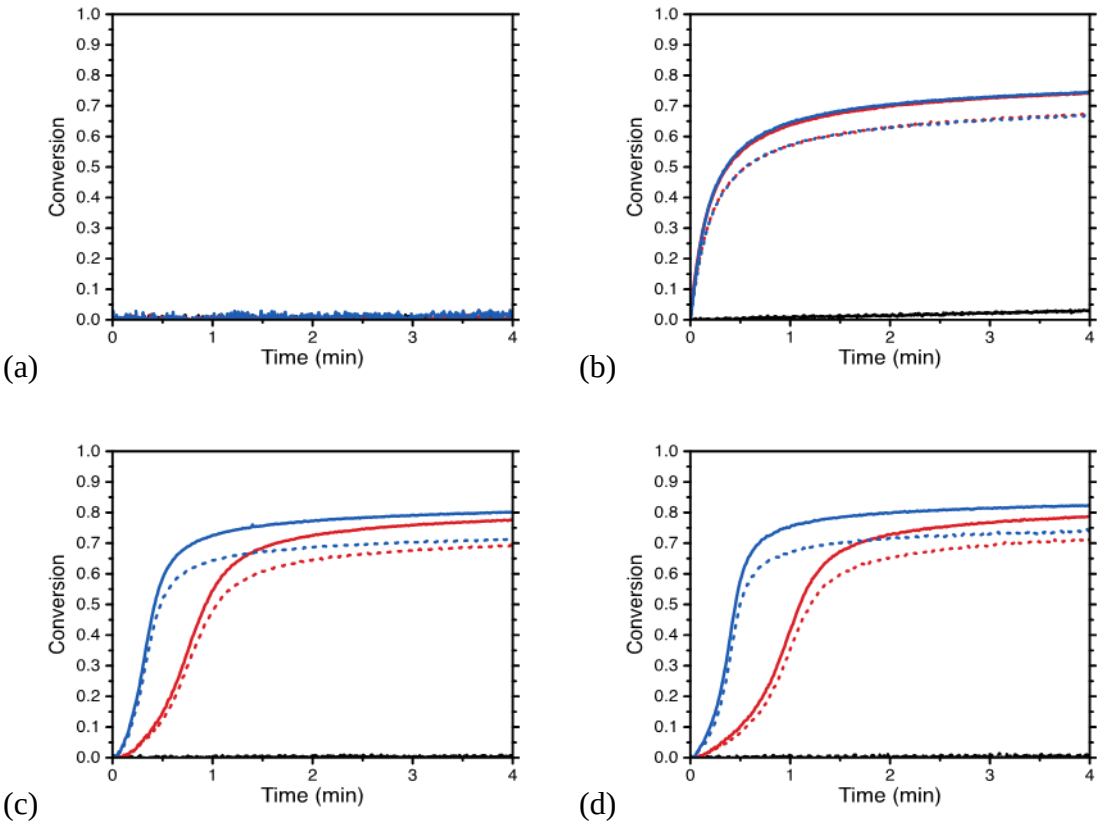

Figure 2.9. *Conversion versus time for the photopolymerization of PETMP/TATATO irradiated at 1 mW·cm^{-2} with 469 (black), 405 (red), and 365 (blue) nm light and formulated with 0.1 wt% (a) CQ/EDAB, (b) Irgacure 819, (c) o-Cl-HABI, and (d) p-HOH-HABI. Vinyl conversions are indicated by solid lines, whereas thiol conversions are indicated by dashed lines.*

2.4.4 Viscoelastic properties of cured films

The viscoelastic properties of photopolymerized bisGMA/TEGDMA and PETMP/TATATO films, formulated with 1 wt% CQ/0.5 wt% TDAB and 1 wt% *p*-HOH-HABI, respectively, and irradiated for 20 minutes with 469 nm at 10 mW·cm^{-2} and at 23°C and 37°C, were examined using DMA (see Figure 2.10, summary of results tabulated in Table 2.3). The bisGMA/TEGDMA samples attained methacrylate conversions of 60.3±0.8% and 68.6±0.7% when photopolymerized at 23°C and 37°C,

respectively; however, after the first temperature ramp in the DMA, the methacrylate conversions increased to 85.3±0.5% and 87.3±0.4% for the samples initially photopolymerized at 23°C and 37°C, respectively. The TATATO/PETMP samples attained allyl and thiol conversions of 85.4±0.6% and 77.5±0.5%, respectively, when photopolymerized at 23°C, and allyl and thiol conversions of 86.1±0.5% and 81.4±0.5%, respectively, when photopolymerized at 37°C. After the first DMA temperature ramp, the allyl and thiol conversions increased to 99.1±0.2% and 93.7±0.3%, respectively, for the TATATO/PETMP samples initially photopolymerized at 23°C, while the allyl and thiol conversions increased to 99.6±0.1% and 94.3±0.2%, respectively, for the samples initially photopolymerized at 37°C. The FWHM of the second DMA temperature ramp tan δ curve peaks for the bisGMA/TEGDMA samples initially photopolymerized at 23°C and 37°C (Figure 2.10b) were 75.2±0.5°C and 76.7±0.5°C, respectively. Conversely, the FWHM of the second DMA temperature ramp tan δ curve peaks for the PETMP/TATATO samples initially photopolymerized at 23°C and 37°C (Figure 2.10d) were 15.9±0.1°C and 15.5±0.1°C, respectively.

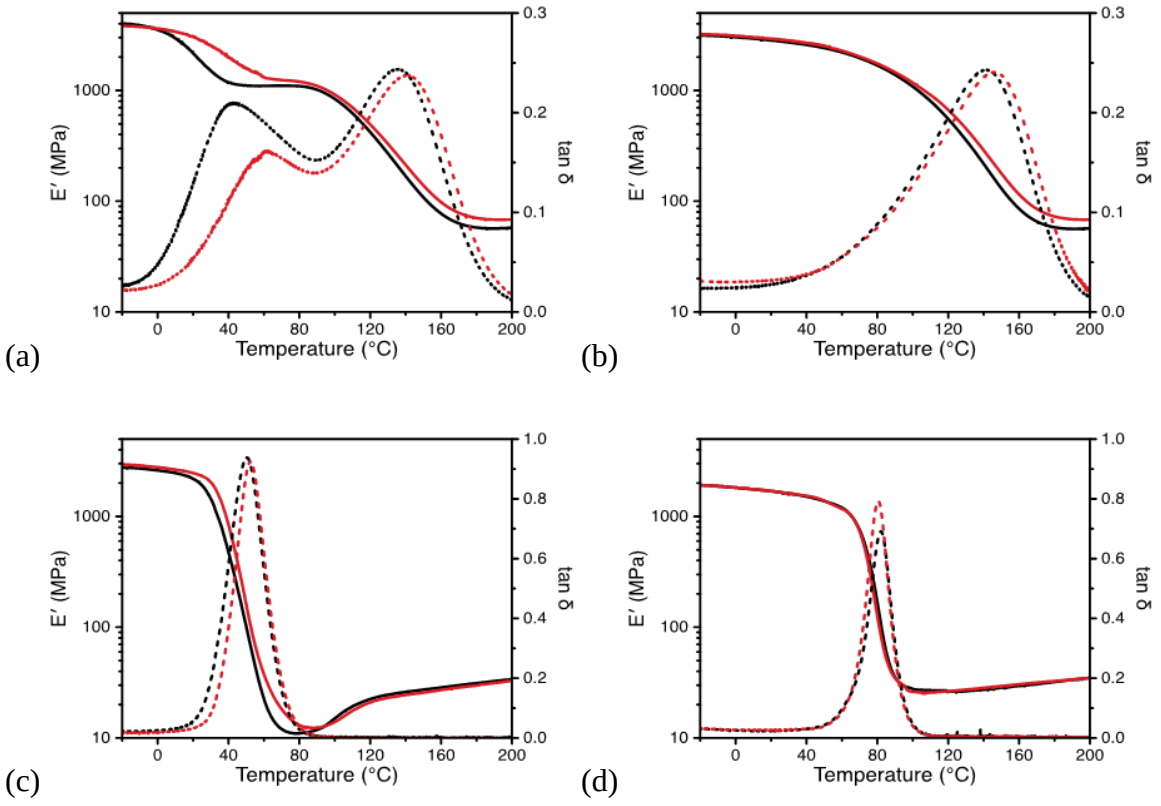

Figure 2.10. *Storage modulus (E', solid lines) and tan δ (dashed lines) versus temperature for photopolymerized films, irradiated for 20 minutes at 10 mW·cm^{-2} with 469 nm and at 23°C (black) or 37°C (red), of (a) bisGMA/TEGDMA formulated with 1 wt% CQ/0.5 wt% EDAB ((b) second temperature ramp), and (c) PETMP/TATATO formulated with 1 wt% p-HOH-HABI ((d) second temperature ramp).*

Table 2.3. *Summary of photopolymerized film viscoelastic properties.*

Summary of photopolymerized film viscoelastic properties.						
Resin formulation	Room temperature photopolymerization			Body temperature photopolymerization		
	E′ at 23°C (GPa)	E′ at 200°C (MPa)	Temp. at tan δ peak(s) (°C)	E′ at 23°C (GPa)	E′ at 200°C (MPa)	Temp. at tan δ peak(s) (°C)
BisGMA/ TEGDMA, 1st ramp	2.1±0.1	57.7 ±1.0	41.0, 138.1±2.0	3.6±0.1	80.4 ±1.0	68.5, 145.2±2.5
BisGMA/ TEGDMA, 2nd ramp	2.7±0.1	57.1 ±1.0	146.2±2.5	2.9±0.1	68.5 ±1.0	148.6±2.0
PETMP/ TATATO, 1st ramp	2.1±0.03	37.2 ±2.1	49.5±0.5	2.3±0.1	31.3 ±1.1	52.2±0.1
PETMP/ TATATO, 2nd ramp	1.7±0.1	35.0 ±0.2	82.0±0.2	1.7±0.1	35.0 ±0.1	81.0±0.1

2.5 Discussion

Composite dental restorative materials are typically photopolymerized *in situ* using visible, blue light, a wavelength range that ensures clinical acceptability. Consequently, CQ, in conjunction with a coinitiator such as a tertiary amine, is the predominant radical-generating photoinitiator for dimethacrylate-based dental resins owing to its well-known blue light absorbance peak, attributable to the $n \rightarrow \pi^*$ transition of the dicarbonyl group.[48,49] Importantly, the absorbance by a photoinitiator at the incident irradiation wavelength must be sufficient to ensure rapid polymerization rates, but not excessive which would limit polymerization depth and thus necessitate multiple, incremental restorative layers to fully address the defect. Thus, the success of CQ as a dental resin photoinitiator is attributable to its moderate absorbance at 469 nm (Table 2.1) which offers an excellent compromise between polymerization rate and cure depth. The ubiquity of CQ has resulted in most conventional halogen- and LED-based dental lamps emitting across a wavelength range tailored to match the CQ visible absorbance peak.[44,50] Thus, compatibility of novel photoinitiators with these legacy dental lamps would promote the rapid clinical adoption of alternate, non-dimethacrylate-based dental resins that are not readily photopolymerized by CQ/coinitiator systems.

HABI photoinitiators are yellow, indicating that they absorb at least somewhat in the blue region of the spectrum (see Figure 2.3). Although the HABI derivatives examined here exhibit lower absorptivity than CQ at 469 nm, a common dental lamp peak emission wavelength, they do afford higher sensitivity than Irgacure 819 (a commercially-available, benzoyl phosphine oxide-based, visible light-active, Type I photoinitiator) at this wavelength (see Table 2.1). Some recently-marketed dental lamps

also emit in the violet region of the spectrum (405 nm),[46,50] a wavelength range where Irgacure 819 and both HABI derivatives exhibit significantly increased sensitivity relative to their absorbance at 469 nm. Of course, photopolymerization initiation rates are not exclusively determined by the photoinitiator absorptivity at the incident irradiation wavelength; rather, the initiating radical quantum yield must be accounted for when determining a photoinitiator's overall efficiency. Although HABI photolysis is very efficient, with quantum yields approaching 2 (i.e., approximately two lophyl radicals generated for each absorbed photon),[39,51] the resultant lophyl radicals are uncommonly stable and do not initiate vinyl polymerizations in the absence of a hydrogen donating thiol coinitiator.[39] Importantly, the stability of the generated lophyl radicals results in sluggish recombination rates (Figure 2.4), where recombination proceeds over several minutes. Thiol–ene formulations, where thiol and vinyl functional groups are present in a 1:1 stoichiometric ratio, inherently provide high thiol concentrations for hydrogen abstraction by lophyl radicals. Thus, the generation of long-lived lophyl radicals in thiol-rich formulations should provide sufficient time for hydrogen abstraction from thiol to proceed prior to significant lophyl radical recombination, yielding highly efficient photoinitiation by HABIs in thiol–ene formulations.

Commercially-available HABI photoinitiators such as *o*-Cl-HABI generally exhibit very low blue light absorbance (Figure 2.3 and Table 2.1) and poor solubility in common resins (Table 2.2). Fortunately, the facile synthetic accessibility of HABIs enables their ready modification to induce particular properties. For example, the solubility of these typically solid materials has been dramatically increased by affixing alkyl substituents,[40,41] and the lophyl radical recombination rate has been decreased, with

a corresponding bathochromic shift in its absorption spectrum, by incorporating extended π-conjugated moieties.[52] In the present study, HABI solubility was increased by affixing flexible, hydroxyhexyl pendant groups to each triphenylimidazoyl moiety. As tabulated in Table 2, this HABI functionalization greatly increased solubility of the resultant HABI, where *p*-HOH-HABI (i.e., the bis(hydroxyhexyl)-functionalized compound) is consistently more soluble in an allyl monomer and polar organic solvents than the unfunctionalized *o*-Cl-HABI. The hydroxyhexyl HABI functionalization was also accompanied by enhanced absorptivity at 469 nm compared with *o*-Cl-HABI (Table 2.1), suggesting a potentially increased photopolymerization rate for *p*-HOH-HABI-containing thiol–ene formulations under conventional dental lamp irradiation.

To establish a benchmark against which thiol–ene photopolymerizations could be compared, the photopolymerization kinetics of methacrylate-based bisGMA/TEGDMA resins formulated with four different photoinitiation systems were examined under several irradiation intensities (Figure 2.5). As the CQ visible absorption peak occurs at approximately 470 nm,[31,32] the rapid photopolymerization observed for the methacrylate-based resin formulated with CQ/EDAB upon 469 nm irradiation is expected. As the commercially-sourced monomers were used as received, the short polymerization induction periods for this system are attributable to radical polymerization inhibitors and dissolved oxygen in the resin. Prior to the onset of polymerization, radicals generated upon irradiation rapidly react with adventitious radical inhibitors and oxygen; however polymerization proceeds immediately upon complete consumption of the inhibiting species. Raised irradiation intensities increase radical generation rates, consuming inhibiting species more quickly and hence reducing the polymerization induction time

(Figure 2.5a). Moreover, the increased radical generation rates at raised intensities afford correspondingly increased polymerization rates (Figure 2.5a). In contrast, as Irgacure 819 exhibits very low absorptivity at 469 nm, the radical generation rate upon irradiation at 469 nm of methacrylate formulations containing this photoinitiator is so low that the consumption of the inhibiting species proceeds over the course of minutes even under a high irradiation intensity. Notably, although *o*-Cl-HABI and *p*-HOH-HABI offer raised absorptivities at 469 nm compared with Irgacure 819, no polymerization was observed at all for bisGMA/TEGDMA resins formulated with these HABI photoinitiators, indicating that the lophyl radicals are inactive towards methacrylate groups.[39]

To determine the relative efficiency of HABI compounds to initiate thiol–ene polymerization upon blue light irradiation, the photopolymerization kinetics of PETMP/TATATO resins formulated with four different photoinitiator systems were similarly examined under several blue light irradiation intensities (Figure 2.6). Interestingly, no polymerization induction period was observed for any system even at low irradiation intensity and correspondingly slow polymerization rates, despite the inclusion of a potent free radical inhibitor (i.e., Q1301) in the resin formulations. This notable absence of induction period may be attributable to the well-known resistance of radical-mediated thiol–ene reaction to oxygen inhibition.[13] Additionally, whereas all PETMP/TATATO resins examined were formulated in a 1:1 thiol to allyl stoichiometric ratio, the unequal monomer consumption rates, where allyl conversion was consistently higher than thiol conversion (see Figures 2.6, 7b, and 9), is attributable to a small amount of allylic homopolymerization.[13]

With the exception of the CQ/EDAB-containing formulation, the relative thiol–ene photopolymerization rates proceed according to the absorptivities at 469 nm for the respective photoinitiators, where the *p*-HOH-HABI-containing formulation reacts most rapidly while blue light initiated photopolymerization of the Irgacure 819-containing formulation proceeds slowest (Figure 2.6). In contrast, despite relatively strong absorbance at 469 nm, the photopolymerization of CQ/EDAB-containing formulations proceeds no more rapidly than Irgacure 819-containing formulations upon blue light irradiation, confirming the poor compatibility of CQ/tertiary amine photoinitiator/coinitiator systems, used ubiquitously in conventional methacrylate-based dental resins, for thiol–ene photopolymerization.

The curves of allyl and thiol conversion versus time for the photopolymerization of both HABI-containing thiol–ene formulations followed distinctive 'S'-shaped trajectories at all examined irradiation intensities (Figures 2.6c and 6d). Similar conversion trajectories are typically associated with polymerization autoacceleration by the gel effect,[53] where the termination reaction rate rapidly drops as radical diffusion is restricted, impeding bimolecular radical-radical reactions and leading to a rise in radical concentration and concomitant increase in polymerization rate. However, as the polymerization rates are observed to increase prior to gelation, attaining their maxima near the gel point conversion (calculated using Flory-Stockmayer theory[54,55] as 40.8% conversion for an ideal tetrathiol/triallyl step growth reaction), and similar conversion trajectories are not observed for the Type I initiation provided by Irgacure 819, autoacceleration does not account for the observed characteristic conversion trajectories afforded by HABI photoinitiators in thiol–ene resins. Furthermore, for ideal free radical

polymerizations where termination is exclusively bimolecular, the polymerization rate (R_p) is anticipated to scale with the square root of the initiation rate (R_i),[30] which for photopolymerizations is proportional to the incident irradiation intensity. The conversion versus time data obtained at different intensities (i.e., Figure 2.6), scaled by R_i to an exponent, are shown in Figure 2.11. As indicated by Figure 2.11a, the classical square root dependence of R_p on R_i (i.e., $R_p \sim R_i^{0.5}$) fails to accurately describe the experimental data; rather the data are well fit by an R_i scaling exponent of 0.84, suggesting concurrent bimolecular and unimolecular termination mechanism in these polymerizations, as has been observed in other thiol–ene systems.[30] As the irradiation intensity emitted at the light guide tip of conventional dental lamps often approaches or even exceeds 1 W·cm^{-2},[45,50] high R_i scaling exponents can provide more rapid polymerization rates of dental restoratives in clinical settings.

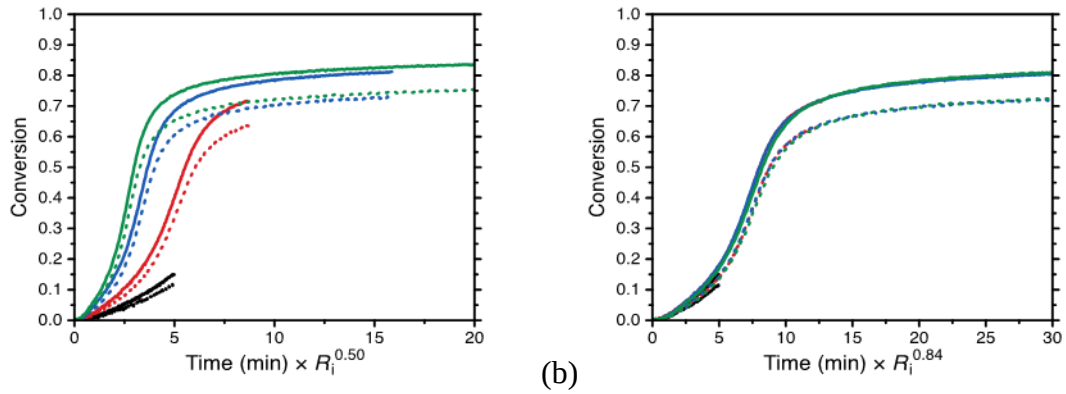

(a) (b)

Figure 2.11. *Conversion versus time, scaled assuming that (a) $R_p \sim R_i^{0.50}$, and (b) $R_p \sim R_i^{0.84}$, for the photopolymerization of PETMP/TATATO formulated with 1 wt% p-HOH-HABI and irradiated with 469 nm light at intensities of 1 (black), 3 (red), 10 (blue), and 20 (green) mW·cm^{-2}. Vinyl conversions are indicated by solid lines, whereas thiol conversions are indicated by dashed lines.*

As seen in Figure 2.7, the CQ/EDAB-containing bisGMA/TEGDMA formulation vitrifies at a relatively low conversion such that a significant amount of unreacted monomer could potentially leach out if this material were in an oral environment. In contrast, the *p*-HOH-HABI-containing PETMP/TATATO formulation, which of the thiol–ene samples reaches the highest conversion contains significantly less unreacted functional groups post-polymerization, and hence it is anticipated to contain significantly less low molecular weight, extractable material.

BisGMA/TEGDMA formulations containing CQ/EDAB and Irgacure 819, photopolymerized slowly using a light intensity of 1 $mW \cdot cm^{-2}$ and a photoinitiator concentration of 0.1 wt%, mitigating both the temperature rise owing to the exothermic polymerization and lessening light intensity gradients through the sample thicknesses at shorter wavelengths, respectively, demonstrate opposing R_p trends for progressively shorter incident irradiation wavelengths (see Figure 2.8). Here, the CQ/EDAB-containing formulation polymerizes fastest under 469 nm irradiation but exhibits negligible polymerization under 365 nm, whereas the Irgacure 819-containing formulation exhibits negligible polymerization under 469 nm irradiation but polymerizes rapidly under both 405 and 365 nm. These trends are readily explained by considering the absorptivities of the two photoinitiators at the relevant wavelengths (Table 2.1). Thus, as CQ exhibits good absorptivity at 469 nm and progressively lower absorptivity at 405 and 365 nm, the R_i for the CQ/EDAB-containing formulation will be reduced at these shorter wavelengths which is reflected in the relative R_ps. Similarly, Irgacure 819 exhibits very low absorptivity at 469 nm but good absorptivity at 405 and 365 nm, reflected in the relative polymerization rates of the Irgacure 819-containing formulations.

Notably, irradiation of the HABI-containing methacrylate formulations again did not afford any observable polymerization, even at shorter wavelengths where both HABIs offer good absorptivity (Table 2.1), confirming lophyl radical inactivity towards methacrylate functional groups.

This relation between R_p and photoinitiator absorptivity is likewise applicable to the photopolymerization of PETMP/TATATO formulations under various incident irradiation wavelengths (Figure 2.9). For the Irgacure 819-containing thiol–ene formulation, the negligible R_p under 469 nm but rapid photopolymerization at shorter wavelengths is a consequence of the relative absorptivity of this photoinitiator at the relevant wavelengths. Interestingly, the relatively more rapid thiol–ene polymerization of the *o*-Cl-HABI-containing formulation versus the *p*-HOH-HABI-containing formulation under 405 nm irradiation, again a consequence of the relative absorptivities of the two photoinitiators at this wavelength, would afford reduced cure time in a clinical setting where the dental lamp used emits violet light. However, unlike the commonplace blue light emitted by conventional dental lamps, 405 nm has yet to see widespread clinical use and thus the raised R_p for *o*-Cl-HABI at this wavelength is less relevant than the higher relative R_p for *p*-HOH-HABI under blue light irradiation. The very low R_ps afforded by irradiation of CQ/EDAB-containing PETMP/TATATO formulations again illustrates the poor compatibility of this photoinitiator system for thiol–ene photopolymerizations.

As composite dental restorative materials are polymerized *in situ* at defect sites, vitrification of the continuous resin phase as the polymerization proceeds is essential to approximate tooth mechanical properties and fully recover the utility of this hard tissue. To determine the capacity of *p*-HOH-HABI to act as a thiol–ene photoinitiator and yield

cross-linked, vitrified polymers, DMA was performed on the model *p*-HOH-HABI-containing thiol–ene and, for comparison, CQ/EDAB-containing dimethacrylate formulations. In the absence of polymerization during a DMA temperature ramp experiment, the tan δ curve peak preceding the rubbery plateau is assigned as the T_g. The two distinct tan δ peaks and corresponding storage modulus reductions displayed by the dimethacrylate films photopolymerized at both room and body temperature (Figure 2.10a) could be the result of either radicals, generated during irradiation but trapped in the vitrified matrix, gaining sufficient mobility during the temperature ramp to induce dark polymerization, or could result from a phase separated film. Notably, the significant methacrylate conversion increase observed after the first DMA experiments and the single thermal transition revealed upon second DMA temperature ramps (Figure 2.10b) discounted phase separation and confirmed the two transitions as attributable to polymerization mediated by trapped radicals; nevertheless, although this dark polymerization prevents accurate assessment of the T_g in these methacrylate-based materials, they are vitrified at room temperature with storage moduli in excess of 2 GPa (Table 2.3).

In contrast to the methacrylate-based materials, the single tan δ curve peaks exhibited by the thiol–ene films photopolymerized at room and body temperature upon a first DMA temperature ramp (Figure 2.10c) indicates that the temperature at the tan δ peak for these samples closely reflected the T_g. Thus, the T_gs for these samples of approximately 50°C, in conjunction with storage moduli in excess of 2 GPa at room temperature, demonstrates that *p*-HOH-HABI is capable of photoinitiating thiol–ene formulations to afford vitrified polymeric matrices. Interestingly, a small increase in

storage modulus towards the end of the glass transition, but prior to the rubbery plateau, is observed during the first temperature ramp of both thiol–ene samples. Given the raised allyl and thiol conversion after the first DMA temperature ramp and the absence of similar storage moduli increases during the second temperature ramp, we again attribute the observed storage moduli increases to dark polymerization. The notably narrower tan δ curve peak FWHMs, obtained from the second DMA temperature ramp experiments, for the thiol–ene films as compared to the dimethacrylate films demonstrates the homogeneity of cross-linked thiol–ene networks (Figure 2.10b and 10d), a consequence of their step-growth polymerization mechanism.[13] Finally, although the monomer conversion is raised, a significant decrease in the room temperature storage modulus for the thiol–ene films is observed after the polymer networks have been subject to the first temperature ramp (Figure 2.10c and 10d, Table 2.3); indeed, the storage moduli of the thiol–ene films are lower than those of the methacrylate-based materials, and a similar storage modulus drop is observed for the bisGMA/TEGDMA sample polymerized at body temperature after its first temperature ramp (Figure 2.10a and 10b, Table 2.3). Similar results have been previously observed in cross-linked epoxy/amine polymer networks, where the modulus passed through a maximum value with increasing fractional chemical conversion.[56] This counterintuitive effect was attributed to 'self-antiplasticization', where the unreacted functional groups can decrease the T_g but increase the modulus of certain glassy, polymeric networks.[56] Consequently, this suggests a path to yield thiol–ene polymer networks with increased moduli by employing rigid, high functionality monomers that vitrify at low conversions, thus enhancing the

antiplasticization effect; however, the associated leachability of low molecular weight species from such materials limits the potential utility of this approach.

2.6 Conclusion

Upon irradiation with UV or short wavelength visible light, HABI compounds generate lophyl radicals that are inactive towards methacrylate groups but are capable of abstracting thiol hydrogens to afford thiyl radicals. Unlike the conventional CQ/tertiary amine photoinitiator system, HABI compounds were shown to be efficient as visible- and UV-active initiators for thiol–ene photopolymerizations owing to the aforementioned thiol hydrogen abstraction mechanism. To address the shortcomings of *o*-Cl-HABI, a commercially-available HABI photoinitiator with limited solubility and low visible light absorptivity, a novel, bis(hydroxyhexyl)-functionalized HABI was successfully synthesized and demonstrated improved solubility in monomer and organic solvents, in addition to raised blue light absorbance, resulting in increased thiol–ene photopolymerization rates upon blue light irradiation. Notably, both examined HABI compounds exhibited good absorptivity and afforded rapid thiol–ene polymerization rates upon 405 nm irradiation, demonstrating their compatibility with emergent violet LED dental light sources.

The potential for *p*-HOH-HABI to act as photoinitiator of a glass-forming, thiol–ene based dental restorative was demonstrated using a model thiol–ene formulation. Extended blue light irradiation of the resin formulation yielded vitrified, cross-linked polymer matrices that were significantly more homogeneous than methacrylate based

polymer networks photopolymerized under equivalent irradiation conditions. The observed disparity in network homogeneity was attributed to the different polymerization mechanisms for the two examined systems.

2.7 References

(1) Peutzfeldt, A. Resin composites in dentistry: The monomer systems. *European Journal of Oral Sciences* **1997**, *105*, 97-116.

(2) Ferracane, J. L. Resin composite - State of the art. *Dental Materials* **2011**, *27*, 29-38.

(3) Rueggeberg, F. A.; Margeson, D. H. The Effect of Oxygen Inhibition on an Unfilled/Filled Composite System. *Journal of Dental Research* **1990**, *69*, 1652-1658.

(4) Gauthier, M. A.; Stangel, I.; Ellis, T. H.; Zhu, X. X. Oxygen inhibition in dental resins. *Journal of Dental Research* **2005**, *84*, 725-729.

(5) Cramer, N. B.; Stansbury, J. W.; Bowman, C. N. Recent advances and developments in composite dental restorative materials. *Journal of Dental Research* **2011**, *90*, 402-416.

(6) Leprince, J. G.; Palin, W. M.; Hadis, M. A.; Devaux, J.; Leloup, G. Progress in dimethacrylate-based dental composite technology and curing efficiency. *Dental Materials* **2013**, *29*, 139-156.

(7) Schweikl, H.; Schmalz, G. Triethylene glycol dimethacrylate induces large deletions in the hprt gene of V79 cells. *Mutation Research - Genetic Toxicology and Environmental Mutagenesis* **1999**, *438*, 71-78.

(8) Darmani, H.; Al-Hiyasat, A. S. The effects of BIS-GMA and TEG-DMA on female mouse fertility. *Dental Materials* **2006**, *22*, 353-358.

(9) Davidson, C. L.; Feilzer, A. J. Polymerization shrinkage and polymerization shrinkage stress in polymer-based restoratives. *Journal of Dentistry* **1997**, *25*, 435-440.

(10) Lu, H.; Stansbury, J. W.; Bowman, C. N. Towards the elucidation of shrinkage stress development and relaxation in dental composites. *Dental Materials* **2004**, *20*, 979-986.

(11) Winkler, M. M.; Katona, T. R.; Paydar, N. H. Finite element stress analysis of three filling techniques for class V light-cured composite restorations. *Journal of Dental Research* **1996**, *75*, 1477-1483.

(12) Braga, R. R.; Ballester, R. Y.; Ferracane, J. L. Factors involved in the development of polymerization shrinkage stress in resin-composites: A systematic review. *Dental Materials* **2005**, *21*, 962-970.

(13) Lu, H.; Carioscia, J. A.; Stansbury, J. W.; Bowman, C. N. Investigations of step-growth thiol-ene polymerizations for novel dental restoratives. *Dental Materials* **2005**, *21*, 1129-1136.

(14) Cramer, N. B.; Couch, C. L.; Schreck, K. M.; Boulden, J. E.; Wydra, R.; Stansbury, J. W.; Bowman, C. N. Properties of methacrylate-thiol-ene formulations as dental restorative materials. *Dental Materials* **2010**, *26*, 799-806.

(15) Weinmann, W.; Thalacker, C.; Guggenberger, R. Siloranes in dental composites. *Dental Materials* **2005**, *21*, 68-74.

(16) Palin, W. M.; Fleming, G. J. P.; Nathwani, H.; Burke, F. J. T.; Randall, R. C. In vitro cuspal deflection and microleakage of maxillary premolars restored with novel low-shrink dental composites. *Dental Materials* **2005**, *21*, 324-335.

(17) Gong, T.; Adzima, B. J.; Baker, N. H.; Bowman, C. N. Photopolymerization reactions using the photoinitiated copper (I)-catalyzed azide-alkyne cycloaddition (CuAAC) reaction. *Advanced Materials* **2013**, *25*, 2024-2028.

(18) Carioscia, J. A.; Lu, H.; Stanbury, J. W.; Bowman, C. N. Thiol-ene oligomers as dental restorative materials. *Dental Materials* **2005**, *21*, 1137-1143.

(19) Cramer, N. B.; Couch, C. L.; Schreck, K. M.; Carioscia, J. A.; Boulden, J. E.; Stansbury, J. W.; Bowman, C. N. Investigation of thiol-ene and thiol-ene-methacrylate based resins as dental restorative materials. *Dental Materials* **2010**, *26*, 21-28.

(20) Reinelt, S.; Tabatabai, M.; Moszner, N.; Fischer, U. K.; Utterodt, A.; Ritter, H. Synthesis and photopolymerization of thiol-modified triazine-based monomers and oligomers for the use in thiol-ene-based dental composites. *Macromolecular Chemistry and Physics* **2014**, *215*, 1415-1425.

(21) Hoyle, C. E.; Lee, T. Y.; Roper, T. Thiol-enes: Chemistry of the past with promise for the future. *Journal of Polymer Science, Part A: Polymer Chemistry* **2004**, *42*, 5301-5338.

(22) Hoyle, C. E.; Bowman, C. N. Thiol-Ene Click Chemistry. *Angewandte Chemie-International Edition* **2010**, *49*, 1540-1573.

(23) Patel, M. P.; Braden, M.; Davy, K. W. M. Polymerization shrinkage of methacrylate esters. *Biomaterials* **1987**, *8*, 53-56.

(24) Cook, W. D. Photopolymerization kinetics of dimethacrylates using the camphorquinone/amine initiator system. *Polymer* **1992**, *33*, 600-609.

(25) Jakubiak, J.; Allonas, X.; Fouassier, J. P.; Sionkowska, A.; Andrzejewska, E.; Linden, L. Å.; Rabek, J. F. Camphorquinone-amines photoinitating systems for the initiation of free radical polymerization. *Polymer* **2003**, *44*, 5219-5226.

(26) Fouassier, J. P.; Lalevée, J.: *Photoinitiators for Polymer Synthesis: Scope, Reactivity and Efficiency*, 2012.

(27) Moszner, N.; Fischer, U. K.; Ganster, B.; Liska, R.; Rheinberger, V. Benzoyl germanium derivatives as novel visible light photoinitiators for dental materials. *Dental Materials* **2008**, *24*, 901-907.

(28) Senyurt, A. F.; Hoyle, C. E. Three component ketocoumarin, amine, maleimide photoinitiator II. *European Polymer Journal* **2006**, *42*, 3133-3139.

(29) Uygun, M.; Tasdelen, M. A.; Yagci, Y. Influence of type of initiation on thiol-ene "click" Chemistry. *Macromolecular Chemistry and Physics* **2010**, *211*, 103-110.

(30) Scott, T. F.; Kloxin, C. J.; Draughon, R. B.; Bowman, C. N. Nonclassical dependence of polymerization rate on initiation rate observed in thiol-ene photopolymerizations. *Macromolecules* **2008**, *41*, 2987-2989.

(31) Chen, Y. C.; Ferracane, J. L.; Prahl, S. A. Quantum yield of conversion of the photoinitiator camphorquinone. *Dental Materials* **2007**, *23*, 655-664.

(32) Scott, T. F.; Kowalski, B. A.; Sullivan, A. C.; Bowman, C. N.; McLeod, R. R. Two-color single-photon photoinitiation and photoinhibition for subdiffraction photolithography. *Science* **2009**, *324*, 913-917.

(33) Kolczak, U.; Rist, G.; Dietliker, K.; Wirz, J. Reaction mechanism of monoacyl- and bisacylphosphine oxide photoinitiators studied by P-31-, C-13-, and H-1-CIDNP and ESR. *Journal of the American Chemical Society* **1996**, *118*, 6477-6489.

(34) Davidenko, N.; Garcia, O.; Sastre, R. The efficiency of titanocene as photoinitiator in the polymerization of dental formulations. *J. Biomater. Sci.-Polym. Ed.* **2003**, *14*, 733-746.

(35) Kitano, H.; Ramachandran, K.; Bowden, N. B.; Scranton, A. B. Unexpected visible-light-induced free radical photopolymerization at low light intensity and high viscosity using a titanocene photoinitiator. *Journal of Applied Polymer Science* **2013**, *128*, 611-618.

(36) Hayashi, T.; Maeda, K. Preparation of a New Phototropic Substance. *Bulletin of the Chemical Society of Japan* **1960**, *33*, 565-566.

(37) Berdzinski, S.; Horst, J.; Straßburg, P.; Strehmel, V. Recombination of lophyl radicals in pyrrolidinium-based ionic liquids. *ChemPhysChem* **2013**, *14*, 1899-1908.

(38) Kawano, M.; Sano, T.; Abe, J.; Ohashi, Y. The first in situ direct observation of the light-induced radical pair from a hexaarylbiimidazolyl derivative by X-ray crystallography. *Journal of the American Chemical Society* **1999**, *121*, 8106-8107.

(39) Berdzinski, S.; Strehmel, N.; Lindauer, H.; Strehmel, V.; Strehmel, B. Extended mechanistic aspects on photoinitiated polymerization of 1,6-hexanediol diacrylate by hexaarylbisimidazoles and heterocyclic mercapto compounds. *Photochem. Photobiol. Sci.* **2014**, *13*, 789-798.

(40) Shi, Y. T.; Yin, J.; Kaji, M.; Yori, H. Photopolymerization of acrylate derivatives initiated by hexaarylbiimidazole with ether groups. *Polym. Int.* **2006**, *55*, 330-339.

(41) Shi, Y.; Yin, J.; Kaji, M.; Yori, H. Synthesis of a novel hexaarylbiimidazole with ether groups and characterization of its photoinitiation properties for acrylate derivatives. *Polymer Engineering and Science* **2006**, *46*, 474-479.

(42) Lovell, L. G.; Berchtold, K. A.; Elliott, J. E.; Lu, H.; Bowman, C. N. Understanding the kinetics and network formation of dimethacrylate dental resins. *Polymers for Advanced Technologies* **2001**, *12*, 335-345.

(43) Caspar, J. V.; Khudyakov, I. V.; Turro, N. J.; Weed, G. C. ESR Study of Lophyl Free Radicals in Dry Films. *Macromolecules* **1995**, *28*, 636-641.

(44) Neumann, M. G.; Miranda Jr, W. G.; Schmitt, C. C.; Rueggeberg, F. A.; Correa, I. C. Molar extinction coefficients and the photon absorption efficiency of dental photoinitiators and light curing units. *Journal of Dentistry* **2005**, *33*, 525-532.

(45) Price, R. B. T.; Felix, C. A.; Andreou, P. Knoop hardness of ten resin composites irradiated with high-power LED and quartz-tungsten-halogen lights. *Biomaterials* **2005**, *26*, 2631-2641.

(46) Kameyama, A.; Kato, J.; Yoshinari, M.; Kotoku, Y.; Akashi, G.; Hirai, Y. Ultimate micro-tensile strength of dental adhesives cured at different light source. *Journal of Photopolymer Science and Technology* **2008**, *21*, 31-35.

(47) Vandewalle, K. S.; Roberts, H. W.; Andrus, J. L.; Dunn, W. J. Effect of light dispersion of LED curing lights on resin composite polymerization. *Journal of Esthetic and Restorative Dentistry* **2005**, *17*, 244-254.

(48) Tsai, L.; Charney, E. The triplet states of α-dicarbonyls. Camphorquinone. *Journal of Physical Chemistry* **1969**, *73*, 2462-2463.

(49) Teshima, W.; Nomura, Y.; Tanaka, N.; Urabe, H.; Okazaki, M.; Nahara, Y. ESR study of camphorquinone/amine photoinitiator systems using blue light-emitting diodes. *Biomaterials* **2003**, *24*, 2097-2103.

(50) Brandt, W. C.; Schneider, L. F. J.; Frollini, E.; Correr-Sobrinho, L.; Sinhoreti, M. A. C. Effect of different photo-initiators and light curing units on degree of conversion of composites. *Brazilian oral research* **2010**, *24*, 263-270.

(51) Zhu, Q. Q.; Fink, M.; Seitz, F.; Schneider, S.; Schnabel, W. On the photolysis of bis[2-(*o*-chlorophenyl)-4,5-diphenylimidazole] sensitized by 2-isopropylthioxanthone or Michler's ketone. *J. Photochem. Photobiol. A-Chem.* **1991**, *59*, 255-263.

(52) Kikuchi, A.; Iyoda, T.; Abe, J. Electronic structure of light-induced lophyl radical derived from a novel hexaarylbiimidazole with pi-conjugated chromophore. *Chemical Communications* **2002**, 1484-1485.

(53) Soh, S. K.; Sundberg, D. C. Diffusion-Controlled Vinyl Polymerization. I. The Gel Effect. *J. Polym. Sci. Pol. Chem.* **1982**, *20*, 1299-1313.

(54) Flory, P. J. Molecular size distribution in three dimensional polymers. I. Gelation. *Journal of the American Chemical Society* **1941**, *63*, 3083-3090.

(55) Stockmayer, W. H. Theory of molecular size distribution and gel formation in branched-chain polymers. *J. Chem. Phys.* **1943**, *11*, 45-55.

(56) Venditti, R. A.; Gillham, J. K.; Jean, Y. C.; Lou, Y. Free Volume After Cure vs. Fractional Conversion for a High-Tg Epoxy/Amine Thermosetting System. *Journal of Applied Polymer Science* **1995**, *56*, 1207-1220.

Chapter 3

Re-examining the photomediated dissociation and recombination kinetics of hexaarylbiimidazoles

3.1 Abstract

The recombination of lophyl radicals generated by the photodissociation of hexaarylbiimidazole (HABI) compounds has been previously reported to proceed as either first, 3/2, or second order reactions. Here, we re-examine the recombination of HABI-derived lophyl radicals to resolve these disparate reported recombination reaction orders. EPR spectroscopy was used to monitor the radical concentration for two HABI-based compounds in solution both during irradiation until steady state was achieved, then in the dark where only the radical recombination reaction proceeded. Over short dark periods, lophyl radical recombination could be adequately described by second order reaction kinetics. To better evaluate these reactions, UV-vis spectrophotometry measurements were performed over longer dark recombination periods. The molar absorptivities of the lophyl radical species were determined and used to express UV-vis absorbance data as radical concentrations. Analysis of these radical concentration curves over extended dark periods revealed that the recombination reactions at low initial HABI concentrations and incident irradiation intensities were well fit as 3/2 and second order reactions for the two respective parent HABI compounds; however, raised initial HABI concentrations and irradiation intensities progressively increased deviation from the

reaction order fits. The fitted recombination and corresponding photodissociation rate constants were validated by predicting radical concentration curves using stepped irradiation intensity profiles, which were compared against experimentally-determined radical concentrations obtained under identical reaction conditions.

3.2 Introduction

Free radicals, atomic or molecular species with an unpaired valence electron, are common reactive species in many chemical reactions; indeed, radicals participate in many naturally-occurring biological processes where they both fulfill essential functions as well as are linked to the cause of many diseases.[1-3] Radical species find particularly wide application in polymerization chemistry as the active propagating centers in both chain- and step-growth polymerizations.[4,5] Although radical are typically extremely reactive species with negligible recombination activation energies, resulting in diffusion-controlled termination rates, several examples of stable radical species exist. For example, trityl (i.e., triphenylmethyl) radicals in solution exist in equilibrium with their dimer form owing to the radical stability afforded by resonance and steric stabilization.[6] Additionally, the unpaired electron of nitroxides, resonance-stabilized and sterically-shielded nitroxyl radical species, is persistent and commonly employed for oxidation catalysis[7,8] and as mediator for controlled radical polymerizations.[9-11]

One particularly interesting class of radical-generating compounds consists of hexaarylbiimidazoles (HABIs) which have been the focus of significant research activity owing to their photochromic, piezochromic, and thermochromic nature for more than five decades[12-19] and have found industrial utility as radical polymerization initiators. First

synthesized by Hayashi and Maeda in 1960,[20] they have since been investigated for use in photographic films as leuco dye photooxidants, color proofing systems,[21] and as radical polymerization photoinitiators.[22,23] HABIs exhibit photochromism where, upon irradiation, they undergo homolytic cleavage to yield two strongly colored lophyl (i.e., triphenylimidazolyl) radicals (Figure 3.1) that are relatively stable in oxygen-saturated surroundings and show slow recombination rates; thus, analogous to the influence of temperature on the trityl radical/quinoid dimer equilibrium, light can be employed to shift the lophyl radical/HABI dimer equilibrium, an attribute that allows for lophyl radical generation and recombination kinetics to be readily studied.

The recombination kinetics of thermally- and photolytically-generated lophyl radicals have been previously studied spectroscopically[22,24-27] and efforts to explain the complex recombination behavior described. The photodissociation rate of a parent HABI compound into lophyl radicals is anticipated to scale with its absorptivity at the irradiation wavelength, the irradiation intensity, the quantum yield, and the concentration of the HABI solution itself. To better utilize the transient HABI photodissociation and its concomitant photochromic and chemically reactive properties, a more comprehensive understanding of the lophyl radical/HABI system reaction kinetics is required. Initial studies by Hayashi and Maeda found that lophyl radical recombination was a first order reaction, however they later revised this assessment to second order.[28] Subsequently, Wilks and Willis found lophyl radical recombination to be better described as 3/2 order rather than second order and postulated a complex recombination mechanism incorporating ionic species to account for their observations.[29] Notably, their experimental data was ill-fit by this perhaps unexpected 3/2 reaction order at long

reaction times whereupon a first order reaction mechanism emerged. In recent years, HABI derivatives based on rigid, bridged imidazole dimers have been synthesized that exhibit rapid, first order lophyl radical recombination, attributable to radical diffusion suppression.[30-34] In disagreement with the previously observed 3/2 reaction order for lophyl radical recombination, studies on conventional HABI compounds have employed second order reaction kinetics to describe the lophyl radical recombination reactions.[35-38] Here, we re-examine the reaction kinetics of HABI photodissociation and subsequent lophyl radical recombination in an attempt to better understand and resolve the apparent disagreement between reported reaction orders. Two HABI compounds, one commercially available and one synthesized for improved solubility and visible light absorption, are examined to assess the influence of the HABI structure on the subsequent recombination rates.

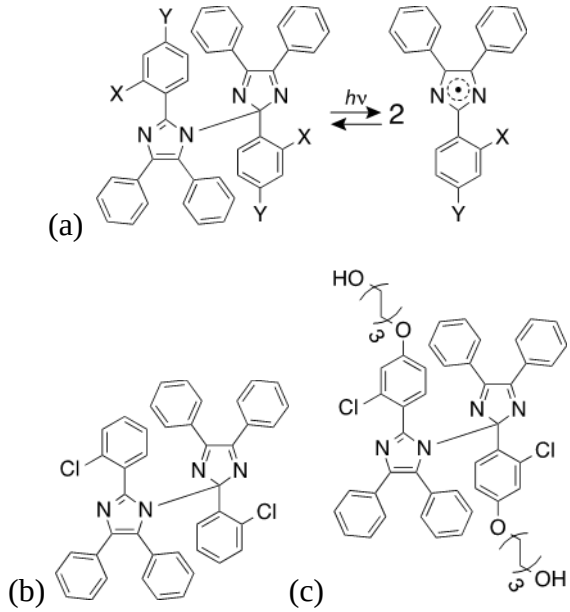

Figure 3.1. *Upon irradiation, the inter-imidazole HABI bond undergoes homolytic cleavage, reversibly generating two relatively stable, long-lived lophyl radicals. (b) o-Cl-HABI, and (c) p-HOH-HABI.*

3.3 Experimental

3.3.1 Materials

Two visible light-active HABI compounds were used for comparison throughout this study. 2,2′-Bis(2-chlorophenyl)-4,4′,5,5′-tetraphenyl-1,2′-biimidazole (*o*-Cl-HABI, TCI America) was used as received, whereas 2,2′-bis(2-chloro-4-hexan-1-ol-phenoxy)-4,4′,5,5′-tetraphenyl-1,2′-biimidazole (*p*-HOH-HABI) was synthesized. 2,2-Diphenyl-1-picrylhydrazyl (DPPH, Sigma-Aldrich) was used as received for standard radical concentration solutions. Toluene (Fisher Chemical) was used as solvent for all samples.

3.3.2 Methods

3.3.2.1 Light sources and intensity measurement

All samples were irradiated with blue light provided by a collimated, LED-based illumination source (Thorlabs model M455L2-C1) with an emittance centered at 455 nm (FWHM 20 nm), used in combination with a current-adjustable LED driver (Thorlabs model LEDD1B) for intensity control. Irradiation intensities were measured with an International Light IL1400A radiometer, equipped with a broadband silicon detector (model SEL033), a 10× attenuation neutral density filter (model QNDS1), and a quartz diffuser (model W), by positioning the detector at the sample site and irradiating it both before and after each experiment to ensure that the light intensity had not changed during the experiments.

3.3.2.2 Ultraviolet-visible spectrophotometry

Ultraviolet-visible (UV-vis) spectrophotometry was performed using an Agilent Technologies Cary 60 UV-Vis Spectrophotometer. Spectra were collected from 650 to 350 nm at 4800 $nm.min^{-1}$ on HABI solutions in toluene using a 1 mm pathlength quartz cuvette both in the dark and under irradiation. HABI photodissociation and subsequent recombination were examined while the sample solutions were either irradiated with 455 nm light, supplied by the Thorlabs LED light source positioned approximately 20 cm from the sample, or in the dark by monitoring the absorbance at 554 nm and 598 nm for *o*-Cl-HABI and *p*-HOH-HABI, respectively, wavelengths where the visible light absorbance by the generated lophyl radicals was greatest (i.e., λ_{max}). All experiments were performed in triplicate.

3.3.2.3 Electron paramagnetic resonance spectroscopy

Electron paramagnetic resonance (EPR) spectroscopy was performed with a Bruker EMX spectrometer. The spectrometer was equipped with a TE_{102} cavity (Bruker model ER 4102ST), and a frequency of 9.717 GHz, 2.05 mW microwave power, 5.02×10^3 receiver gain, 100 kHz modulation frequency, and 1 G modulation amplitude were used for all experiments. Optical access to the cavity was afforded by a 10 mm × 23 mm grid providing 50% light transmittance to the sample. A 3.2 mm inner diameter quartz sample tube was filled with 190 μL of sample solution and inserted into the spectrometer cavity for analysis. Photodissociation and subsequent recombination was monitored at a 3453 G static field, the first derivative signal intensity maximum for both HABI compounds under irradiation, while the sample solutions were irradiated with 455 nm

light, again supplied by the Thorlabs LED light source positioned approximately 60 cm from the sample, for 5 minutes to ensure reaction equilibrium, then for a further 15 minutes in the dark. All experiments were performed at room temperature. Radical concentrations were quantified by calibrating the EPR spectrum integral against known concentration solutions of DPPH in toluene using the same sample geometry, volume, and acquisition conditions employed for the HABI solutions (Figure 3.2).

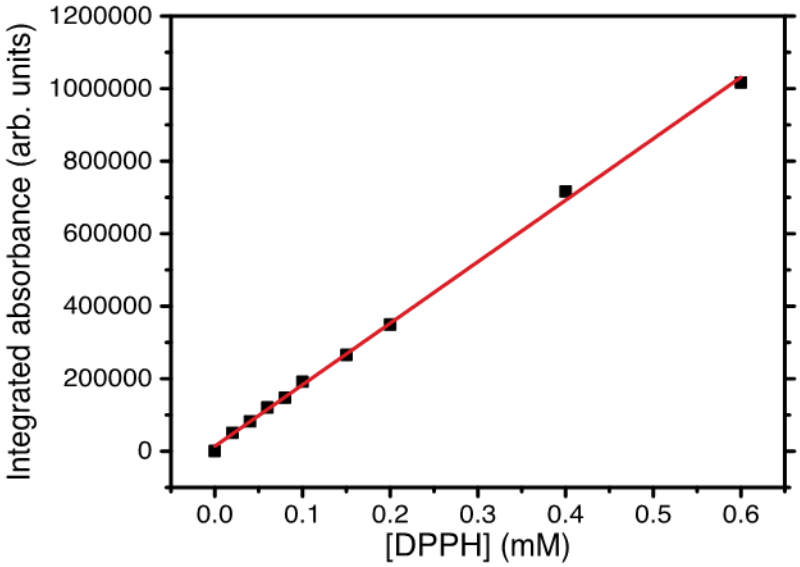

Figure 3.2. *Integrated absorbance, as determined by EPR spectroscopy, versus DPPH concentration in toluene for 190 μL of solution (black squares) and least squares linear fit (red line, y = 13851 + 1696070x, r^2 = 0.999).*

3.4 Results and discussion

Dissolution of HABI compounds typically affords yellow solutions that exhibit moderate absorbance in the violet to blue region of the spectrum; however, these solutions undergo a dramatic color change upon irradiation, generating colors ranging from indigo to teal and attributable to the photoinduced dissociation of HABIs to yield

strongly colored lophyl radical species.[39] This color change suggests UV-vis spectrophotometry as a convenient and sensitive approach to monitor the photodissociation of HABIs and subsequent dark recombination of the generated lophyl radicals. The evolution of ultraviolet/visible light absorbance of 5 mM solutions of *o*-Cl-HABI and *p*-HOH-HABI in toluene in the dark and upon irradiation with 455 nm light at 10 $mW \cdot cm^{-2}$ until the reactions attain steady state are shown in Figure 3.3a and 3b, respectively. Here, the unirradiated HABI species display slight absorbance at 455 nm and the increase in absorbance at this wavelength while the solutions are under irradiation is relatively low (Figure 3.3a and 3b). Consequently, 455 nm light was selected as the irradiation wavelength throughout this study to effect HABI photolysis while avoiding excessive light attenuation and concomitant concentration inhomogeneity through the sample thicknesses. The peak absorbance wavelengths (i.e., λ_{max}) of the *o*-Cl-HABI and *p*-HOH-HABI solutions while under irradiation (554 and 598 nm, respectively) are not overlapped by the absorbance spectra of the respective parent HABI solutions, enabling the lophyl radical concentration curves to be readily determined by simply monitoring λ_{max} without any additional steps deconvoluting the radical absorbance from an underlying absorbance by the parent compound. Notably, the absorbances at these wavelengths do not provide a direct measure of the radical concentration; rather, the as-yet-unknown molar absorptivity of the radical species at λ_{max} must be employed to obtain radical concentration information.

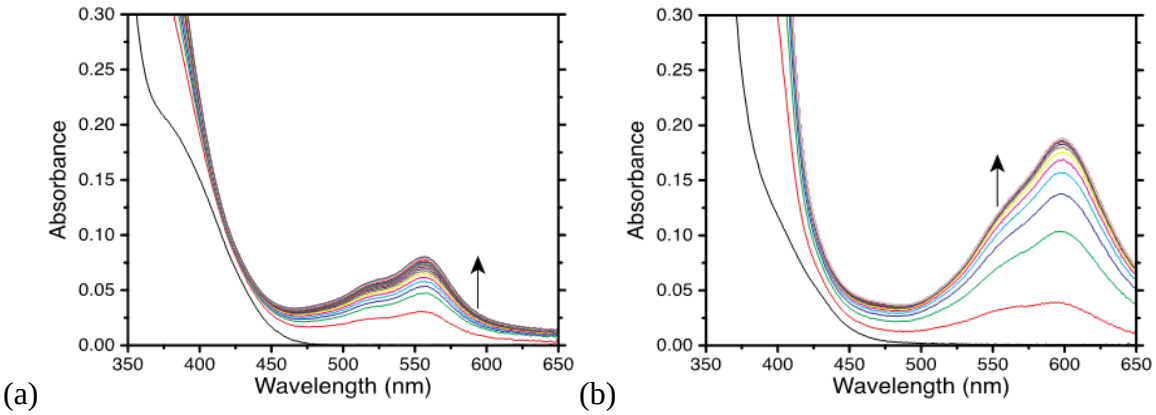

Figure 3.3. *UV-vis absorption spectra for 5 mM solutions of (a) o-Cl-HABI and (b) p-HOH-HABI in toluene prior to (black) and under irradiation at 10 mW·cm^{-2}. An individual wavelength scan took 3.75 seconds and scans were collected at 5.3 second intervals.*

Although perhaps less convenient than UV-vis spectrophotometry owing to sample geometry and spectrometer cavity constraints, EPR spectroscopy does have the advantage of allowing for direct measurement of radical concentration in solution. Here, the influences of varying initial HABI concentration and incident irradiation intensity on photoinduced dissociation and dark recombination were examined by *in situ* sample irradiation in an EPR spectrometer. Whereas studies examining photoinitiator photolysis typically employ either spin traps[40] or severely restricted molecular mobility at low temperatures[41] to attain sufficient radical concentrations for detection, the stability of the lophyl radicals generated by HABI photolysis affords readily detectable radical concentrations in solution and at room temperature, even at moderate HABI concentrations and irradiation intensities. Upon irradiation, the radical concentrations for all samples rapidly increased to a plateau value and, upon irradiation cessation, decreased ultimately to undetectable levels over several minutes (see Figure 3.4). The radical generation rates and steady state radical concentrations for both HABI compounds

increased with raised irradiation intensity and initial HABI concentration (Figure 3.4), and the steady state radical concentrations for all conditions examined are tabulated in Table 3.1. At the highest HABI concentration and applied irradiation intensity (i.e., 5 mM and 5 $mW \cdot cm^{-2}$), the steady state radical concentrations of 0.081 mM and 0.12 mM for *o*-Cl-HABI and *p*-HOH-HABI (Table 3.1) indicate reaction extents of 0.0081 and 0.012, respectively. That is, the instantaneous percentage of HABI interimidazole C–N bonds cleaved at steady state are 0.81% and 1.23% for *o*-Cl-HABI and *p*-HOH-HABI, respectively, under these reaction conditions. Interestingly, the steady state radical concentrations achieved under the reaction conditions used here are similar to those typically attained upon gelation and vitrification during radical-mediated cross-linking polymerizations,[42] where the precipitous termination rate decrease owing to restricted radical mobility leads to a dramatic radical concentration increase,[43] despite no mobility restrictions imposed on lophyl radicals in solution. Moreover, irradiation of *p*-HOH-HABI solutions yielded higher radical concentrations than *o*-Cl-HABI solutions under equivalent reaction conditions for all conditions investigated, attributable in part to the raised molar absorptivity at 455 nm of *p*-HOH-HABI (21.3 $M^{-1} \cdot cm^{-1}$) compared with that of *o*-Cl-HABI (16.0 $M^{-1} \cdot cm^{-1}$).

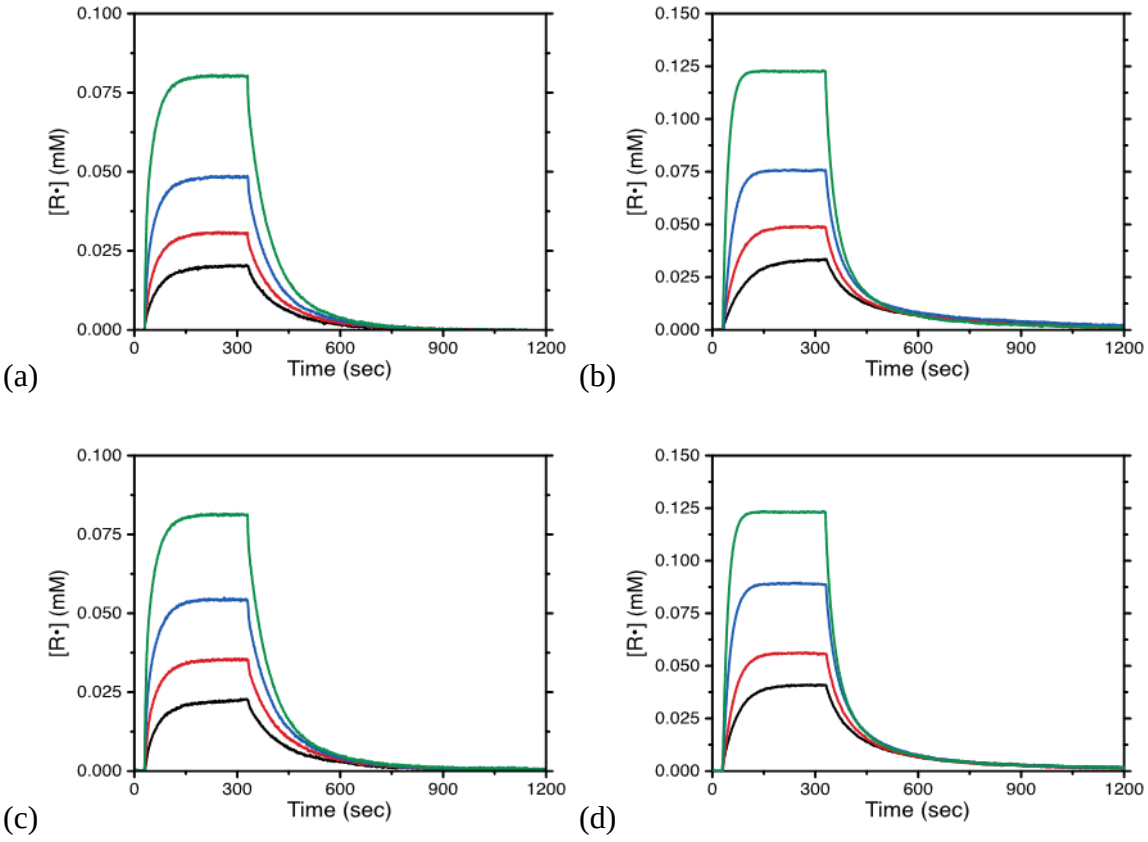

Figure 3.4. *Lophyl radical concentration, as determined by EPR spectroscopy, versus time for 5 mM solutions of (a) o-Cl-HABI and (b) p-HOH-HABI in toluene, irradiated at intensities of 0.5 (black), 1.0 (red), 2.0 (blue), and 5.0 (green) mW·cm^{-2}, and for solutions of (c) o-Cl-HABI and (d) p-HOH-HABI in toluene at concentrations of 0.5 (black), 1.0 (red), 2.5 (blue), and 5.0 (green) mM, irradiated at 5 mW·cm^{-2}. All solutions were irradiated from 30 seconds to 330 seconds (i.e., 5 minutes irradiation), and were otherwise in the dark.*

The reaction scheme described in Figure 3.1a suggests that, whereas HABI photodissociation is a first order reaction with a rate constant that scales with the incident irradiation intensity, lophyl radical recombination in dilute solution to form dimeric HABI species should proceed as a second order reaction with respect to the lophyl radical concentration. Thus, the radical generation rate can be described by the relation:

$$-2\frac{d[\mathrm{HABI}]}{dt} = \frac{d[\mathrm{R}\bullet]}{dt} = k_{dis}[\mathrm{HABI}] - 2k_{rec}[\mathrm{R}\bullet]^2, \qquad (1)$$

where k_{dis} is the photodissociation rate constant, the value of which is directly proportional to the irradiation intensity, k_{rec} is the recombination rate constant, and α is the recombination reaction order and equal to 2 for a simple, bimolecular, second order reaction. At steady state, where the radical concentration is invariant, the forward and reverse reactions proceed at the same rate such that Equation 1 simplifies to:

$$k_{dis}[\mathrm{HABI}]_0\left(1-x_{ss}\right)=2k_{rec}[\mathrm{R}\bullet]_{ss}^{\alpha}, \qquad (2)$$

where $[\text{species}]_0$ denotes the initial species concentration, $[\text{species}]_{ss}$ the steady state species concentration, and x_{ss} the steady state reaction extent. Thus, under two different reaction conditions, labeled 1 and 2, respectively, Equation 2 under these two conditions can be expressed by the ratio:

$$\frac{k_{dis_2}[\mathrm{HABI}]_{0_2}\left(1-x_{ss_2}\right)}{k_{dis_1}[\mathrm{HABI}]_{0_1}\left(1-x_{ss_1}\right)}=\frac{2k_{rec_2}[\mathrm{R}\bullet]_{ss_2}^{\alpha}}{2k_{rec_1}[\mathrm{R}\bullet]_{ss_1}^{\alpha}}, \qquad (3)$$

To the best of our knowledge, evidence of photomediated recombination of lophyl radicals has not been previously described, such that we assume k_{rec} to be independent of both incident irradiation intensity and $[\mathrm{HABI}]_0$. Moreover, as described above, monomolecular photodissociation reaction rates scale with the irradiation intensity at a given wavelength, such that $\frac{k_{dis_2}}{k_{dis_1}}=\frac{I_{0_2}}{I_{0_1}}$, where I_0 is the incident irradiation intensity. Thus, steady state radical concentrations under two different reaction conditions can be compared using the ratio:

$$\frac{[\mathrm{R}\bullet]_{ss_2}}{[\mathrm{R}\bullet]_{ss_1}}=\left(\frac{I_{0_2}[\mathrm{HABI}]_{0_2}\left(1-x_{ss_2}\right)}{I_{0_1}[\mathrm{HABI}]_{0_1}\left(1-x_{ss_1}\right)}\right)^{1/\alpha} \qquad (4)$$

Given the steady state lophyl radical concentration under specific reaction conditions, Equation 4 can be employed to predict the lophyl radical concentration at steady state under different conditions and confirm the recombination reaction order α. The steady state radical concentrations under varying incident irradiation intensities and initial HABI concentrations, as measured using EPR spectroscopy, and predicted radical concentrations using the reference reaction conditions as shown and assuming a second order recombination reaction are tabulated in Table 3.1. Here, the predicted radical concentrations closely match those experimentally determined, where the largest discrepancy between the experimental and predicted radical concentrations is only 12.3% (Table 3.1), indicating that the assumed second order lophyl radical recombination is experimentally supported for both HABI compounds under the reaction conditions examined

Table 3.1. *EPR spectroscopy-measured steady state lophyl radical concentrations for o-Cl-HABI and p-HOH-HABI solutions under varying initial HABI concentrations and incident irradiation intensities, and radical concentrations predicted using reference data assuming second order recombination.*

$[HABI]_0$ (mM)	I_0 ($mW \cdot cm^{-2}$)	*o*-Cl-HABI			*p*-HOH-HABI		
		Experimental $[R\bullet]_{ss}$ (mM)	Predicted $[R\bullet]_{ss}$ (mM)	Difference (%)	Experimental $[R\bullet]_{ss}$ (mM)	Predicted $[R\bullet]_{ss}$ (mM)	Difference (%)
5.0	0.5	0.0207	Reference	-	0.0334	Reference	-
	1.0	0.0305	0.0293	4.1	0.0489	0.0472	3.4
	2.0	0.0491	0.0431	12.3	0.0759	0.0689	9.1
	5.0	0.0811	0.0774	3.2	0.1231	0.1194	2.0
0.5	5.0	0.0228	Reference	-	0.0410	Reference	-
1.0		0.0355	0.0324	8.6	0.0558	0.0579	-3.8
2.5		0.0544	0.0565	-3.9	0.0888	0.0882	0.72
5.0		0.0811	0.0771	4.8	0.1231	0.1256	-2.0

For the experiments shown in Figure 3.4, data for each individual run were collected under two irradiation regimes such that both the forward HABI photodissociation and reverse lophyl radical recombination reactions proceed concurrently during irradiation, resulting in the observed radical concentration increase until steady state is achieved, whereas exclusively radical consumption by recombination occurs in the dark. Consequently, fitting the portion of the curves where irradiation is

ceased enables facile calculation of k_{rec}, the recombination rate constant, under varying initial reaction conditions. In this dark reaction regime, the generalized relation for the radical generation rate (Equation 1) can be simplified to:

$$\frac{d[R\bullet]}{dt} = -2k_{rec}[R\bullet]^{\alpha} \qquad (5)$$

The integral form for this rate expression is given as:

$$\int_{[R\bullet]_{ss}}^{[R\bullet]} [R\bullet]^{-\alpha}\, d[R\bullet] = -2k_{rec}\int_{t_0}^{t} dt \quad (6)$$

where t_0 is the irradiation cessation time whereupon exclusively the radical recombination reaction proceeds. Finally, integrating Equation 6 across its limits yields the relation:

$$\frac{1}{[R\bullet]^{\alpha-1}} - \frac{1}{[R\bullet]_{ss}^{\alpha-1}} = 2(\alpha - 1)k_{rec}(t - t_0) \qquad (7)$$

Thus, assuming second order radical recombination (i.e., $\alpha = 2$), applying linear regression to plots of $\frac{1}{[R\bullet]} - \frac{1}{[R\bullet]_{ss}}$ versus $(t - t_0)$ using experimentally-determined data affords $2k_{rec}$ as the fitted slope. Such second order plots using the previously-obtained EPR spectroscopy data (see Figure 3.4) and corresponding linear fits are shown in Figure 3.5. Only the first 30 seconds upon irradiation cessation are plotted (i.e., 330 seconds to 360 seconds, Figure 3.4) and fitted as extended reaction times in the dark, where radical concentrations are significantly depleted, result in low signal to noise ratios; however, under the reaction conditions examined, these first 30 seconds are again well-described by second order reaction kinetics and the calculated second order recombination rate

constants are tabulated in Table 3.2. Whereas the second order recombination fits for *p*-HOH-HABI yielded slight variation in k_{rec} values, ranging from 0.159 to 0.205 $mM^{-1}\cdot sec^{-1}$, equivalent second order recombination fits for *o*-Cl-HABI by over a factor of 3, from 0.12 to 0.395 $mM^{-1}\cdot sec^{-1}$. This suggests that, although *p*-HOH-HABI-derived lophyl radical recombination appears well-described by second order reaction kinetics, the recombination of *o*-Cl-HABI-derived radicals may be better described by alternative reaction order exponents.

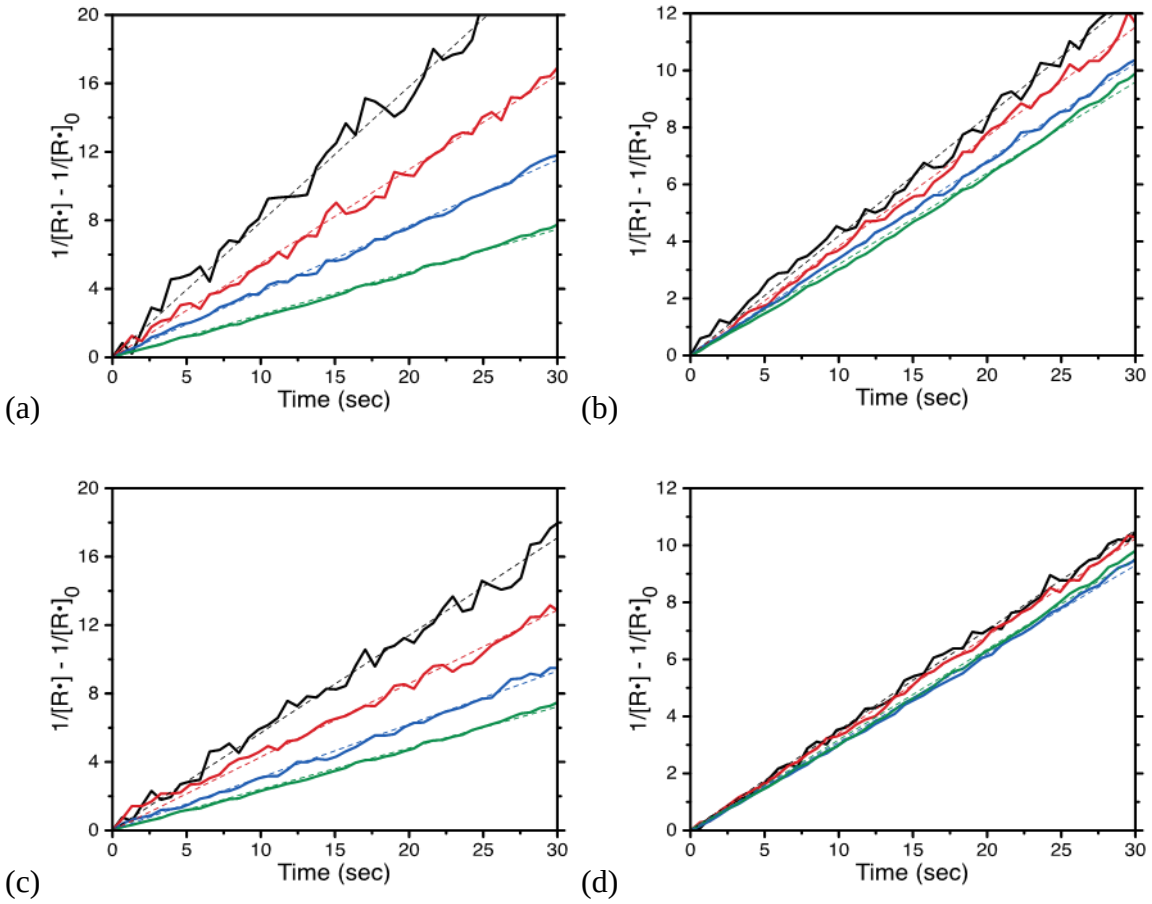

Figure 3.5. *Second order plots of EPR spectroscopy-measured dark lophyl radical concentration decay for (a) o-Cl-HABI and (b) p-HOH-HABI at varying initial incident irradiation intensities (0.5 (black), 1.0 (red), 2.0 (blue), and 5.0 (green) mW·cm^{-2}), and (c) o-Cl-HABI and (d) p-HOH-HABI at varying initial HABI concentrations (0.5 (black), 1.0 (red), 2.5 (blue), and 5.0 (green) mM). Experimental data and corresponding linear regression fits are shown as solid and dashed lines, respectively.*

Having determined k_{rec}, assuming second order radical recombination, and given forward and reverse reaction rate equality at steady state under irradiation, the dissociation rate constant, k_{dis}, can be readily calculated. By expressing $[R\bullet]_{ss}$ as the product $2x_{ss}[HABI]_0$, Equation 2 can be simplified and rearranged in terms of k_{dis} to yield:

$$k_{dis} = 2^{a+1} k_{rec} [\mathrm{HABI}]_0^{a-1} \int_0^{x_{ss}} \left(\frac{x^a}{1-x} \right) \quad (8)$$

Again assuming second order lophyl radical recombination and applying values for x_{ss} and k_{rec} determined previously (Tables 3.1 and 3.2, respectively), k_{dis} for each reaction condition was calculated and tabulated in Table 3.2. Here, the k_{dis} for *p*-HOH-HABI increases by an order of magnitude as the incident irradiation intensity is raised by a factor of ten, and remains constant at constant irradiation intensity as $[\mathrm{HABI}]_0$ is varied, in good agreement with the anticipated photodissociation rate scaling with irradiation intensity and further affirming second order reaction kinetics to accurately describe *p*-HOH-HABI-derived lophyl radical recombination. In contrast, the fitted k_{dis} for *o*-Cl-HABI decrease by nearly a factor of two with a ten-fold $[\mathrm{HABI}]_0$ increase at constant intensity (Table 3.2), again suggesting that the *o*-Cl-HABI-derived lophyl radical recombination is not accurately described as a second order reaction.

Table 3.2. *Second order lophyl radical recombination and first order HABI photodissociation rate constants for EPR spectroscopy-measured HABI photolysis in toluene solution under irradiation with 455 nm light and in the dark.*

$[HABI]_0$ (mM)	I_0 ($mW \cdot cm^{-2}$)	*o*-Cl-HABI		*p*-HOH-HABI	
		k_{rec} ($mM^{-1} \cdot sec^{-1}$)	k_{dis} (sec^{-1})	k_{rec} ($mM^{-1} \cdot sec^{-1}$)	k_{dis} (sec^{-1})
5.0	0.5	3.95×10^{-1}	0.68×10^{-4}	2.05×10^{-1}	0.92×10^{-4}
	1.0	2.75×10^{-1}	1.02×10^{-4}	1.95×10^{-1}	1.88×10^{-4}
	2.0	1.92×10^{-1}	1.86×10^{-4}	1.73×10^{-1}	4.01×10^{-4}
	5.0	1.25×10^{-1}	3.22×10^{-4}	1.66×10^{-1}	9.97×10^{-4}
0.5	5.0	2.85×10^{-1}	6.08×10^{-4}	1.77×10^{-1}	12.36×10^{-4}
1.0		2.15×10^{-1}	5.50×10^{-4}	1.72×10^{-1}	11.01×10^{-4}
2.5		1.55×10^{-1}	3.71×10^{-4}	1.59×10^{-1}	10.20×10^{-4}
5.0		1.20×10^{-1}	3.20×10^{-4}	1.63×10^{-1}	10.02×10^{-4}

Owing to the low signal to noise ratios typically achieved by EPR spectroscopy, plots of lophyl radical concentration, as determined by that technique, versus time become progressively noisy as the recombination reaction proceeds and reaction order fits become unreliable after even relatively short dark periods. Consequently, increasing the time period over which the reaction order fits maintain accuracy necessitates utilizing characterization techniques with improved sensitivity, such as UV-vis spectrophotometry. By performing both EPR spectroscopic and UV-vis spectrophotometric measurements using solutions with varying HABI concentrations while at steady state under identical

irradiation conditions with 455 nm light, the λ_{max} absorbances for given radical concentrations were obtained and the molar absorptivities at λ_{max} for each of the HABI-derived lophyl radicals calculated (see Table 3.3), enabling the UV-vis absorption versus time data to be expressed as radical concentration curves (Figure 3.6). A comparison of Figure 3.6 with Figure 3.4 reveals similar radical concentration curves under equivalent reaction conditions where the radical generation rates upon irradiation and steady state reaction extents increase with raised irradiation intensities and $[HABI]_0$. However, the signal to noise ratios, particularly after extended periods in the dark are improved. The small error bars demonstrate the consistency of the data acquisition performed in triplicate. Whereas no radical concentration decrease during irradiation was observed by EPR spectroscopy, UV-vis spectrophotometry revealed a small radical concentration drop at long irradiation times under reaction conditions using the highest $[HABI]_0$ and I_0, potentially attributable to radical consumption by reaction with dissolved oxygen to afford non-photochromic peroxide adducts.[44,45]

Table 3.3. *Molar absorptivities of HABI-sourced lophyl radicals in toluene solution.*

Parent HABI	Lophyl radical molar absorptivity at λ_{max} ($M^{-1}\cdot cm^{-1}$)
o-Cl-HABI	6132 ± 122
p-HOH-HABI	9610 ± 26

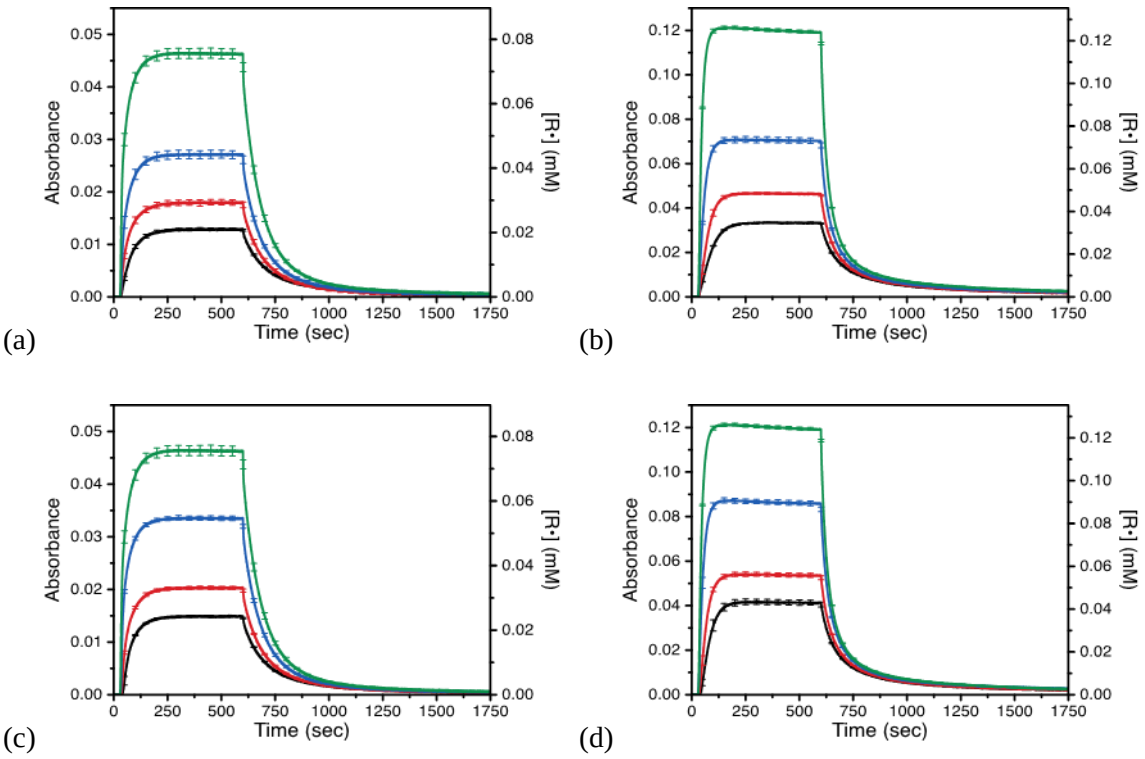

Figure 3.6. *Absorbance at λ_{max} and lophyl radical concentration, as determined by UV-vis spectrophotometry, versus time for 5 mM solutions of (a) o-Cl-HABI and (b) p-HOH-HABI in toluene, irradiated at intensities of 0.5 (black), 1.0 (red), 2.0 (blue), and 5.0 (green) mW·cm^{-2}, and for solutions of (c) o-Cl-HABI and (d) p-HOH-HABI in toluene at concentrations of 0.5 (black), 1.0 (red), 2.5 (blue), and 5.0 (green) mM, irradiated at 5 mW·cm^{-2}. All solutions were irradiated from 30 seconds to 600 seconds, and were otherwise in the dark. Error bars represent standard error for triplicate experiments.*

As performed above, Equation 7 was fit to the dark lophyl radical recombination data obtained by UV-vis spectrophotometry (i.e., 600 seconds on, Figure 3.6); however, instead of assuming second order recombination reaction behavior, the reaction order α was allowed to vary. Notably, plots of $\frac{1}{[R\bullet]^{\alpha-1}} - \frac{1}{[R\bullet]_{ss}^{\alpha-1}}$ versus $(t - t_0)$ for the experimentally-determined data did not achieve linearity over extended dark periods at high initial $[R\bullet]_{ss}$ for any single α value (Figure 3.7); rather, whereas the radical recombinations at low initial $[R\bullet]_{ss}$ were well-described by 3/2 and second order reaction

kinetics for *o*-Cl-HABI- and *p*-HOH-HABI-derived lophyl radicals, respectively) demonstrated by the excellent linearity achieved under low $[HABI]_0$ and reduced irradiation intensity reaction conditions (e.g., Figure 3.7a and 7b, 0.5 $mW \cdot cm^{-2}$ and 5 mM), the fitted experimental data exhibited progressively earlier deviation from linearity as the $[HABI]_0$ and irradiation intensity were raised (e.g., Figure 3.7c and 7d, 5 $mW \cdot cm^{-2}$ and 5 mM). Similar initial recombination rate order deviations were previously observed where consistent deviations from 3/2 recombination reaction order at extended dark lophyl radical recombination times for a simple, non-functionalized HABI were reported,[29] attributed to a change in the recombination mechanism, although the nature of this varying recombination mechanism remains elusive. To demonstrate the influence of α as a fitting parameter, the reaction orders for the two HABIs examined were swapped (i.e., second and 3/2 order reaction kinetics for *o*-Cl-HABI- and *p*-HOH-HABI-derived lophyl radicals plots, respectively); however, the experimental data was ill-described by these reaction orders other than over very short periods after irradiation cessation, even at low initial $[R\bullet]_{ss}$ (see Figure 3.8). Values for k_{rec} for *p*-HOH-HABI-derived radical recombination were similar across all examined experimental conditions (Table 3.4). Moreover, values for *p*-HOH-HABI k_{dis} approximately scaled with the irradiation intensity and were consistent for several $[HABI]_0$ solutions under the same irradiation intensity (Table 3.4), confirming *p*-HOH-HABI photodissociation and subsequent lophyl radical recombination being well-described as first and second order reactions, respectively. In contrast, despite the initial linearity observed for the 3/2 order rate plots under low $[HABI]_0$ and I_0 conditions, values for k_{rec} for *o*-Cl-HABI-derived radical

recombination varied significantly over the examined experimental conditions, and calculated values for *o*-Cl-HABI k_{dis} were inconsistent with first order photodissociation.

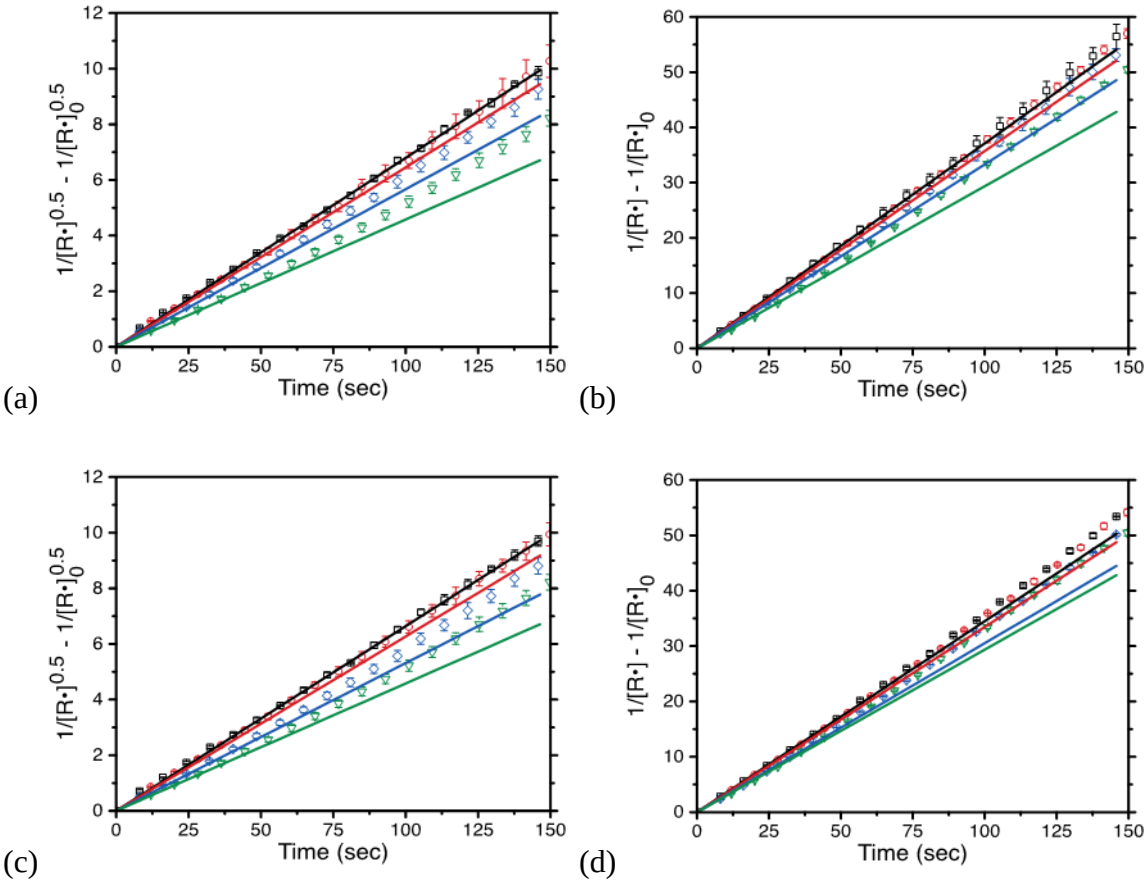

Figure 3.7. *3/2 and second order plots of UV-vis spectrophotometry-measured dark lophyl radical concentration decay for (a) o-Cl-HABI and (b) p-HOH-HABI at varying initial incident irradiation intensities (0.5 (black), 1.0 (red), 2.0 (blue), and 5.0 (green) mW·cm^{-2}), and (c) o-Cl-HABI and (d) p-HOH-HABI at varying initial HABI concentrations (0.5 (black), 1.0 (red), 2.5 (blue), and 5.0 (green) mM). Experimental data and corresponding linear regression fits are shown as symbols and dashed lines, respectively. Error bars represent standard error for triplicate experiments. For clarity, not all experimental data points are plotted.*

Table 3.4. *3/2 and second order o-Cl-HABI- and p-HOH-HABI-derived lophyl radical recombination, respectively, and first order HABI photodissociation rate constants for UV-vis spectrophotometry-measured HABI photolysis in toluene solution under irradiation with 455 nm light and in the dark.*

$[HABI]_0$ (mM)	I_0 (mW·cm^{-2})	*o*-Cl-HABI		*p*-HOH-HABI	
		k_{rec} (mM$^{-0.5}$·sec^{-1}) × 10^2	k_{dis} (sec^{-1}) × 10^4	k_{rec} (mM^{-1}·sec^{-1}) × 10^1	k_{dis} (sec^{-1}) × 10^4
5.0	0.5	4.25 ± 0.03	0.51 ± 0.01	1.86 ± 0.03	0.83 ± 0.01
	1.0	4.04 ± 0.10	0.86 ± 0.02	1.79 ± 0.02	1.71 ± 0.01
	2.0	3.55 ± 0.09	1.55 ± 0.04	1.67 ± 0.03	3.86 ± 0.07
	5.0	2.87 ± 0.10	2.62 ± 0.09	1.47 ± 0.01	8.83 ± 0.02
0.5	5.0	4.16 ± 0.08	5.87 ± 0.11	1.73 ± 0.01	12.06 ± 0.07
1.0		3.92 ± 0.10	5.33 ± 0.14	1.67 ± 0.01	10.71 ± 0.08
2.5		3.33 ± 0.10	3.42 ± 0.10	1.52 ± 0.01	9.80 ± 0.02
5.0		2.87 ± 0.10	2.67 ± 0.10	1.46 ± 0.01	9.01 ± 0.02

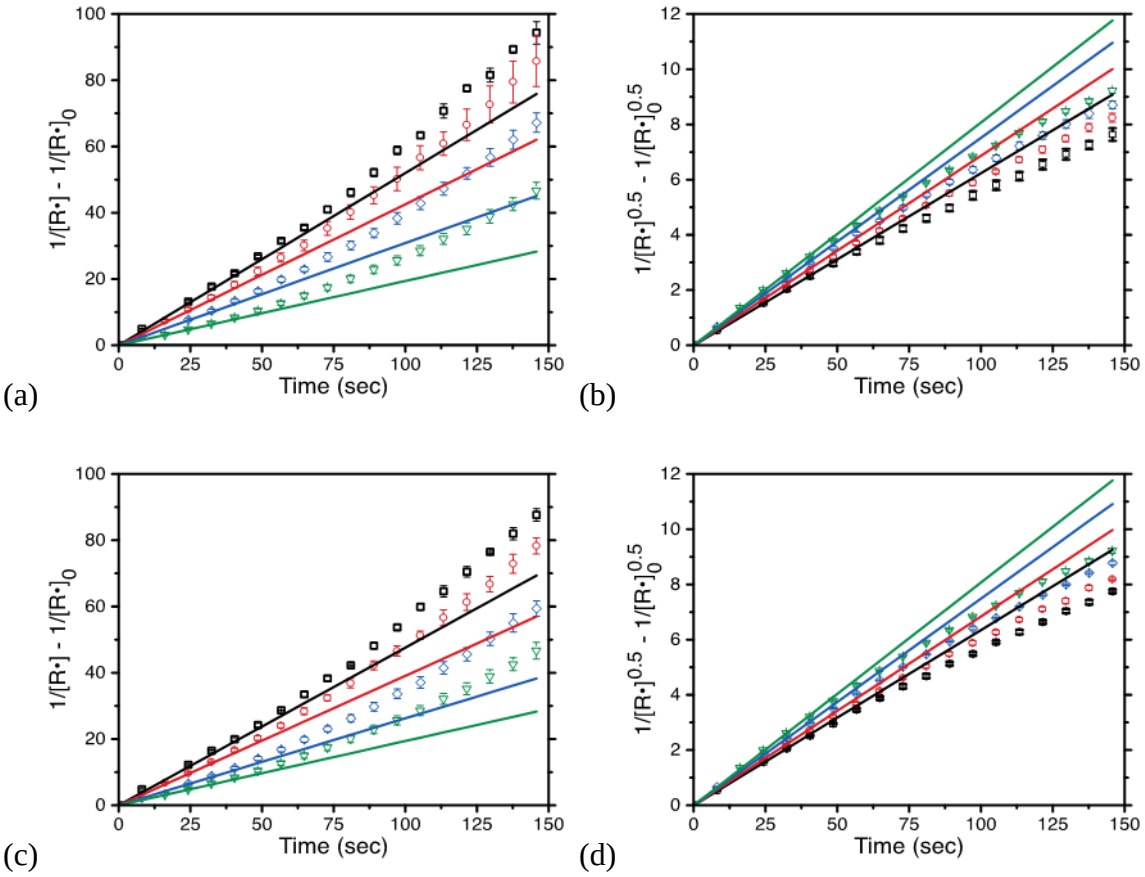

Figure 3.8. *Second and 3/2 order plots of UV-vis spectrophotometry-measured dark lophyl radical concentration decay for (a) o-Cl-HABI and (b) p-HOH-HABI at varying initial incident irradiation intensities (0.5 (black), 1.0 (red), 2.0 (blue), and 5.0 (green) mW·cm^{-2}), and (c) o-Cl-HABI and (d) p-HOH-HABI at varying initial HABI concentrations (0.5 (black), 1.0 (red), 2.5 (blue), and 5.0 (green) mM). Experimental data and corresponding linear regression fits are shown as symbols and dashed lines, respectively. Error bars represent standard error for triplicate experiments. For clarity, not all experimental data points are plotted.*

To validate the reaction orders determined above, the obtained HABI photodissociation and lophyl radical recombination rate constants were used to predict radical concentration curves anticipated from a stepped irradiation intensity profile and compared to experimental data. Here, the radical concentration evolution in 5 mM solutions of *o*-Cl-HABI and *p*-HOH-HABI in toluene were monitored by EPR spectroscopy where the samples were initially in the dark then subject to irradiation with

455 nm light under an irradiation intensity profile from 0.5 $mW \cdot cm^{-2}$ with step intensity increases every 300 seconds to 1.0, 2.0 and finally 5.0 $mW \cdot cm^{-2}$, followed by step intensity decreases every 300 seconds in the reverse irradiation intensity order (see Figure 3.9). The applied 300 second step periods are sufficient for steady state to be achieved for both increasing and decreasing irradiation intensities. The radical concentration curves were predicted by applying the fitted rate constants for each reaction condition (see Table 3.2, Table 3.4, and Table 3.5) to the generalized radical generation rate relation, Equation 1, solutions for which are superimposed on the experimental data in Figure 3.9. The predicted *p*-HOH-HABI-derived lophyl radical concentrations using second order rate constants fitted from EPR spectroscopy and UV-vis spectrophotometry experiments both closely parallel the shape and steady state concentrations observed experimentally for *p*-HOH-HABI (Figure 3.9, red and blue curves), although the predicted curves slightly underestimate the actual radical concentration at high irradiation intensity, confirming that the recombination of *p*-HOH-HABI-derived lophyl radicals is well-described as a second order reaction as depicted in Figure 3.1a. The predicted *o*-Cl-HABI-derived lophyl radical concentrations using second order rate constants fitted from EPR spectroscopy similarly match the experimental steady state radical concentrations for *o*-Cl-HABI; however, the concentration curves do not match, where the predicted radical concentrations approach steady state more rapidly than experimentally observed (Figure 3.9, black and orange curves). Conversely, radical concentrations predicted using fitted 3/2 order rate constants from UV-vis and EPR experiments closely match both the steady state radical concentrations and concentration curves that were experimentally measured (Figure 3.9, black and green curves), indicating that the simple bimolecular

reaction of identical species described in Figure 3.1a does not fully capture the recombination mechanism of *o*-Cl-HABI-derived lophyl radicals. This in part resolves the disparate recombination reaction orders reported previously whereby lophyl radical recombinations cannot be categorized as a class of second order reactions. Rather, depending on the structure of the parent HABI compound, lophyl radical recombination can either proceed as a second order reaction or can exhibit complex recombination behavior that is more closely modeled as a 3/2 order reaction.

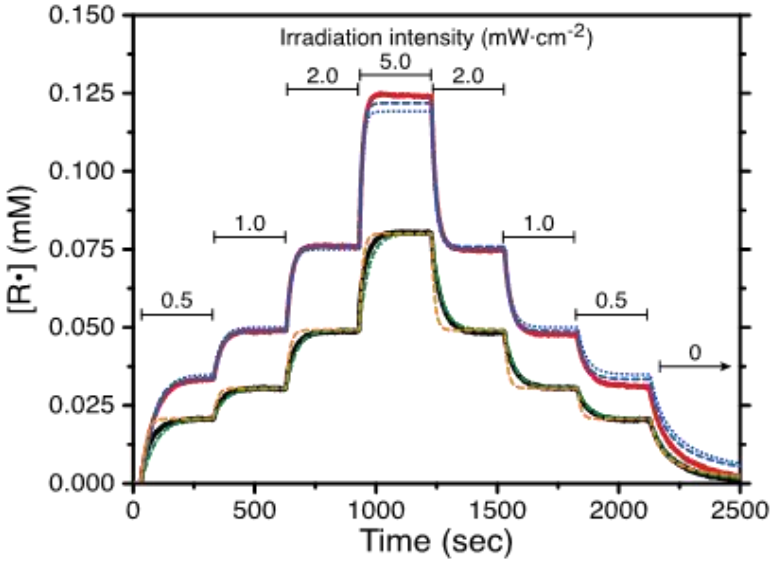

Figure 3.9. *Lophyl radical concentration versus time for 5 mM solutions of o-Cl-HABI (black) and p-HOH-HABI (red) in toluene, irradiated at varying intensities as shown. Radical concentration predictions for p-HOH-HABI (blue) and o-Cl-HABI (green) solutions were performed using second and 3/2 order rate constants, respectively derived from EPR (dashed lines) and UV-vis (dotted lines) experiments. A radical concentration prediction for the o-Cl-HABI solution was also performed using second order rate constants derived from EPR (orange dashed line).*

Table 3.5. *3/2 order o-Cl-HABI-derived lophyl radical recombination and first order o-Cl-HABI photodissociation rate constants for EPR spectroscopy-measured HABI photolysis in toluene solution under irradiation with 455 nm light and in the dark.*

$[HABI]_0$ (mM)	I_0 (mW·cm^{-2})	k_{rec} (mM$^{-0.5}$·sec^{-1})	k_{dis} (sec^{-1})
5.0	0.5	4.68×10^{-2}	0.56×10^{-4}
	1.0	4.21×10^{-2}	0.90×10^{-4}
	2.0	3.75×10^{-2}	1.64×10^{-4}
	5.0	3.28×10^{-2}	2.99×10^{-4}
0.5	5.0	3.89×10^{-2}	5.49×10^{-4}
1.0		3.40×10^{-2}	4.62×10^{-4}
2.5		3.23×10^{-2}	3.31×10^{-4}
5.0		3.17×10^{-2}	2.95×10^{-4}

3.5 Conclusion

The recombination of lophyl radicals generated by HABI photodissociation proceeds *via* a complex mechanism that cannot always be described by simple bimolecular reactions that obey second order kinetics and is dependent on the HABI molecular structure. The investigated photodissociation kinetics reveal that, upon irradiation at relatively low intensities, HABI compounds rapidly generate appreciable lophyl radical concentrations in solution that are comparable to those obtained during cross-linking polymerization reactions, radicals which subsequently recombine over

several minutes upon irradiation cessation. Careful real-time lophyl radical concentration measurement during the photodissociation of two different HABI compounds in solution, *o*-Cl-HABI and *p*-HOH-HABI, and recombination of the generated lophyl radicals on irradiation cessation, revealed apparent second order radical recombination over short periods in the dark. However, over longer dark periods, the recombination rates were not adequately described by second order rate fits for *o*-Cl-HABI, although good second order recombination rate fits were maintained over extended dark periods for *p*-HOH-HABI at low initial HABI concentrations and low irradiation intensities, with increasing deviation from the described rate orders at raised initial HABI concentrations and incident irradiation intensities.

Examination of the dark recombination of *o*-Cl-HABI-derived lophyl radicals over extended time periods revealed improved description of the reaction as 3/2 order. The lophyl radical recombination rate constants calculated postulating a 3/2 order kinetic rate fit for *o*-Cl-HABI and a second order rate fit for *p*-HOH-HABI, in conjunction with steady state lophyl radical measurements, give HABI dissociation constants that, as expected, vary in direct proportion to irradiation intensity for *p*-HOH-HABI but deviate from this trend for *o*-Cl-HABI, suggesting a complex mechanism accounting for the 3/2 order recombination kinetics of *o*-Cl-HABI. For predictive purposes however, the rate constants for 3/2 order and second order lophyl radical recombination for *o*-Cl-HABI and *p*-HOH-HABI, respectively, and first order HABI photodissociation proved capable of accurately simulating radical concentration curves for both examined compounds under equivalent reaction conditions.

3.6 References

(1) Dröge, W. Free radicals in the physiological control of cell function. *Physiological Reviews* **2002**, *82*, 47-95.

(2) Halliwell, B.; Whiteman, M. Measuring reactive species and oxidative damage in vivo and in cell culture: How should you do it and what do the results mean? *British Journal of Pharmacology* **2004**, *142*, 231-255.

(3) Valko, M.; Leibfritz, D.; Moncol, J.; Cronin, M. T. D.; Mazur, M.; Telser, J. Free radicals and antioxidants in normal physiological functions and human disease. *International Journal of Biochemistry and Cell Biology* **2007**, *39*, 44-84.

(4) Braunecker, W. A.; Matyjaszewski, K. Controlled/living radical polymerization: Features, developments, and perspectives. *Prog. Polym. Sci.* **2007**, *32*, 93-146.

(5) Coseri, S. Phthalimide-N-oxyl (PINO) radical, a powerful catalytic agent: Its generation and versatility towards various organic substrates. *Catalysis Reviews - Science and Engineering* **2009**, *51*, 218-292.

(6) Sabacky, M. J.; Johnson Jr, C. S.; Smith, R. G.; Gutowsky, H. S.; Martin, J. C. Triarylmethyl radicals. Synthesis and electron spin resonance studies of sesquixanthydryl dimer and related compounds. *J. Am. Chem. Soc.* **1967**, *89*, 2054-2058.

(7) Amorati, R.; Lucarini, M.; Mugnaini, V.; Pedulli, G. F.; Minisci, F.; Recupero, F.; Fontana, F.; Astolfi, P.; Greci, L. Hydroxylamines as oxidation catalysts: Thermochemical and kinetic studies. *Journal of Organic Chemistry* **2003**, *68*, 1747-1754.

(8) Anderson, C. D.; Shea, K. J.; Rychnovsky, S. D. Strategies for the generation of molecularly imprinted polymeric nitroxide catalysts. *Organic Letters* **2005**, *7*, 4879-4882.

(9) Benoit, D.; Chaplinski, V.; Braslau, R.; Hawker, C. J. Development of a universal alkoxyamine for "living" free radical polymerizations. *J. Am. Chem. Soc.* **1999**, *121*, 3904-3920.

(10) Hawker, C. J.; Bosman, A. W.; Harth, E. New polymer synthesis by nitroxide mediated living radical polymerizations. *Chemical Reviews* **2001**, *101*, 3661-3688.

(11) Benoit, D.; Chaplinski, V.; Braslau, R.; Hawker, C. J. Development of a universal alkoxyamine for 'living' free radical polymerizations. *Journal of the American Chemical Society* **1999**, *121*, 3904-3920.

(12) White, D. M.; Sonnenberg, J. Oxidation of Triarylimidazoles. Structures of the Photochromic and Piezochromic Dimers of Triarylimidazyl Radicals. *Journal of the American Chemical Society* **1966**, *88*, 3825-3829.

(13) Maeda, K.; Hayashi, T. The Mechanism of Photochromism, Thermochromism and Piezochromism of Dimers of Triarylimidazolyl. *Bull. Chem. Soc. Jpn.* **1970**, *43*, 429-438.

(14) Riem, R. H.; MacLachlan, A.; Coraor, G. R.; Urban, E. J. The flash photolysis of a substituted hexaarylbiimidazole and reactions of the imidazolyl radical. *J Org Chem* **1971**, *36*, 2272-2275.

(15) Cohen, R. L. Substituent Effects on the Reactivity of Triarylimidazolyl Free Radicals toward Tris(2-methyl-4-diethylaminophenyl)methane. *Journal of Organic Chemistry* **1971**, *36*, 2280-2284.

(16) Cescon, L. A.; Coraor, G. R.; Dessauer, R.; Silversmith, E. F.; Urban, E. J. Some Properties of Triarylimidazolyl Radicals and Their Dimers. *Journal of Organic Chemistry* **1971**, *36*, 2262-2267.

(17) Kikuchi, A.; Iyoda, T.; Abe, J. Electronic structure of light-induced lophyl radical derived from a novel hexaarylbiimidazole with π-conjugated chromophore. *Chem. Commun.* **2002**, 1484-1485.

(18) Kishimoto, Y.; Abe, J. A fast photochromic molecule that colors only under UV light. *Journal of the American Chemical Society* **2009**, *131*, 4227-4229.

(19) Hatano, S.; Horino, T.; Tokita, A.; Oshima, T.; Abe, J. Unusual negative photochromism via a short-lived imidazolyl radical of 1,1′-binaphthyl-bridged imidazole dimer. *Journal of the American Chemical Society* **2013**, *135*, 3164-3172.

(20) Hayashi, T.; Maeda, K. Preparation of a new phototropic substance. *Bull. Chem. Soc. Jpn.* **1960**, *33*, 565-566.

(21) Dessauer, R.: The Invention of Dylux® Instant-Access Imaging Materials and the Development of HABI Chemistry—A Personal History. In *Adv. Photochem.*; John Wiley & Sons, Inc., 2005; pp 129-261.

(22) Liu, A. D.; Trifunac, A. D.; Krongauz, V. V. Photodissociation of hexaarylbiimidazole. 2. Direct and sensitized dissociation. *Journal of Physical Chemistry* **1992**, *96*, 207-211.

(23) Shi, Y.; Yin, J.; Kaji, M.; Yori, H. Synthesis of a novel hexaarylbiimidazole with ether groups and characterization of its photoinitiation properties for acrylate derivatives. *Polym. Eng. Sci.* **2006**, *46*, 474-479.

(24) Qin, X. Z.; Liu, A.; Trifunac, A. D.; Krongauz, V. V. Photodissociation of hexaarylbiimidazole. 1. Triplet-state formation. *Journal of Physical Chemistry* **1991**, *95*, 5822-5826.

(25) Lin, Y.; Liu, A.; Trifunac, A. D.; Krongauz, V. V. Investigation of electron transfer between hexaarylbiimidazole and visible sensitizer. *Chemical Physics Letters* **1992**, *198*, 200-206.

(26) Caspar, J. V.; Khudyakov, I. V.; Turro, N. J.; Weed, G. C. ESR study of lophyl free radicals in dry films. *Macromolecules* **1995**, *28*, 636-641.

(27) Abe, J.; Sano, T.; Kawano, M.; Ohashi, Y.; Matsushita, M. M.; Iyoda, T. Epr and density functional studies of light-induced radical pairs in a single crystal of a hexaarylbiimidazolyl derivative. *Angewandte Chemie - International Edition* **2001**, *40*, 580-582.

(28) Hayashi, T.; Maeda, K.; Takeuchi, M. A Kinetic Study of the Photochromism of 2,2′,4,4′,5,5′-Hexaphenyl-1,1′-biimidazolyl with Electron Spin Resonance. *Bull. Chem. Soc. Jpn.* **1964**, *37*, 1717-1718.

(29) Wilks, M. A. J.; Willis, M. R. Kinetics of the photochromic decay reaction of solutions of 2,2′,4,4′,5,5′-hexaphenyl bi-imidazolyl [11]. *Nature* **1966**, *212*, 500-502.

(30) Iwahori, F.; Hatano, S.; Abe, J. Rational design of a new class of diffusion-inhibited HABI with fast back-reaction. *Journal of Physical Organic Chemistry* **2007**, *20*, 857-863.

(31) Hatano, S.; Abe, J. Activation parameters for the recombination reaction of intramolecular radical pairs generated from the radical diffusion-inhibited HABI derivative. *Journal of Physical Chemistry A* **2008**, *112*, 6098-6103.

(32) Fujita, K.; Hatano, S.; Kato, D.; Abe, J. Photochromism of a radical diffusion-inhibited hexaarylbiimidazole derivative with intense coloration and fast decoloration performance. *Organic Letters* **2008**, *10*, 3105-3108.

(33) Takizawa, M.; Kimoto, A.; Abe, J. Photochromic organogel based on [2.2]paracyclophane-bridged imidazole dimer with tetrapodal urea moieties. *Dyes and Pigments* **2011**, *89*, 254-259.

(34) Kawai, S.; Yamaguchi, T.; Kato, T.; Hatano, S.; Abe, J. Entropy-controlled thermal back-reaction of photochromic [2.2]paracyclophane-bridged imidazole dimer. *Dyes and Pigments* **2012**, *92*, 872-876.

(35) Sato, H.; Kasatani, K.; Murakami, S. Magnetic field effects on the photochromism of hexaphenylbiimidazolyl. *Chemical Physics Letters* **1988**, *151*, 97-101.

(36) Miyamoto, Y.; Kikuchi, A.; Iwahori, F.; Abe, J. Synthesis and photochemical properties of a photochromic iron(II) complex of hexaarylbiimidazole. *Journal of Physical Chemistry A* **2005**, *109*, 10183-10188.

(37) Strehmel, V.; Wishart, J. F.; Polyansky, D. E.; Strehmel, B. Recombination of photogenerated lophyl radicals in imidazolium-based ionic liquids. *ChemPhysChem* **2009**, *10*, 3112-3118.

(38) Berdzinski, S.; Horst, J.; Straßburg, P.; Strehmel, V. Recombination of lophyl radicals in pyrrolidinium-based ionic liquids. *ChemPhysChem* **2013**, *14*, 1899-1908.

(39) Hayashi, T.; Maeda, K. Chemiluminescence of 2,3,4,5-Tetraphenylpyrrole. *B Chem Soc Jpn* **1962**, *35*, 2058-2059.

(40) Alberti, A.; Benaglia, M.; Macciantelli, D.; Rossetti, S.; Scoponi, M. Further EPR-spin trapping studies of the photoinitiating activity of Irgacure 369. *European Polymer Journal* **2008**, *44*, 3022-3027.

(41) Shida, T.; Maeda, K.; Hayashi, T. Optical and ESR Studies on Triphenylimidazolyl Radicals Produced by Photolysis and Radiolysis at Low Temperature. *B Chem Soc Jpn* **1970**, *43*, 652-657.

(42) Scott, T. F.; Cook, W. D.; Forsythe, J. S.; Bowman, C. N.; Berchtold, K. A. FTIR and ESR spectroscopic studies of the photopolymerization of vinyl ester resins. *Macromolecules* **2003**, *36*, 6066-6074.

(43) Berchtold, K. A.; Randolph, T. W.; Bowman, C. N. Propagation and termination kinetics of cross-linking photopolymerizations studied using electron paramagnetic resonance spectroscopy in conjunction with near IR spectroscopy. *Macromolecules* **2005**, *38*, 6954-6964.

(44) Hatano, S.; Abe, J. A peroxide-bridged imidazole dimer formed from a photochromic naphthalene-bridged imidazole dimer. *Physical Chemistry Chemical Physics* **2012**, *14*, 5855-5860.

(45) Edkins, R. M.; Probert, M. R.; Fucke, K.; Robertson, C. M.; Howard, J. A. K.; Beeby, A. The formation of peroxide degradation products of photochromic triphenylimidazolyl radical-dimers. *Phys. Chem. Chem. Phys.* **2013**, *15*, 7848-7853.

Chapter 4

Rapid, photo-mediated healing of hexaarylbiimidazole-based covalently cross-linked gels

4.1 Abstract

The intrinsic healing of covalently cross-linked polymer networks is commonly effected *via* the utilization of backbone-borne functional groups able to reversibly cleave or rearrange, thereby enabling mixing and co-reaction of network strands that bridge contacted interfaces; however, such materials often exhibit slow healing rates and are susceptible to creep under load. To address these deficiencies, we incorporated hexaarylbiimidazole (HABI) functionalities, groups that are homolytically cleavable to yield relatively low reactivity lophyl radicals under UV or visible light irradiation and which, in the absence of light, spontaneously recombine without significantly participating in deleterious side reactions, into the backbone of poly(ethylene glycol)-based polymeric gels. Whereas the network connectivity of these HABI-incorporating gels was stable in the dark, they exhibited significant creep upon irradiation. The influence of swelling solvent on the reaction kinetics of backbone-borne HABI photolysis and lophyl radical recombination were examined and revealed that gels swollen with 1,1,2-trichloroethane (TCE) exhibited higher radical concentrations than those swollen with either acetonitrile or water under equivalent irradiation conditions, attributable to the relative solvent affinity for the hydrophobic HABI functionalities affording more rapid

HABI cleavage and slower radical recombination rates in TCE than in water. The fastest healing rates for cleaved samples brought into contact and irradiated with visible light was observed for TCE-swollen gels, although rapid restoration of mechanical integrity was achieved for gels swollen with any of the solvents examined where tensile strengths approached those of the pristine materials after 1 to 3 minutes of light exposure.

4.2 Introduction

Significant research attention has been devoted towards reversible crack-healing and autonomic healing of cross-linked polymeric matrices in recent years owing to the potential for successful implementations to yield tremendous improvements in reconfigurability, longevity, and reliability of these materials.[1-3] To date, crack-healing approaches in covalently cross-linked polymers typically utilize either systems that incorporate non-load bearing, liquid-filled inclusions, such as capsules or channels, whose contents flow upon rupture and polymerize *in situ* to bridge the flaw interfaces,[4-6] or that incorporate dynamic covalent functional groups, moieties able to be rearranged or reverted back to their constituent reactants under specific reaction conditions, in their backbone to effect transient depolymerization or bond rearrangement.[7] Unfortunately, despite their utility, the incorporation of continuously-active dynamic covalent chemistries in the network strands of a cross-linked polymer often results in creep under mechanical loads at ambient temperature,[8-12] a significantly deleterious trait for stress-bearing materials. Additionally, the healing rates typically exhibited by these materials are relatively slow, where the healing processes proceed over the course of hours to days.[11-14] More desirable would be the incorporation of a dynamic chemistry that only

proceeds upon application of a specific stimulus, mitigating the potential for creep. Moreover, achieving intrinsic crack healing in cross-linked polymers necessitates not only bond rearrangement, but the rearrangement reaction should ideally occur on a sufficiently long timescale to allow segmental diffusion and mixing to quickly bridge the fracture surfaces and effect rapid healing of the damaged region.

A commonly employed stimulus to afford an intrinsic healing ability in cross-linked polymers is heat, where the incorporation of thermally-reversible adducts in network strands provides a mechanism for bond cleavage and rearrangement at raised temperatures which, if above the material's glass transition temperature, concurrently affords the molecular mobility necessary to bridge defects and effect healing.[15] Although the typically poor spatial and temporal reaction confinement of this healing stimulus can be addressed in part by photothermal heating,[16,17] enabling heating to be confined to the vicinity of the defect in the polymer network, intolerance of the raised temperatures necessary for bond rearrangement in these materials precludes their consideration for many applications.[18] In contrast, the incorporation of functional groups that undergo triggered, reversible cleavage or bond rearrangement reactions at ambient temperatures would afford healable materials with broader utility.

Unlike thermoreversible networks, photoreversible networks only undergo bond rearrangement upon irradiation, otherwise exhibiting little to no creep or adaptation in the absence of irradiation. Furthermore, photochemical approaches enable three-dimensional spatial control of the healing reaction as well as the ability to remotely trigger a process on and off. Several approaches to photochemically triggered rearrangeable polymer networks have been developed, including photoinduced cyclization and photo-mediated

metathesis, among other reactions.[19,20] The photocyclization reactions, exhibited by functional groups such as cinnamate,[21,22] coumarin,[23-25] and anthracene[26,27] derivatives, exhibit limited relative response rates as at most a single cross-link is reversibly broken for each absorbed photon at relatively low quantum yields,[28,29] and require irradiation at ultraviolet (UV) wavelengths to realize both the forward and reverse reactions.[30] Conversely, photo-mediated metathesis reactions are effected in covalently cross-linked polymer networks by incorporating functional groups which undergo a network rearrangement cascade, such as disulfides,[31] thiuram disulfides,[13] allyl sulfides,[32,33] and trithiocarbonates,[34] where multiple reversible bond breaking and re-forming reactions occur for each absorbed photon.[33] However, as the chain transfer mechanism does not afford any significant fraction of network strands being cleaved at a given instant,[32,33] this approach again results in sluggish healing rates[13,34] owing to limited segmental diffusion. Several other reactions employed for the photo-mediated repair of cross-linked polymers include the photodissociation of alkoxyamine groups,[35] radical-mediated polyurea-to-polyurethane conversion in oxetane- and oxolane-substituted chitosan-polyurethane networks,[36,37] and Si–O–Si covalent bond reformation mediated by Cu–O coordination complexes,[38] each of which proceeds under UV irradiation for multiple hours.

Here, we describe an approach to address the deficiencies of contemporary, intrinsically-healable cross-linked polymers by incorporating hexaarylbiimidazole (HABI) functionalities, dimers of triphenyl-substituted imidazoles,[39] in the backbone of polymeric gels. HABIs are photosensitive groups that undergo reversible, homolytic cleavage of the carbon-nitrogen (C–N) bond between the imidazole rings to efficiently afford two teal-colored 2,4,5-triarylimidazoyl (lophyl) radicals which thermally

recombine to reproduce the original imidazole dimer (see Scheme 4.1a).[40] With some notable exceptions (e.g., nitroxides), organic radicals are typically highly reactive species that recombine at diffusion-controlled rates;[41] in contrast, the lophyl radicals generated by HABI homolysis are insensitive to atmospheric oxygen and show extraordinarily slow recombination rates,[42] attributable to their unique chemical structure affording stabilization by steric hindrance and electron delocalization.[43] Thus, owing to the low reactivity and long lifetime of the lophyl radicals originating from HABI photolysis, cross-linked polymers bearing HABI-containing network strands offer a unique mechanism for intrinsically-healable materials.

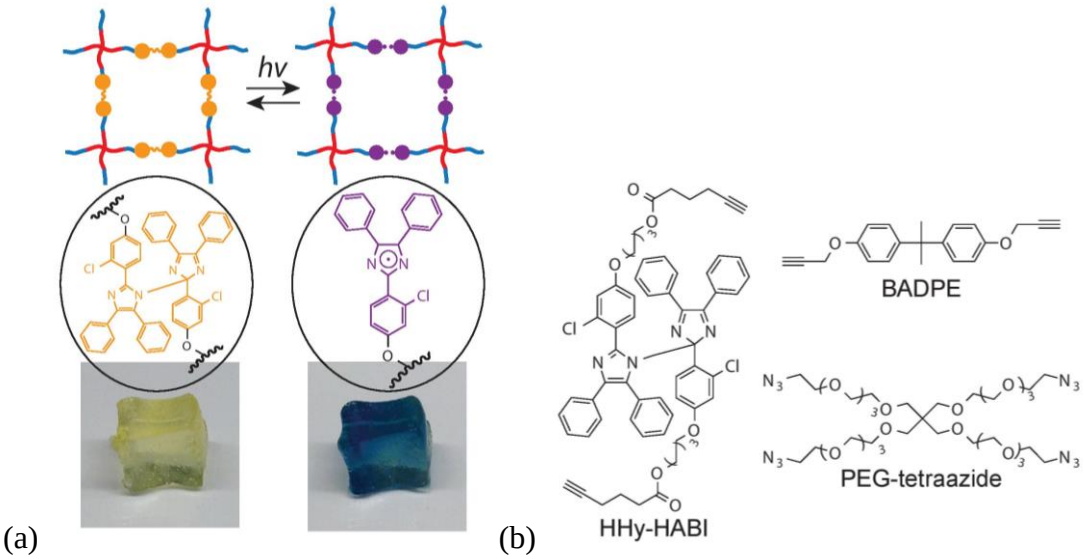

(a) (b)

Scheme 4.1. *Mechanism and structures of materials used. (a) Reversible photocleavage of cross-linked gels incorporating HABI moieties upon visible light irradiation to afford lophyl radicals, the recombination of which proceeds over several minutes, is visualized as a yellow/teal color change. (b) Dialkynyl monomers 2,2'-bis-(2-chloro-4-hexyl hex-5-ynoate-phenoxy)-4,4',5,5'-tetraphenyl-1,2'-biimidazole (HHy-HABI) and bisphenol A dipropargyl ether (BADPE), and a tetra-azide monomer (PEG tetra-azide).*

4.3 Experimental

4.3.1 Materials

Four-arm PEG tetra-azide (molecular weight = 10 kg·mol^{-1}, Creative PEGWorks), copper(II) sulfate pentahydrate (Sigma-Aldrich), (+)-sodium L-ascorbate (Sigma-Aldrich), and 2,2-diphenyl-1-picrylhydrazyl (DPPH, Sigma-Aldrich) were used as received. Acetonitrile (Sigma-Aldrich), dimethylformamide (DMF, Fisher Chemical), and 1,1,2-trichloroethane (TCE, Acros Organics) were used as solvent for all samples. 2,2′-Bis(2-chloro-4-hexan-1-ol-phenoxy)-4,4′,5,5′-tetraphenyl-1,2′-biimidazole (**1**) was synthesized as described previously,[42] whereas the dialkynyl monomers were synthesized as described below. Structures of all monomers used in this study are shown in Scheme 4.1b.

4.3.2 Synthesis

4.3.2.1 Synthesis of 2,2'-bis-(2-chloro-4-hexyl-hex-5-ynoate-phenoxy)-4,4',5,5'-tetraphenyl-1,2'-biimidazole (HHy-HABI).

A mixture of **1** (1.00 g, 1.12 mmol), 5-hexynoic acid (0.370 mL, 3.36 mmol), *N*,*N*′-diisopropylcarbodiimide (0.520 mL, 3.36 mmol), and 4-dimethylaminopyridine (74.5 mg, 0.610 mmol) in dichloromethane (50 mL) was stirred at room temperature for 16 hours under nitrogen. The solvent was removed under reduced pressure, and then the crude product was collected and purified by silica gel chromatography eluting with hexane/ethyl acetate (2/1, v/v) to afford 0.890 g of the dialkyne-substituted HHy-HABI (73.6% yield). ^{1}H NMR (400 MHz, DMSO-d_6), δ: 1.10-1.19 (m, 4H), 1.36-1.40 (m, 6H),

1.65-1.70 (m, 10H), 1.99-2.18 (m, 4H), 2.30-2.38 (m, 4H), 2.77-2.79 (m, 2H), 3.85-3.99 (m, 4H), 4.00-4.07 (m, 4H), 6.20-7.54 (m, 26H).

4.3.2.2 Synthesis of bisphenol A dipropargyl ether (BADPE).

Bisphenol A (5.00 g, 21.9 mmol) and potassium carbonate (9.08 g, 65.7 mmol) were added to 50 mL of DMF and the mixture stirred. Propargyl bromide solution (80 wt% in toluene, 7.32 mL, 65.7 mmol) was then added and the mixture heated at 70°C for 16 hours under nitrogen. After cooling to room temperature, the mixture was filtered to remove potassium carbonate, DMF was evaporated under reduced pressure, and the residue was purified by silica gel chromatography eluting with hexane/ethyl acetate (2/1, v/v), yielding 5.45 g of bisphenol A dipropargyl ether (81.8% yield). ^{1}H NMR (400 MHz, DMSO-d_6), δ: 1.59 (s, 6H), 3.50-3.51 (t, 2H), 4.74-4.76 (d, 4H), 6.85-6.89 (m, 4H), 7.11-7.15 (m, 4H).

4.3.2.3 Synthesis of cross-linked polymeric gels.

Dialkyne-functionalized monomer, either HHy-HABI (130 mg, 0.12 mmol) or BADPE (36.5 mg, 0.12 mmol), four-arm PEG tetra-azide (MW=10 kg·mol^{-1}, 0.602 g, 0.060 mmol), copper(II) sulfate pentahydrate (5.94 mg, 0.0238 mmol), and (+)-sodium L-ascorbate (23.6 mg, 0.119 mmol) were dissolved in *N*,*N*-dimethylformamide (DMF, 4.32 g). Gel films were fabricated by sandwiching the formulated monomer solutions between glass microscope slides separated by 250 μm shims. After polymerization overnight, the cross-linked polymeric films were removed from the glass slides and immersed in

acetonitrile for 24 hours then in water for a further 24 hours to ensure thorough extraction of residual solvent, copper catalyst, and reducing agent. Finally, the sample films were immersed in the desired solvent for 24 hours to complete the solvent exchange prior to use. For gels swollen with 1,1,2-trichloroethane (TCE), samples were initially immersed in acetonitrile prior to immersion in TCE owing to the immiscibility of deionized water and TCE.

Cylindrical gels were fabricated by injecting the formulated monomer solutions described above into 6 mm inner diameter poly(tetrafluoroethylene) tubing. After polymerization overnight, approximately 1 cm long sections of tubing were carefully removed from around the enclosed gels and the cylindrical samples were subjected to the extraction and solvent exchange steps described above. The residual copper content in HABI-incorporating gels digested by nitric acid prior to and after extraction, determined by inductively coupled plasma optical emission spectroscopy (ICP-OES, Perkin-Elmer Optima 2000 DV), revealed that the extraction procedure yielded a five-fold copper concentration decrease.

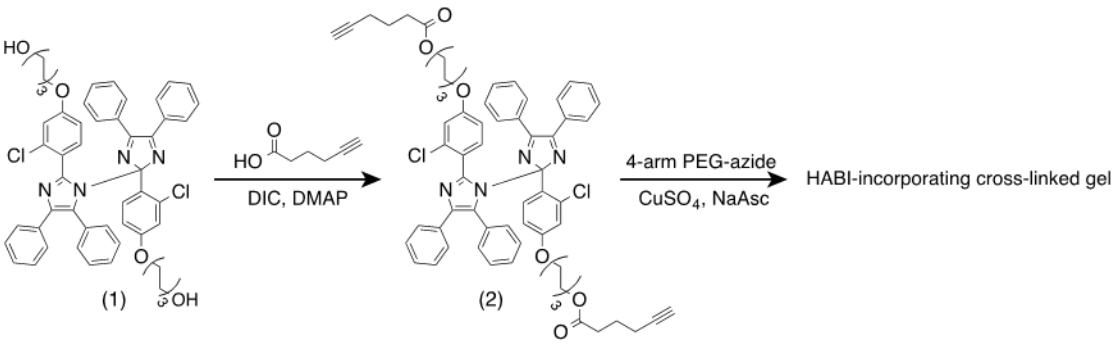

Scheme 4.2. *Synthesis of 2,2'-bis-(2-chloro-4-hexylhex-5-ynoate-phenoxy))-4,4',5,5'-tetraphenyl-1,2'-biimidazole (HHy-HABI, 2), a dialkyne-substituted HABI, and its subsequent polymerization via copper(I)-catalyzed azide-alkyne cycloaddition (CuAAC) to afford a HABI-incorporating cross-linked polymer gel.*

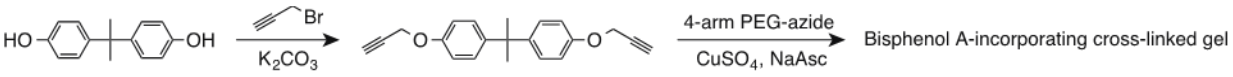

Scheme 4.3. *Synthesis of bisphenol A dipropargyl ether (BADPE) and subsequent polymerization via CuAAC to afford a cross-linked polymer gel unable to undergo homolytic cleavage under violet light irradiation and used as a negative control.*

4.3.3 Light sources and intensity measurement.

For the spectroscopy experiments, violet light was provided by a collimated, LED-based illumination source (Thorlabs M405L2-C) with an emittance centered at 405 nm (FWHM 13 nm), used in combination with a current-adjustable LED driver (Thorlabs LEDD1B) for intensity control. For the photo-mediated healing experiments, violet light was provided by 405 nm LED-based illumination source (Arroyo Instruments, 226 TEC LED Lasermount), used in combination with a current-adjustable LED driver (Arroyo Instruments, 6340 ComboSource Laser Diode Controller) and delivered via a bifurcated light guide. Irradiation intensities were measured with an International Light IL1400A

radiometer equipped with a broadband silicon detector (model SEL033), a 10× attenuation neutral density filter (model QNDS1), and a quartz diffuser (model W).

4.3.4 Ultraviolet-visible spectroscopy

UV-vis spectroscopy was performed on 250 μm thick film samples using an Agilent Technologies Cary 60 UV-vis spectrophotometer. Spectra were collected from 200 to 800 nm both in the dark and under irradiation once the radical concentration reached equilibrium. HABI photodissociation and subsequent recombination were examined by monitoring 609 nm, 597 nm, and 604 nm for the HABI-incorporating gels swollen by water, acetonitrile, and TCE, respectively, the wavelengths where the visible light absorbance by the generated lophyl radicals was greatest (i.e., λ_{max}), while the samples were irradiated with 405 nm for 2.5 min to ensure radical concentration equilibration and then for a further 7.5 min after the light was turned off. All kinetics experiments were performed in triplicate.

4.3.5 Electron paramagnetic resonance spectroscopy

Electron paramagnetic resonance (EPR) spectroscopy was performed with a Bruker EMX spectrometer. The spectrometer was equipped with a TE_{102} cavity (Bruker model ER 4102ST), and a frequency of 9.712 GHz, 2.05 mW microwave power, 5.02×10^4 receiver gain, 100 kHz modulation frequency, and 1 G modulation amplitude were used for all experiments. Optical access to the cavity was afforded by a 10 mm × 23 mm grid providing 50% light transmittance to the sample. For the sample preparation, a 1.1

mm inner diameter glass capillary tube was filled with 20 μL of sample formulation and allowed to react for 24 hours. After polymerization, each sample was rigorously extracted with acetonitrile and water to remove residual solvent, copper catalyst, and reducing agent, then immersed in the desired solvent to complete the solvent exchange prior to use. Each sample capillary tube was then inserted into a 3.2 mm inner diameter quartz sample tube and inserted again into the spectrometer cavity for analysis. The samples were irradiated *in situ* with 405 nm light and spectra were collected after 90 s when the radical concentration had reached steady state. Kinetics of photo-dissociation and dark recombination was performed by monitoring at a 3453 G static field, the first derivative signal intensity maximum for the HABI-incorporating gel under irradiation. All experiments were performed at room temperature. Radical concentrations were quantified by calibrating the EPR spectrum integral against known concentration solutions of DPPH in three solvents (water, acetonitrile, and TCE) using the same sample geometry, volume, and acquisition conditions employed for the HABI-incorporating polymeric gels (see Figure 4.1).

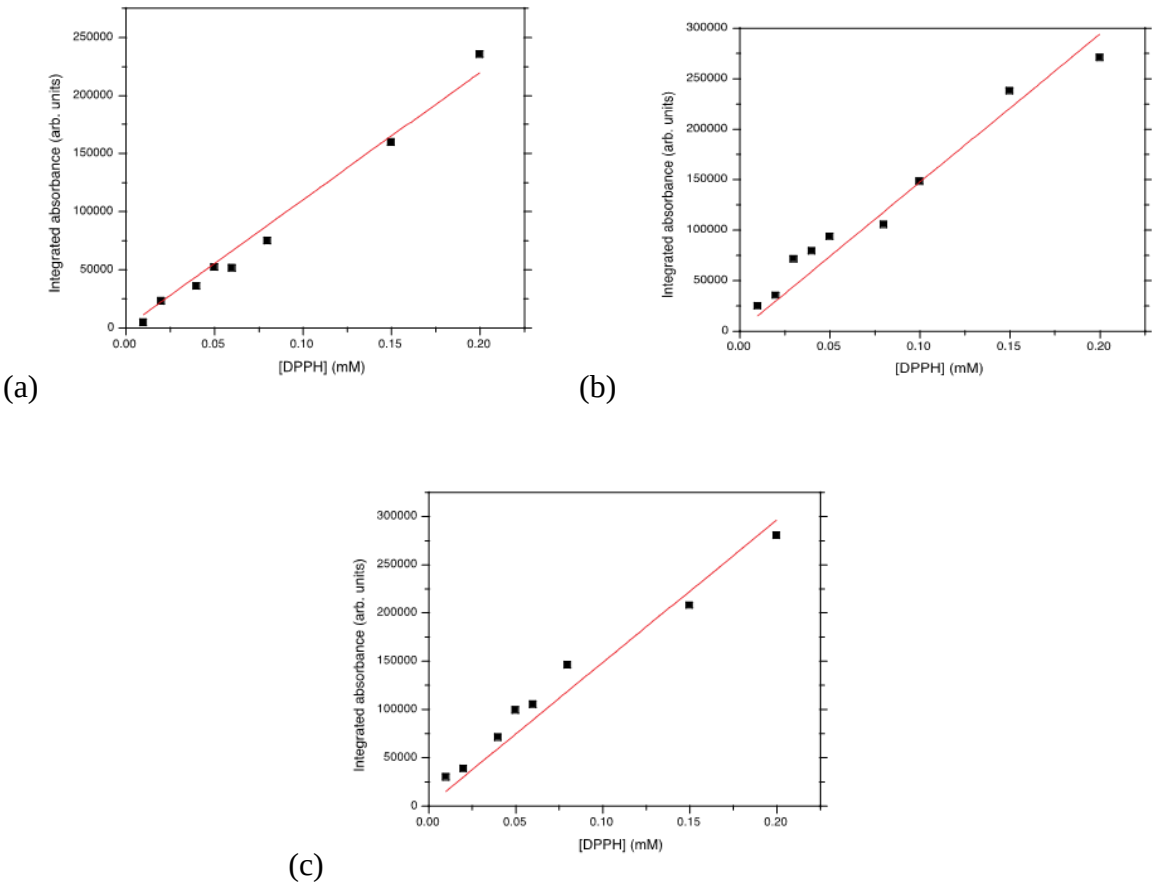

Figure 4.1. *EPR radical concentration calibration curves. Integrated absorbance, as determined by EPR spectroscopy, versus DPPH concentration for 20 μL of solution (black squares) in (a) water (least squares fit depicted by red line, y = 1062930x, r^2 = 0.983), (b) acetonitrile (red line, y = 1467580x, r^2 = 0.984), and (c) TCE (red line, y = 1477790x, r^2 = 0.983).*

4.3.6 Rheometry

Rheological measurements to monitor the polymerization of HABI- and bisphenol A-incorporating cross-linked gels were performed using a TA Instruments AR-G2 rheometer equipped with a 60 mm diameter parallel plate geometry. Immediately after preparation as described in the Experimental Section, 500 μL of a monomer formulation incorporating either HHy-HABI or BADPE was pipetted onto the lower plate of the rheometer fixture and the upper plate was lowered to achieve a gap of 300 μm. Time

sweep measurements were recorded at a rate of approximately one point every 9 seconds while applying a strain of 1% at a frequency of 1 Hz.

Photo-mediated creep tests were performed using the TA Instruments AR-G2 rheometer equipped with a parallel plate, UV-LED curing accessory consisting of a 20 mm diameter upper plate and a transparent, a quartz bottom plate, below which an LED array provides irradiation to the sample at a wavelength of 365 nm. HABI-containing cross-linked polymeric gel films were prepared as described in the Experimental Section, although 500 μm thick shims were used to separate the microscope slides, immersed in acetonitrile for solvent exchange, and mounted on the UV-LED test fixture. During the measurement, no shear stress was applied to the sample from t = 0 to 1 minute; however, from 1 minute through to the end of the experiment, a constant shear stress of 100 Pa was applied. From 3 minutes through 6 minutes, the gel films gels were subjected to alternating irradiation and dark periods of 15 and 45 seconds, respectively.

4.3.7 Swelling measurement

A 15 wt% HABI-incorporating gel was prepared and its swelling behavior in water, acetonitrile, and TCE was calculated from the volume of the polymeric gels in their dry and swollen states at room temperature. The swelling degree (*Q*), defined as the ratio of the volume of absorbed solvent to that of the dry polymer, was determined using the equation (eq. 1):

$$Q = \frac{V_{wet} - V_{dry}}{V_{dry}} \qquad (1)$$

where V_{wet} and V_{dry} are the volumes of the swollen and dry polymeric gels, respectively. The volume of absorbed solvent was determined from both the mass change of an initially dry sample after immersion in solvent for 24 hours in the dark and the density of the solvent.

4.3.8 Photo-mediated healing and mechanical testing

6 mm diameter cylindrical gel samples were sectioned perpendicular to their axes using a razor blade and the exposed surfaces were re-contacted immediately. The samples were then irradiated at room temperature with 405 nm light at 10 $mW \cdot cm^{-2}$, delivered to the vicinity of the re-contacted gel surfaces *via* a bifurcated light guide to ensure sufficient light penetration through the sample thickness, for different periods of time.

Pristine or healed polymeric gel samples were deformed in tension under air at room temperature using an electromechanical test machine (TestResources 100Q1000) equipped with a 25 lb load cell (TestResources SM-25-294) at a crosshead speed of 0.1 $mm \cdot sec^{-1}$. All experiments were performed in triplicate.

4.4 Results and discussion

The utilization of reactive functional groups such as HABIs to afford intrinsically-healable, covalently cross-linked polymers necessitates the incorporation of these functionalities in the network backbone. Cross-linked polymers incorporating HABI functional groups have been synthesized previously,[44-47] one approach being to treat

polymers bearing triaryl-substituted imidazole pendant groups, synthesized *via* a radical-mediated, chain growth polymerization mechanism, with potassium ferricyanide to oxidize the imidazole groups and yield HABI cross-links.[44,46,47] Notably, this synthetic approach affords cross-linked particles which would require further treatment to yield monolithic materials. In contrast, the cross-linked gels examined here were synthesized by treating solutions of PEG tetra-azide and a dialkynyl monomer, where the polymerizable moieties flank either side of the monomer core, in DMF with $CuSO_4$ and sodium ascorbate to effect polymerization by Cu(I)-catalyzed azide-alkyne cycloaddition (CuAAC), thereby ensuring incorporation of either the HABI or bisphenol A functional groups in the backbone of the resultant cross-linked, monolithic gels. The progress of these CuAAC polymerizations were monitored by parallel plate rheometry (see Figure 4.2a and 2b), revealing that gelation, determined here by the crossover in the storage and loss moduli,[48] occurred after approximately 10 minutes and 75 minutes for the HABI- and bisphenol A-based formulations, respectively. Although unexpected, the relatively rapid reaction rate observed for the HABI-based system is perhaps a result of the imidazole moiety acting as a ligand for the generated Cu(I) species,[49,50] increasing its stability and improving its catalytic activity. Nevertheless, a storage modulus plateau of ~10 kPa was achieved within 4 hours for both systems, indicating reaction completion after that time and assuring that the overnight reaction used to synthesize cross-linked samples was sufficient for full polymerization.

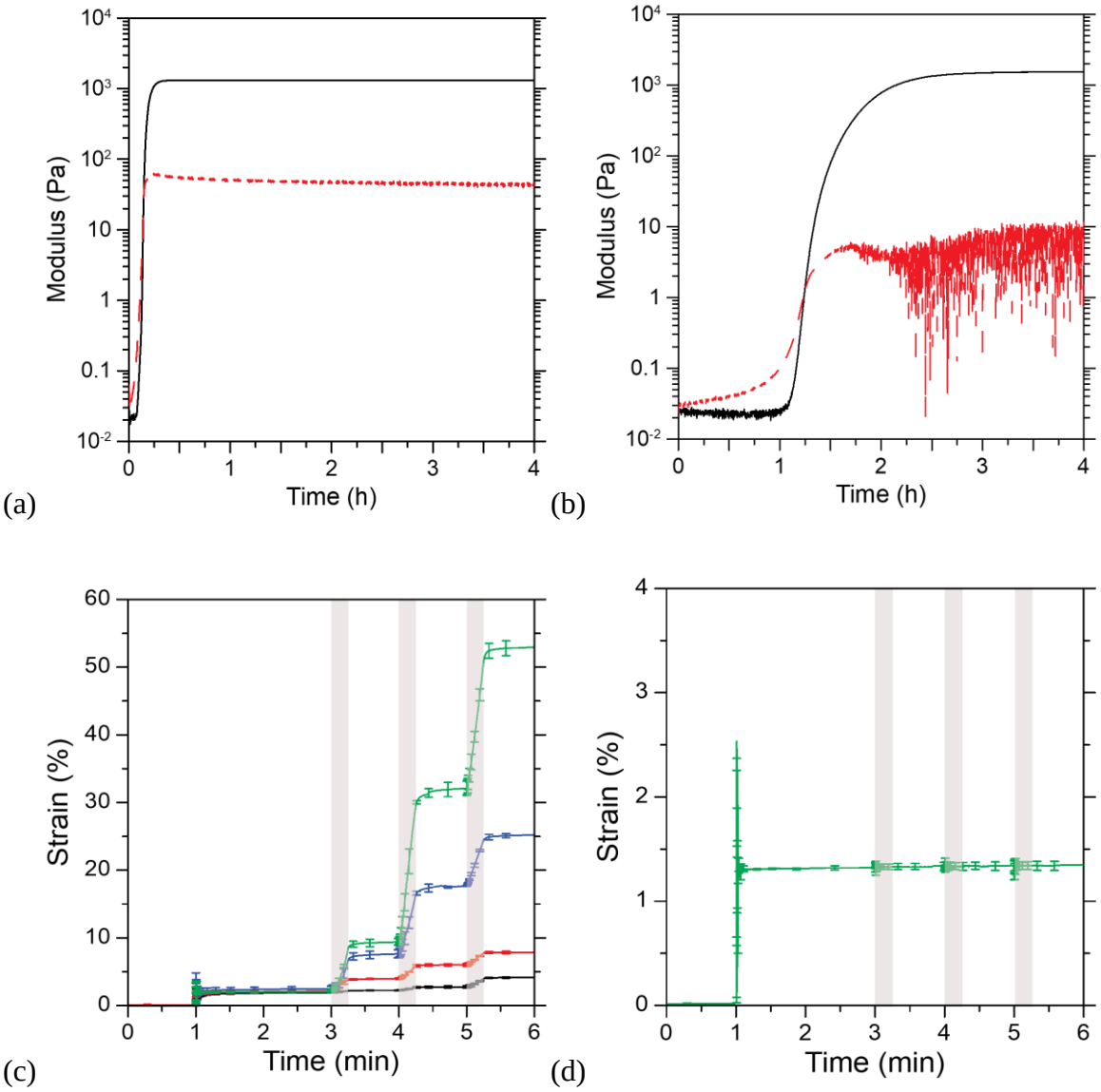

Figure 4.2. *Rheological characterization of covalently cross-linked gels. The CuAAC-mediated polymerization between a 4-arm PEG tetra-azide and either (a) HHy-HABI or (b) BADPE in DMF solution, monitored by oscillatory parallel plate rheometry (storage modulus, solid black line; loss modulus, dashed red line). The photo-induced creep of gel films, swollen with acetonitrile and incorporating (c) HABI or (d) bisphenol A functional groups in their backbone, under 100 Pa shear stress (initially applied at 1 min) and intermittently irradiated with 365 nm light at 0.5 (black), 1 (red), 3 (blue), and 5 (green) mW·cm^{-2}. The periods of irradiation are indicated by the shaded regions, and the experiments were performed in triplicate.*

As noted above, covalently cross-linked, photo-reversible networks undergo network connectivity rearrangement exclusively under irradiation and consequently should undergo plastic deformation upon irradiation while not exhibiting significant creep in the absence of exposure to light. To confirm whether the HABI-incorporating gels exhibited this property and thus held promise as photo-healable materials, gel films swollen with acetonitrile were mounted in a parallel plate rheometer, equipped with a UV curing accessory to enable irradiation of the sample, and subjected to a constant shear stress with alternating periods of irradiation and darkness (see Figure 4.2c and 2d). The initial application of shear stress in the dark to the HABI-incorporating films resulted in consistent elastic deformation of the samples with no discernable creep for the duration of the experiment; however, significant plastic deformation proceeded immediately upon exposure of the samples to UV irradiation for all intensities examined (Figure 4.2c), indicating that the network rearrangement necessary for the photo-mediated healing of this material does proceed under light exposure. Increasing the irradiation intensity afforded raised rates and extents of plastic deformation, attributable to the photolysis reaction equilibrium progressively tending towards the cleaved state (see Scheme 4.1a), increasing the network rearrangement rate. Notably, the observed creep under irradiation did not discontinue immediately upon cessation of light exposure; rather, although the creep rate did rapidly decrease, plastic deformation continued for several seconds after terminating the irradiation, an effect most apparent at the highest light intensity examined. This delayed cessation of plastic deformation is indicative of the stability and slow recombination of lophyl radicals, resulting in a continued, though progressively diminished, capacity for network rearrangement immediately after exposure of the

samples to light is ceased. The bisphenol A-based gel films, employed here as a light-insensitive, negative control material, similarly exhibited constant elastic deformation upon application of shear stress; however, in contrast to the HABI-incorporating films, they did not exhibit any discernable creep under irradiation (Figure 4.2d), indicating an absence of photo-induced network rearrangement in this material.

The photo-mediated cleavage of HABI moieties within polymeric gels in response to visible light irradiation at 405 nm was further examined using UV-vis spectrophotometry by *in situ* sample irradiation to determine the influence of varying incident irradiation intensity and swelling solvent (see Figure 4.6). Prior to irradiation, the HABI-incorporating gels exhibited weak absorption tails extending into the visible spectral region; however, irradiation at 405 nm irradiation resulted in a dramatic color change from yellow to teal (see Scheme 4.1a) and the emergence of an absorbance peak in the visible region (λ_{max} = 609, 597, and 604 nm in water, acetonitrile, and TCE, respectively), which became progressively stronger with raised irradiation intensity (Figure 4.3 and 4.6a), attributable to generation of the visible light-absorbing lophyl radical.[42] Subsequently ceasing irradiation of the gels resulted in complete reversion of their color from teal back to yellow and corresponding disappearance of the visible region absorption peak over the course of several minutes. The capacity of the gels in the three solvents examined (i.e., water, acetonitrile, and TCE) to generate radicals in response to 405 nm irradiation was confirmed by EPR spectroscopy. Whereas studies examining photoinitiator photolysis commonly employ spin traps[51] or the severely restricted molecular mobility at low temperatures[52] to attain detectable radical concentrations, the low recombination rates of lophyl radicals generated by HABI

photolysis affords sufficient radical concentrations for facile detection at room temperature.[40,42,53] Although no radicals were observed in the EPR spectra of the HABI-incorporating gels in the absence of light, significant radical formation proceeded upon irradiation, the concentration of which increased with raised irradiation intensity (Figure 4.3 and 4.6b), establishing the visible absorbance peaks as attributable to HABI-derived lophyl radical formation.[42,53] In contrast, no radicals were observed in the bisphenol A-incorporating gels under any of the irradiation intensities at 405 nm examined, irrespective of the solvent employed to swell the gels (see Figure 4.4), confirming the stability of this polymer network under visible light irradiation.

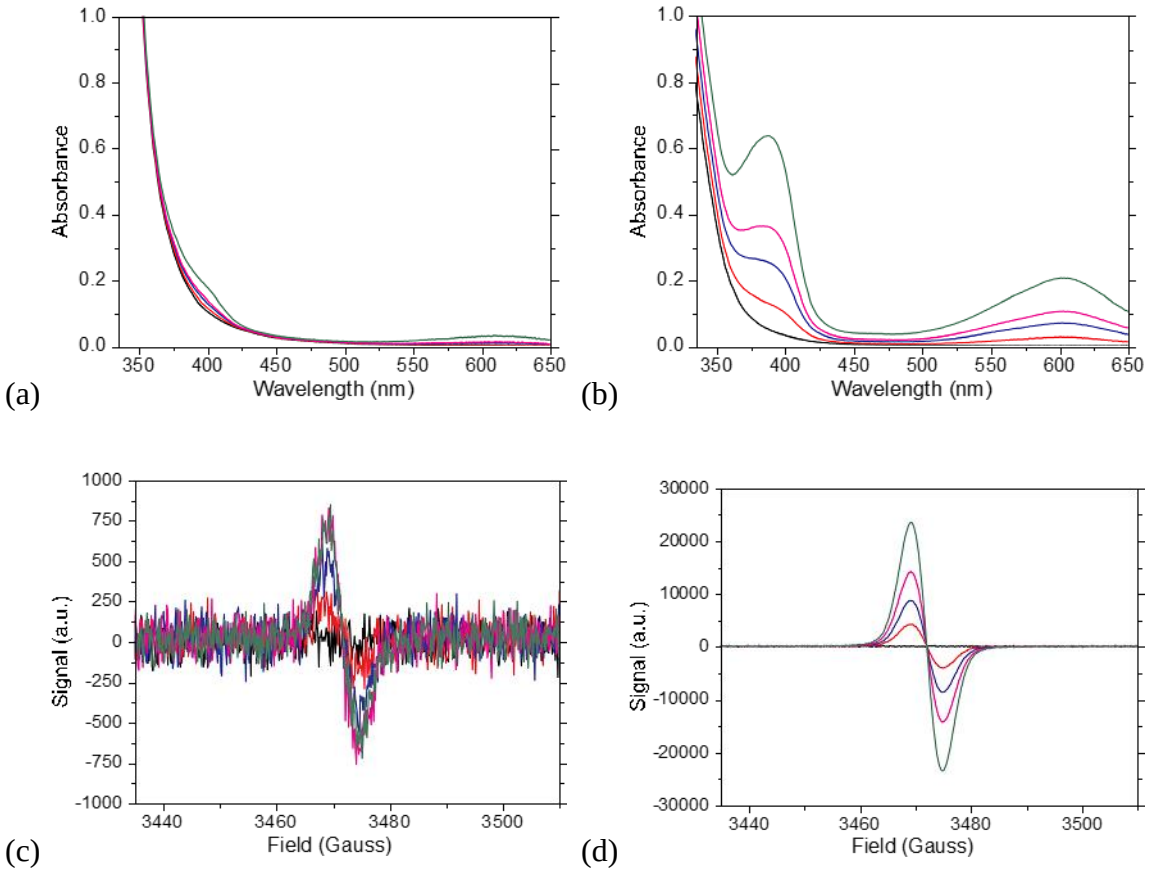

Figure 4.3. *UV-vis absorbance spectra of HABI-based gels in (a) water and (b) TCE, and EPR spectra of HABI-based gels in (c) water and (d) TCE, prior to (black) and at equilibrium during 405 nm irradiation at intensities of 1 mW·cm^{-2} (red), 5 mW·cm^{-2} (blue), 10 mW·cm^{-2} (magenta), and 50 mW·cm^{-2} (green).*

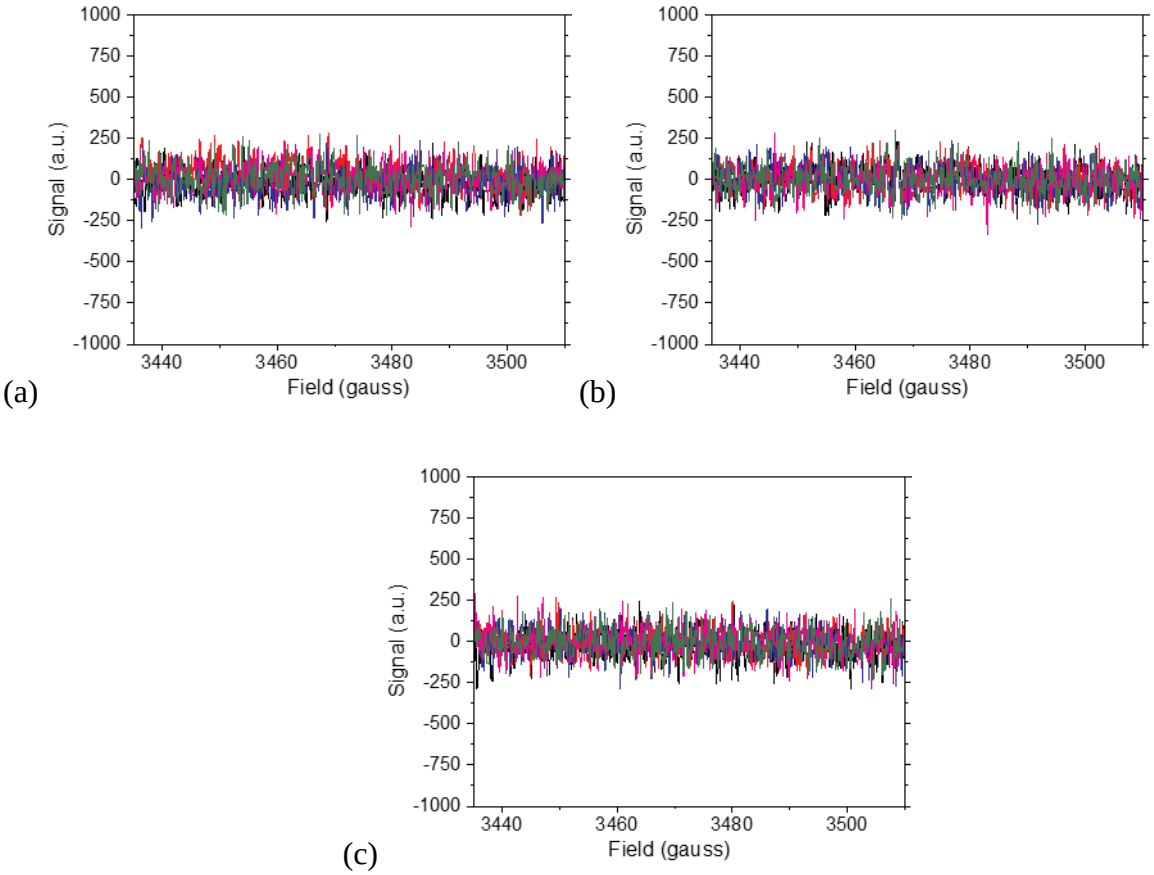

Figure 4.4. *EPR spectra of bisphenol A-based gels in (a) water, (b) acetonitrile, and (c) TCE, prior to (black) and after 90 s irradiation under 405 nm at intensities of 1 mW·cm^{-2} (red), 5 mW·cm^{-2} (blue), 10 mW·cm^{-2} (magenta), and 50 mW·cm^{-2} (green).*

To further characterize the influence of solvent and irradiation intensity on network strand cleavage of the HABI-incorporating gels, reaction kinetics experiments to examine photodissociation and lophyl radical recombination rates were performed. Here, HABI-incorporating gels were subjected to cycles of alternating light and dark periods at progressively raised irradiation intensities while monitoring either λ_{max} by UV-vis spectrophotometry (Figure 4.6c) or the radical concentration by EPR spectroscopy (Figure 4.6d). Whereas UV-vis spectrophotometry data were used to examine reaction rate orders owing to their low noise, data obtained by EPR spectroscopy were used to

determine kinetic rate constants given the direct measurement of radicals afforded by that technique. As is apparent from this spectroscopic characterization, the solvent used to swell the gels greatly affected the concentration of lophyl radicals generated. The equilibrium functional group dissociation in TCE was approximately double that in acetonitrile and an order of magnitude greater than that in water (Figure 4.6d), attributable to a higher affinity of the hydrophobic HABI groups and, upon photolysis, resultant lophyl radicals for TCE than for acetonitrile or water. This is supported by swelling measurements performed in the dark where, in contrast to previously-reported swelling behavior of cross-linked, PEG diacrylate gels which were most swollen by water and less so by acetonitrile and toluene,[54] the HABI-incorporating gels were most swollen by, and hence had the highest affinity for, TCE and least by water (see Figure 4.5). Notably, since two lophyl radicals result from every HABI bond broken, the maximum percentage of cleaved network strands was 0.07, 0.35, and 0.64% for HABI-incorporating gels swollen with water, acetonitrile, and TCE, respectively, under 405 nm light irradiation at 50 $mW \cdot cm^{-2}$, one to two orders of magnitude greater than contemporary polymer networks incorporating radical-mediated, dynamic covalent bonds such as those incorporating diarylbibenzofuranone (DABBF) groups in their backbone where less than 0.01% of the DABBF network strands are dissociated even at 50°C.[55] A small decrease in the absorbance at λ_{max} for the HABI-incorporating gels swollen with water and TCE while under the highest irradiation intensity investigated indicated that, instead of exclusively participating in self-recombination, some of the generated lophyl radicals were being consumed in an irreversible side reaction, potentially owing to the

susceptibility of the residual copper azide-alkyne cycloaddition catalyst to radical-mediated reduction from Cu(II) to Cu(I).[56]

(a) 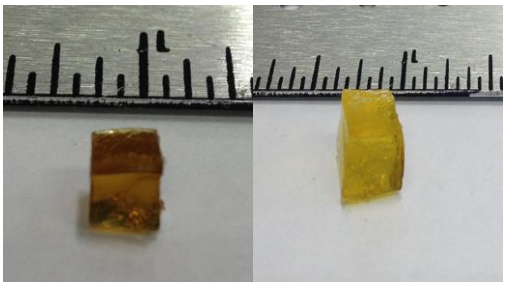 (b) 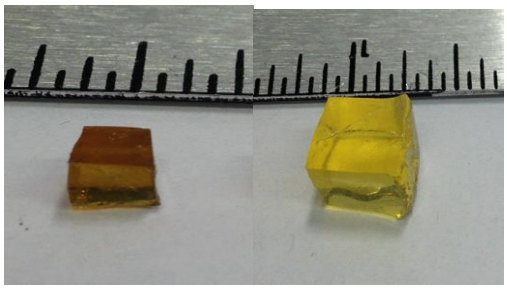

(c) 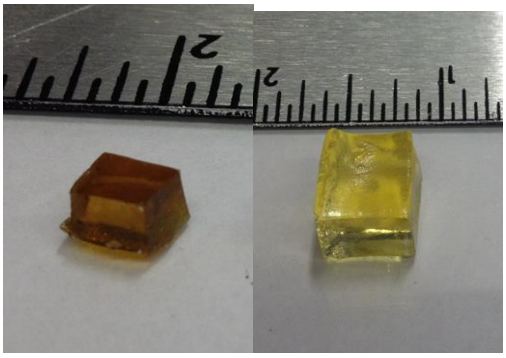

(d)

Solvent	*Q*
Water	4.4
Acetonitrile	8.3
TCE	10.8

Figure 4.5. *Swelling behavior of HABI-incorporating gels swollen with different solvents. Photographs of 15 wt% HABI-incorporating polymeric gels in their dry (left) and swollen (right) state in (a) water, (b) acetonitrile, and (c) TCE, and (d) their swelling degrees (Q).*

The reversible HABI photocleavage mechanism described in Scheme 4.1a suggests that the lophyl radical recombination should proceed as a second order reaction; however, we previously established that this reaction can be described by either 1.5 or second order reaction kinetics, depending on the structure of the parent HABI compound.[42] Although fitting of the λ_{max} absorbance curves (presented in Figure 4.6c) during lophyl radical recombination in the dark revealed that lophyl recombination was

well described as a near-second order reaction for HABI-incorporating gels swollen with TCE (see Figure 4.7), the recombination reaction for acetonitrile- and water-swollen gels was better fit by 1.6 and 1.2 order kinetics, respectively (Figure 4.7). Notably, radical diffusion-inhibited HABI derivatives have exhibited rapid, first order lophyl radical recombination kinetics.[57,58] Thus, the respective reaction orders for the recombination of network backbone-borne lophyl radicals suggest that, whereas the HABI groups for gels swollen with TCE are not subject to significant diffusion inhibition, HABIs in gels swollen with acetonitrile or water may be subject to partial diffusion inhibition, yielding sub-second order recombination behavior. Thus, despite the structural similarity between the respective chromophores of HHy-HABI and **1**, a HABI-derived compound which affords radicals that recombine according to second order kinetics,[42] we analyzed the HHy-HABI photolysis and lophyl radical recombination results shown in Figure 4.6d by assuming first and sub-second order reactions, respectively (see Table 4.1). As expected, the dissociation rate constant k_{dis} increased with raised irradiation intensity. Moreover, under equivalent irradiation conditions, k_{dis} was lowest for water and highest for TCE, attributable to the relative affinities the HABI functional group had for the examined solvents as described above. Although their dissimilar reaction orders impede direct comparison of the recombination rate constants (k_{rec}) for each respective gel, only minor k_{rec} variation was observed for each gel as the irradiation intensity was varied.

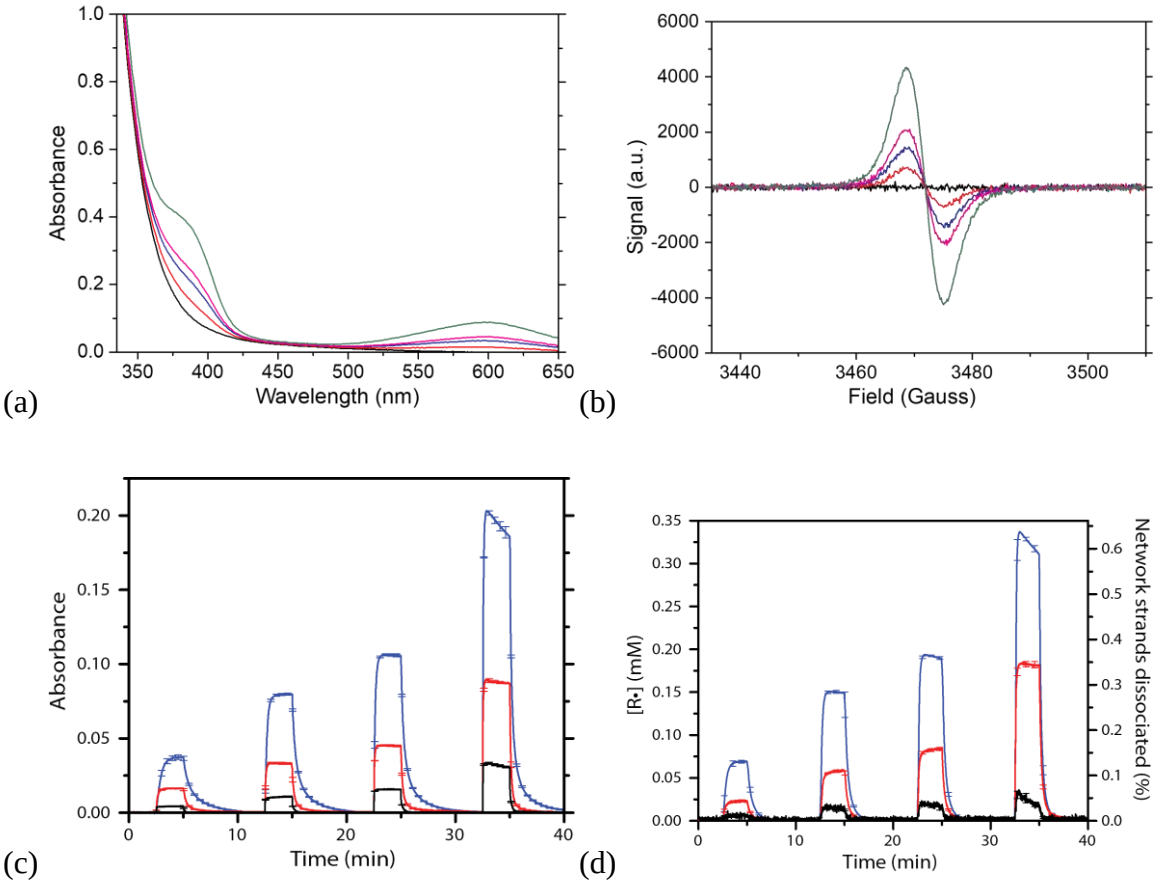

Figure 4.6. *UV-Vis and EPR with kinetics. (a) UV-vis and (b) EPR spectra of HABI-incorporating gels swollen with acetonitrile at equilibrium under irradiation with 405 nm light at 0 (black), 1 (red), 5 (blue), 10 (green), and 50 (magenta) mW·cm^{-2}. (c) Absorbance at λ_{max} as determined by UV-vis spectrophotometry, and (d) lophyl radical concentration and network strands dissociated as determined by EPR spectroscopy, of HABI-incorporating gels swollen with water (black), acetonitrile (red), and TCE (blue) under alternating conditions of darkness and irradiation with 405 nm light at 1 (2.5 – 5 minutes), 5 (12.5 – 15 minutes), 10 (22.5 – 25 minutes), and 50 (32.5 – 35 minutes) mW·cm^{-2}.*

Table 4.1. *Sub-second-order lophyl radical recombination (k_{rec}) and first order HABI photodissociation (k_{dis}) rate constants for photolysis under varying irradiation intensities (I_0) with 405 nm light and in the dark of HABI-incorporating gels swollen with varying solvents.*

I_0 (mW·cm^{-2})	$k_{rec} \times 10^1$		
	Water (mM$^{-0.2}$·sec^{-1})	Acetonitrile (mM$^{-0.6}$·sec^{-1})	TCE (mM$^{-0.9}$·sec^{-1})
5	1.13 ± 0.03	1.96 ± 0.04	1.86 ± 0.09
10	1.06 ± 0.03	1.54 ± 0.02	1.45 ± 0.07
50	0.94 ± 0.02	1.36 ± 0.03	1.46 ± 0.05
I_0 (mW·cm^{-2})	k_{dis} (sec^{-1}) × 10^4		
	Water	Acetonitrile	TCE
5	0.58 ± 0.02	1.55 ± 0.03	3.88 ± 0.20
10	0.81 ± 0.02	2.19 ± 0.03	4.96 ± 0.23
50	1.32 ± 0.03	6.75 ± 0.13	14.06 ± 0.53

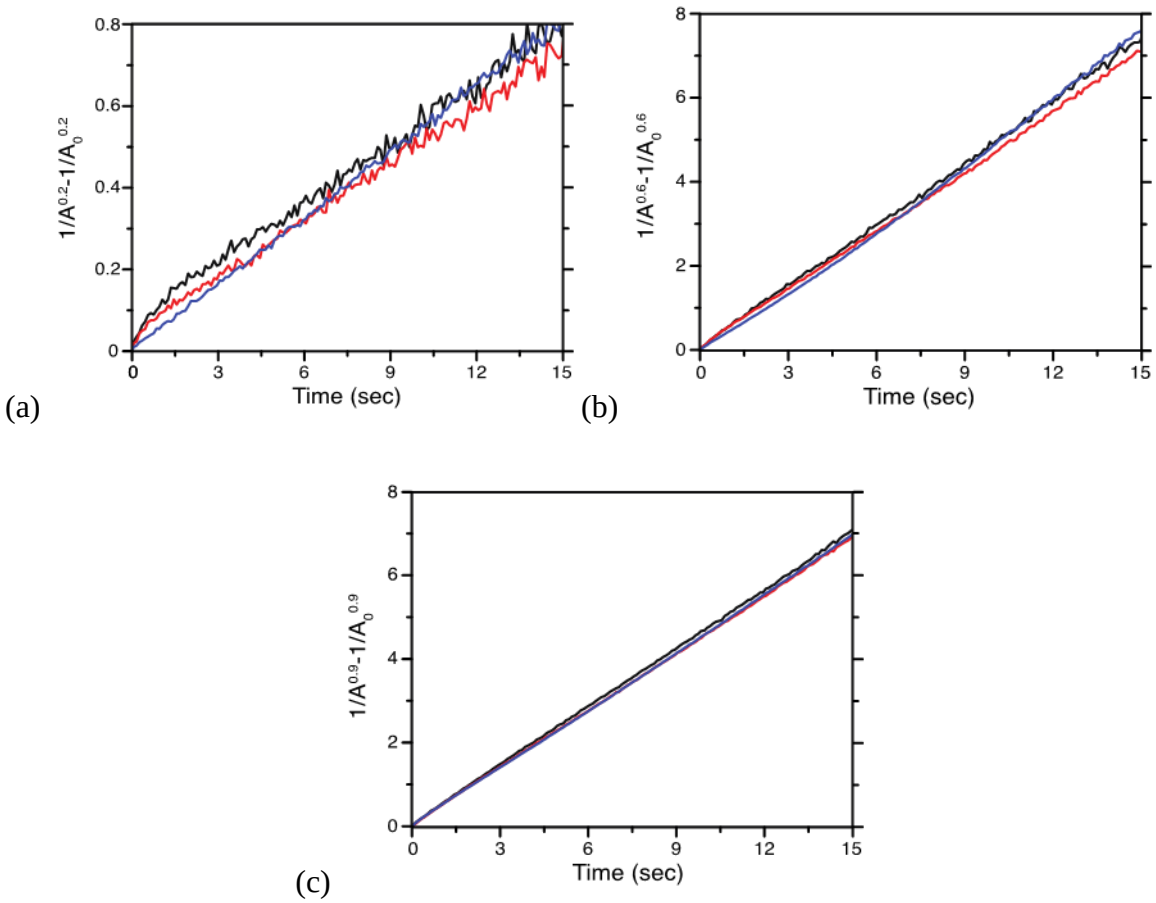

Figure 4.7. *(a) 1.2-, (b) 1.6-, and (c) 1.9-order plots of UV-vis spectrophotometry-measured dark lophyl radical concentration for HABI-incorporating gel swollen by (a) water, (b) acetonitrile, and (c) TCE at varying initial incident irradiation intensities (5 (black), 10 (red), and 50 (blue) mW·cm^{-2}).*

Having established the solvent-dependent backbone cleavage behavior in the presence of light and recombination in its absence, the photo-mediated healing capability of the HABI-incorporating gels was investigated at room temperature and under aerobic conditions. To demonstrate this, the exposed surfaces of sectioned gel cylinders, swollen in one the three solvents examined (i.e., water, acetonitrile, or TCE) were brought into contact and irradiated with visible light to effect cleavage and rearrangement of network strands at the interface of contacted surfaces; these healed materials, as well as the

pristine gels, were subsequently subjected to tensile testing. The exposed region of each HABI-incorporating gel again turned from yellow to teal upon irradiation and back to yellow upon irradiation cessation, confirming the backbone cleavage and subsequent recombination necessary for healing, whereas no light-induced color change was observed for the bisphenol A-incorporating gels. Although many backbone-borne, dynamic functional groups have been employed to achieve intrinsically-healable polymeric gels and elastomers,[59] effective restoration of mechanical properties upon contacting fracture surfaces can take several hours or days,[13,14] while more rapid healing rates afforded by materials with a more dynamic network connectivity are generally accompanied by correspondingly faster stress relaxation or creep.[10] In contrast, by inducing reversible, photo-mediated cleavage of network strands, far more rapid healing rates can be attained in polymer networks that, in the absence of light, are not susceptible to creep under load. As shown in Figure 4.8 and tabulated in Table 4.2, the healing rate order corresponds to the radical under equivalent irradiation conditions, where the HABI-incorporating gel with the highest light-induced radical concentration (i.e., the TCE-swollen gel) afforded the most rapid tensile strength recovery upon healing while the water-swollen gel recovered its tensile strength slowest. Nevertheless, all of the HABI-incorporating gels had recovered over half of their tensile strength after only 30 seconds of visible light irradiation and were approaching the tensile strength of the pristine materials after 3 minutes irradiation, demonstrating the rapid healing attainable in these materials even under a moderate irradiation intensity. No photo-mediated healing was observed for the bisphenol A-incorporating material upon irradiation at any of the conditions examined (Figure 4.8d), establishing that cleavage of the backbone-borne

HABI functional group was responsible for the observed photo-mediated healing of these covalently cross-linked networks.

Table 4.2. *Tensile strength (TS) of 15 wt% HABI-incorporating gels prior to and after photo-mediated healing.*

Solvent	TS of pristine gel (kPa)	% recovery of TS after irradiation		
		30 s	1 minute	3 minutes
Water	71.6±1.3	56.2±1.8	83.9±1.4	94.7±1.0
Acetonitrile	58.2±1.8	65.9±1.7	88.4±1.1	97.6±1.1
TCE	58.6±1.8	67.1±2.0	97.1±1.3	>99

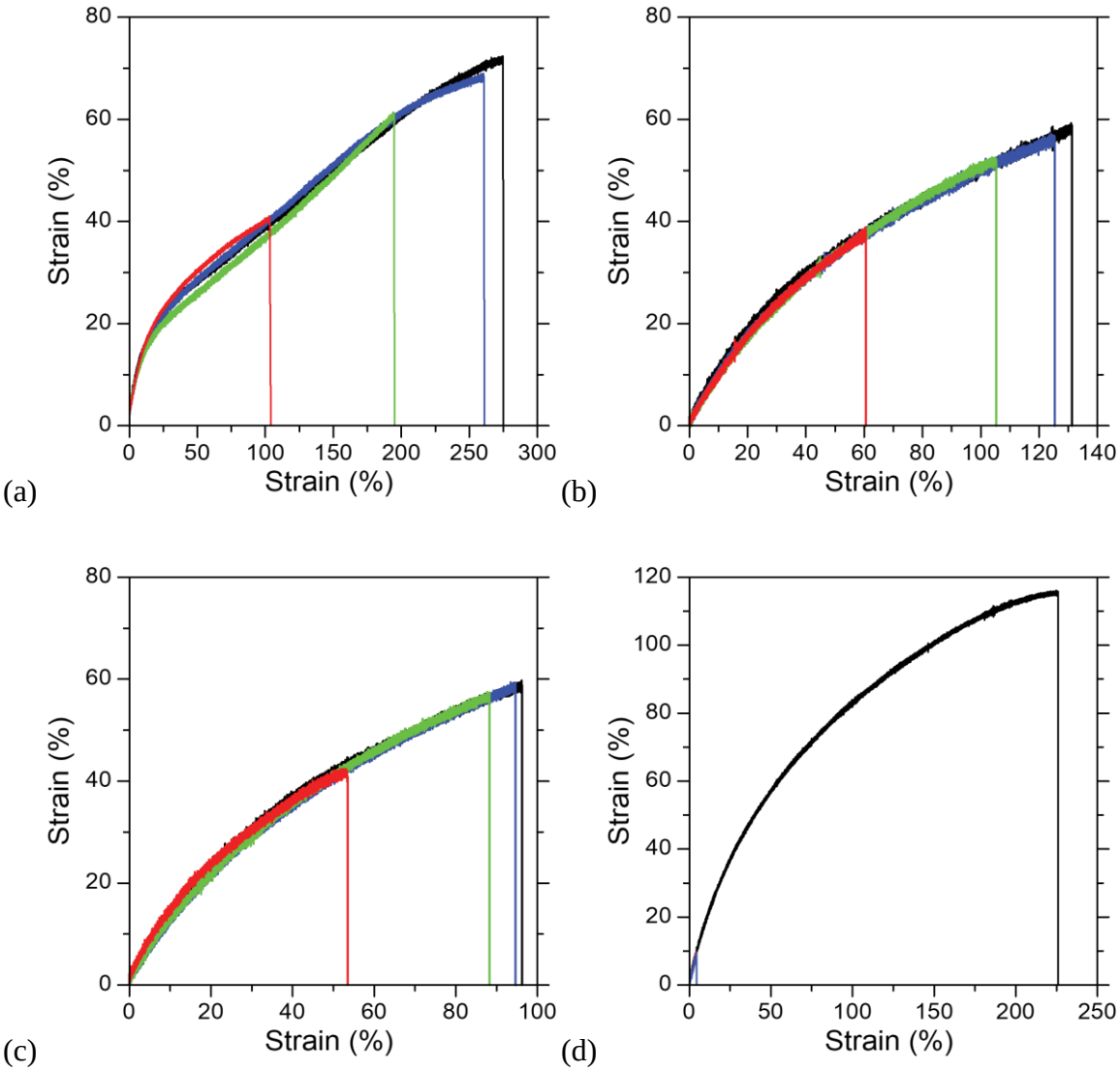

Figure 4.8. *Mechanical testing of healed polymer networks. Stress-strain curves for cylindrical samples under tensile deformation were determined for 15 wt% HABI-incorporating gels swollen with (a) water, (b) acetonitrile, and (c) TCE, and for (d) 15 wt% bisphenol A-incorporating gels swollen with acetonitrile. Shown are the stress-strain curves of pristine samples (black) and healed samples after irradiation with 405 nm light at 10 mW·cm^{-2} for 30 seconds (red), 1 minute (green), and 3 minutes (blue).*

4.5 Conclusion

In summary, the HABI-incorporating, covalently-cross-linked gels developed here undergo photo-mediated backbone cleavage under irradiation with near-UV or

visible light, temporarily affording reduced cross-link density and dynamic connectivity rearrangement, and revert back to stable, static networks upon irradiation cessation. This network stability in the dark, combined with its highly dynamic nature under irradiation, enables rapid healing rates while decoupling the creep that often accompanies the dynamic connectivity of intrinsically-healable polymer networks. As noted above, molecular mobility is necessary to achieve effective mixing and reaction at the interface of contacted polymeric materials; thus, given the dependence of glass transition temperature on cross-link density, the reduced cross-link density that accompanies the photo-mediated backbone cleavage exhibited by these HABI-incorporating networks may provide a route to achieve sub-glass transition temperature healing of vitrified thermosets.

4.6 References

(1) Wu, D. Y.; Meure, S.; Solomon, D. Self-healing polymeric materials: A review of recent developments. *Prog. Polym. Sci.* **2008**, *33*, 479-522.

(2) Bergman, S. D.; Wudl, F. Mendable polymers. *J. Mater. Chem.* **2008**, *18*, 41-62.

(3) Wojtecki, R. J.; Meador, M. A.; Rowan, S. J. Using the dynamic bond to access macroscopically responsive structurally dynamic polymers. *Nat. Mater.* **2011**, *10*, 14-27.

(4) White, S. R.; Sottos, N. R.; Geubelle, P. H.; Moore, J. S.; Kessler, M. R.; Sriram, S. R.; Brown, E. N.; Viswanathan, S. Autonomic healing of polymer composites. *Nature* **2001**, *409*, 794-797.

(5) Toohey, K. S.; Sottos, N. R.; Lewis, J. A.; Moore, J. S.; White, S. R. Self-healing materials with microvascular networks. *Nat. Mater.* **2007**, *6*, 581-585.

(6) Zavada, S. R.; McHardy, N. R.; Gordon, K. L.; Scott, T. F. Rapid, Puncture-Initiated Healing via Oxygen-Mediated Polymerization. *ACS Macro Lett.* **2015**, *4*, 819-824.

(7) Zhang, M. Q.; Rong, M. Z. Intrinsic self-healing of covalent polymers through bond reconnection towards strength restoration. *Polym. Chem.* **2013**, *4*, 4878-4884.

(8) Reutenauer, P.; Buhler, E.; Boul, P. J.; Candau, S. J.; Lehn, J. M. Room Temperature Dynamic Polymers Based on Diels-Alder Chemistry. *Chem.-Eur. J.* **2009**, *15*, 1893-1900.

(9) Zhang, B.; Digby, Z. A.; Flum, J. A.; Foster, E. M.; Sparks, J. L.; Konkolewicz, D. Self-healing, malleable and creep limiting materials using both supramolecular and reversible covalent linkages. *Polym. Chem.* **2015**, *6*, 7368-7372.

(10) Cromwell, O. R.; Chung, J.; Guan, Z. B. Malleable and Self-Healing Covalent Polymer Networks through Tunable Dynamic Boronic Ester Bonds. *Journal of the American Chemical Society* **2015**, *137*, 6492-6495.

(11) Ying, H. Z.; Zhang, Y. F.; Cheng, J. J. Dynamic urea bond for the design of reversible and self-healing polymers. *Nat. Commun.* **2014**, *5*, 9.

(12) Lei, Z. Q.; Xie, P.; Rong, M. Z.; Zhang, M. Q. Catalyst-free dynamic exchange of aromatic Schiff base bonds and its application to self-healing and remolding of crosslinked polymers. *J. Mater. Chem. A* **2015**, *3*, 19662-19668.

(13) Amamoto, Y.; Otsuka, H.; Takahara, A.; Matyjaszewski, K. Self-Healing of Covalently Cross-Linked Polymers by Reshuffling Thiuram Disulfide Moieties in Air under Visible Light. *Advanced Materials* **2012**, *24*, 3975-3980.

(14) Imato, K.; Nishihara, M.; Kanehara, T.; Amamoto, Y.; Takahara, A.; Otsuka, H. Self-Healing of Chemical Gels Cross-Linked by Diarylbibenzofuranone-Based Trigger-Free Dynamic Covalent Bonds at Room Temperature. *Angew. Chem.-Int. Edit.* **2012**, *51*, 1138-1142.

(15) Liu, Y. L.; Chuo, T. W. Self-healing polymers based on thermally reversible Diels-Alder chemistry. *Polym. Chem.* **2013**, *4*, 2194-2205.

(16) Altuna, F. I.; Antonacci, J.; Arenas, G. F.; Pettarin, V.; Hoppe, C. E.; Williams, R. J. J. Photothermal triggering of self-healing processes applied to the reparation of bio-based polymer networks. *Mater. Res. Express* **2016**, *3*, 11.

(17) Li, Q. T.; Jiang, M. J.; Wu, G.; Chen, L.; Chen, S. C.; Cao, Y. X.; Wang, Y. Z. Photothermal Conversion Triggered Precisely Targeted Healing of Epoxy Resin Based on Thermoreversible Diels−Alder Network and Amino-Functionalized Carbon Nanotubes. *ACS Appl. Mater. Interfaces* **2017**, *9*, 20797-20807.

(18) Wang, H. Y.; Heilshorn, S. C. Adaptable Hydrogel Networks with Reversible Linkages for Tissue Engineering. *Advanced Materials* **2015**, *27*, 3717-3736.

(19) Habault, D.; Zhang, H. J.; Zhao, Y. Light-triggered self-healing and shape-memory polymers. *Chemical Society Reviews* **2013**, *42*, 7244-7256.

(20) Fiore, G. L.; Rowan, S. J.; Weder, C. Optically healable polymers. *Chemical Society Reviews* **2013**, *42*, 7278-7288.

(21) Chung, C. M.; Roh, Y. S.; Cho, S. Y.; Kim, J. G. Crack healing in polymeric materials via photochemical 2+2 cycloaddition. *Chem. Mater.* **2004**, *16*, 3982-3984.

(22) Oya, N.; Sukarsaatmadja, P.; Ishida, K.; Yoshie, N. Photoinduced mendable network polymer from poly(butylene adipate) end-functionalized with cinnamoyl groups. *Polym. J.* **2012**, *44*, 724-729.

(23) Ling, J.; Rong, M. Z.; Zhang, M. Q. Photo-stimulated self-healing polyurethane containing dihydroxyl coumarin derivatives. *Polymer* **2012**, *53*, 2691-2698.

(24) Kiskan, B.; Yagci, Y. Self-Healing of Poly(propylene oxide)-Polybenzoxazine Thermosets by Photoinduced Coumarine Dimerization. *J. Polym. Sci. Pol. Chem.* **2014**, *52*, 2911-2918.

(25) Yu, L. L.; Xu, K. G.; Ge, L. P.; Wan, W. B.; Darabi, A.; Xing, M.; Zhong, W. Cytocompatible, Photoreversible, and Self-Healing Hydrogels for Regulating Bone Marrow Stromal Cell Differentiation. *Macromol. Biosci.* **2016**, *16*, 1381-1390.

(26) Radl, S.; Kreimer, M.; Griesser, T.; Oesterreicher, A.; Moser, A.; Kern, W.; Schlogl, S. New strategies towards reversible and mendable epoxy based materials

employing 4 pi s+4 pi s photocycloaddition and thermal cycloreversion of pendant anthracene groups. *Polymer* **2015**, *80*, 76-87.

(27) Froimowicz, P.; Frey, H.; Landfester, K. Towards the Generation of Self-Healing Materials by Means of a Reversible Photo-induced Approach. *Macromol. Rapid Commun.* **2011**, *32*, 468-473.

(28) Coqueret, X. Photoreactivity of polymers with dimerizable side-groups: Kinetic analysis for probing morphology and molecular organization. *Macromolecular Chemistry and Physics* **1999**, *200*, 1567-1579.

(29) Schreier, W. J.; Schrader, T. E.; Koller, F. O.; Gilch, P.; Crespo-Hernandez, C. E.; Swaminathan, V. N.; Carell, T.; Zinth, W.; Kohler, B. Thymine dimerization in DNA is an ultrafast photoreaction. *Science* **2007**, *315*, 625-629.

(30) Lendlein, A.; Jiang, H. Y.; Junger, O.; Langer, R. Light-induced shape-memory polymers. *Nature* **2005**, *434*, 879-882.

(31) Fairbanks, B. D.; Singh, S. P.; Bowman, C. N.; Anseth, K. S. Photodegradable, Photoadaptable Hydrogels via Radical-Mediated Disulfide Fragmentation Reaction. *Macromolecules* **2011**, *44*, 2444-2450.

(32) Scott, T. F.; Schneider, A. D.; Cook, W. D.; Bowman, C. N. Photoinduced plasticity in cross-linked polymers. *Science* **2005**, *308*, 1615-1617.

(33) Scott, T. F.; Draughon, R. B.; Bowman, C. N. Actuation in crosslinked polymers via photoinduced stress relaxation. *Advanced Materials* **2006**, *18*, 2128-2132.

(34) Amamoto, Y.; Kamada, J.; Otsuka, H.; Takahara, A.; Matyjaszewski, K. Repeatable Photoinduced Self-Healing of Covalently Cross-Linked Polymers through Reshuffling of Trithiocarbonate Units. *Angew. Chem.-Int. Edit.* **2011**, *50*, 1660-1663.

(35) Telitel, S.; Amamoto, Y.; Poly, J.; Morlet-Savary, F.; Soppera, O.; Lalevee, J.; Matyjaszewski, K. Introduction of self-healing properties into covalent polymer networks via the photodissociation of alkoxyamine junctions. *Polym. Chem.* **2014**, *5*, 921-930.

(36) Ghosh, B.; Urban, M. W. Self-Repairing Oxetane-Substituted Chitosan Polyurethane Networks. *Science* **2009**, *323*, 1458-1460.

(37) Ghosh, B.; Chellappan, K. V.; Urban, M. W. UV-initiated self-healing of oxolane-chitosan-polyurethane (OXO-CHI-PUR) networks. *J. Mater. Chem.* **2012**, *22*, 16104-16113.

(38) Wang, Z. H.; Yang, Y.; Burtovyy, R.; Luzinov, I.; Urban, M. W. UV-induced self-repairing polydimethylsiloxane-polyurethane (PDMS-PUR) and polyethylene glycol-polyurethane (PEG-PUR) Cu-catalyzed networks. *J. Mater. Chem. A* **2014**, *2*, 15527-15534.

(39) Riem, R. H.; Maclachl.A; Coraor, G. R.; Urban, E. J. The Flash Photolysis of a Substituted Hexaarylbiimidazole and Reactions of the Imidazolyl Radical. *Journal of Organic Chemistry* **1971**, *36*, 2272-2275.

(40) Caspar, J. V.; Khudyakov, I. V.; Turro, N. J.; Weed, G. C. ESR Study of Lophyl Free Radicals in Dry Films. *Macromolecules* **1995**, *28*, 636-641.

(41) Allen, P. E. M.; Patrick, C. R. Diffusion-Controlled Reactions in Free Radical Polymerisation. *Makromolekulare Chemie* **1961**, *47*, 154-167.

(42) Sathe, S. S.; Ahn, D.; Scott, T. F. Re-examining the Photomediated Dissociation and Recombination Kinetics of Hexaarylbiimidazoles. *Ind. Eng. Chem. Res.* **2015**, *54*, 4203-4212.

(43) Kawano, M.; Sano, T.; Abe, J.; Ohashi, Y. The first in situ direct observation of the light-induced radical pair from a hexaarylbiimidazolyl derivative by X-ray crystallography. *Journal of the American Chemical Society* **1999**, *121*, 8106-8107.

(44) Iwamura, T.; Nakamura, S. Synthesis and properties of de-cross-linkable acrylate polymers based on hexaarylbiimidazole. *Polymer* **2013**, *54*, 4161-4170.

(45) Verstraeten, F.; Gostl, R.; Sijbesma, R. P. Stress-induced colouration and crosslinking of polymeric materials by mechanochemical formation of triphenylimidazolyl radicals. *Chemical Communications* **2016**, *52*, 8608-8611.

(46) Peng, Y.; Yu, H. W.; Chen, H. B.; Huang, Z. C.; Li, H. M. Cross-linking and de-cross-linking of triarylimidazole-based polymer. *Polymer* **2016**, *99*, 529-535.

(47) Iwamura, T.; Sakaguchi, M. A Novel De-Cross-Linking System from Cross-Linked Polymer to Linear Polymer Utilizing Pressure or Visible Light Irradiation. *Macromolecules* **2008**, *41*, 8995-8999.

(48) Winter, H. H. Can the Gel Point of a Cross-linking Polymer Be Detected by the G' - G" Crossover? *Polymer Engineering and Science* **1987**, *27*, 1698-1702.

(49) Asano, K.; Matsubara, S. Effects of a Flexible Alkyl Chain on a Ligand for CuAAC Reaction. *Organic Letters* **2010**, *12*, 4988-4991.

(50) Yamada, Y. M. A.; Sarkar, S. M.; Uozumi, Y. Amphiphilic Self-Assembled Polymeric Copper Catalyst to Parts per Million Levels: Click Chemistry. *Journal of the American Chemical Society* **2012**, *134*, 9285-9290.

(51) Alberti, A.; Benaglia, M.; Macciantelli, D.; Rossetti, S.; Scoponi, M. Further EPR-spin trapping studies of the photoinitiating activity of Irgacure 369. *Eur. Polym. J.* **2008**, *44*, 3022-3027.

(52) von Sonntag, J.; Janovsky, I.; Naumov, S.; Mehnert, R. Free radical copolymerisation of N-methylmaleimide and 2,3-dihydrofuran initiated by their radical cations. A low temperature EPR study of a binary system. *Macromolecular Chemistry and Physics* **2002**, *203*, 580-585.

(53) Sathe, S. S.; Ahn, D.; Scott, T. F. Re-examining the photomediated dissociation and recombination kinetics of hexaarylbiimidazoles. *Industrial and Engineering Chemistry Research* **2015**, *54*, 4203-4212.

(54) Waters, D. J.; Engberg, K.; Parke-Houben, R.; Hartmann, L.; Ta, C. N.; Toney, M. F.; Frank, C. W. Morphology of Photopolymerized End-Linked Poly(ethylene glycol) Hydrogels by Small-Angle X-ray Scattering. *Macromolecules* **2010**, *43*, 6861-6870.

(55) Imato, K.; Ohishi, T.; Nishihara, M.; Takahara, A.; Otsuka, H. Network Reorganization of Dynamic Covalent Polymer Gels with Exchangeable Diarylbibenzofuranone at Ambient Temperature. *Journal of the American Chemical Society* **2014**, *136*, 11839-11845.

(56) Adzima, B. J.; Tao, Y. H.; Kloxin, C. J.; DeForest, C. A.; Anseth, K. S.; Bowman, C. N. Spatial and temporal control of the alkyne-azide cycloaddition by photoinitiated Cu(II) reduction. *Nat. Chem.* **2011**, *3*, 256-259.

(57) Fujita, K.; Hatano, S.; Kato, D.; Abe, J. Photochromism of a radical diffusion-inhibited hexaarylbiimidazole derivative with intense coloration and fast decoloration performance. *Org. Lett.* **2008**, *10*, 3105-3108.

(58) Kishimoto, Y.; Abe, J. A Fast Photochromic Molecule That Colors Only under UV Light. *J. Am. Chem. Soc.* **2009**, *131*, 4227-4229.

(59) Zou, W. K.; Dong, J. T.; Luo, Y. W.; Zhao, Q.; Xie, T. Dynamic Covalent Polymer Networks: from Old Chemistry to Modern Day Innovations. *Advanced Materials* **2017**, *29*, 1606100.

Chapter 5

Sub-T_g photo-mediated welding of vitrified polymer networks

5.1 Abstract

The intrinsic healing of covalently cross-linked polymer networks is commonly obtained by the incorporation of dynamic covalent bonds; however, hard autonomously self-healing materials have been considered a contradiction in terms because dynamic intermolecular interactions necessitate sufficient chain dynamics attainable only above the glass transition temperature (T_g). To address this intractable problem, we incorporated HABI moieties, groups that are homolytically cleavable, to yield relatively low reactivity lophyl radicals under visible light irradiation and which, in the absence of light, spontaneously recombine without significantly participating in deleterious side reaction, into vitrified, polyurethane networks. Owing to the slow recombination of lophyl radicals and photo-mediated backbone cleavage upon irradiation with visible light, temporarily affording reduced cross-link density and dynamic connectivity rearrangement, sub-T_g healing of vitrified thermosets was achieved.

5.2 Introduction

Covalently cross-linked, vitrified polymer networks find utility as structural materials across a wide variety of applications where in situ polymerization, dimensional stability, environmental resistance, and permanence are required. Additional chemical

functionality can be readily introduced to these networks by incorporating desired functional groups in the monomeric precursors employed for material fabrication; however, once set, the reuse, repair, and post-polymerization manipulation of these vitrified polymer networks are, as suggested by their common description as 'thermosets', limited. To address this shortcoming, strategies to afford a capacity for healing in these otherwise intractable polymeric matrices have either necessitated heating the material above its glass transition temperature (T_g) and effect concomitant transient depolymerization[1,2] or bond rearrangement,[3-5] or involved the incorporation of liquid-filled inclusions, such as capsules or channels, whose contents flow upon rupture and polymerize in situ to bridge the flaw interfaces.[6,7] Notably, all of these approaches utilize systems with either significant chain mobility and associated segmental diffusion or simple fluid flow to achieve mass transport and reaction at the damage site. A recent commentary recognized that self-healing mechanisms based on reversible, dynamic intermolecular interactions necessitate sufficient chain dynamics attainable only above the T_g, and asked whether hard autonomous self-healing [supramolecular] materials might be a contradiction in terms.[8] Indeed, the example of a relatively hard self-healing thermoplastic elastomer,[9] reported by Guan et al., exhibited a modulus of 38 MPa,[9] well below that of vitrified, cross-linked polymers which typically exhibit moduli of ~1-3 GPa, or even up to ~10-14 GPa for poly(hexahydrotriazine)s.[10,11] Although certainly attainable in elastomeric materials, achieving analogous sub-T_g, 'cold welding' behavior in thermosets, where chain mobility is severely limited, remains an unmet challenge.

HABIs, first synthesized by Hayashi and Maeda in 1960,[12] are well known as thermo- and photo-chromic materials and photoinitiators that are widely used in proofing

papers, photoimaging, and photoresists. The photochromic behavior of HABI derivatives can be attributed to the photoinduced homolytic, reversible cleavage of carbon-nitrogen (C-N) bond between the imidazole rings. They efficiently produce indigo-colored, 2,4,5-triarylimidazolyl (lophyl) radicals upon either UV or visible light irradiation and can thermally recombine to reproduce the dimer. In comparison to other radical species, lophyl radicals generated by HABI photolysis are insensitive to atmospheric oxygen and exhibit extraordinary long lifetimes, on the order of tens of seconds to minutes or hours, in solution[13] or even when embedded in polymer matrices,[14] attributable to their unique chemical structure affording stabilization by both π-conjugation and steric hindrance.[15] This relatively low reactivity of the lophyl radicals originating from HABI cleavage affords an inherent reversibility where the cleaved covalent bond spontaneously reforms without participating in deleterious side reactions. Notably, HABIs were recently utilized as a new class of dynamic covalent bond to afford photo-mediated healable polymeric gel.[16]

The incorporation of dynamic covalent bonds into cross-linked polymer networks has been widely used to fabricate adaptable networks in recent years.[17,18] However, despite their utility, the incorporation of dynamic covalent chemistries in the network strands of a cross-linked polymer often results in creep under mechanical stress,[16] a significantly deleterious trait for structural materials. Rather, more desirable is the incorporation of a dynamic chemistry that only proceeds upon application of a specific stimulus.[19] Achieving intrinsic crack healing in rigid, cross-linked polymers necessitates not only activated bond rearrangement and recombination, but the reaction needs to occur on a sufficiently long timescale to allow segmental diffusion and mixing to bridge the

fracture surfaces. Thus, both thermodynamic and kinetic elements of a given dynamic covalent reaction must be considered in conjunction with the application and its characteristic time scale. The T_g of cross-linked polymers decreases with reduced cross-link density; consequently, reversibly breaking network strands to afford sufficiently long-lived species would enable a significant, though temporary, reduction in the cross-link density and concomitant reduction in T_g, imparting high chain mobility prior to strand reformation. Here, we describe the incorporation of reversible, photo-latent, long-lived reactive species in the backbone of cross-linked polymers to impart transient high chain mobility and enable temporally-controlled healing of vitrified polymeric networks at sub-T_g ambient temperatures.

5.3 Experimental

5.3.1 Materials

Isophorone diisocyanate (IPDI, Acros) and dibutyltin dilaurate (Sigma-Aldrich) were purchased and used without further purification. Diphenyl-1-picrylhydrazyl (DPPH, Sigma-Aldrich) was used as received for standard radical concentration solutions. Dimethylformamide (DMF, Fisher Chemical), anhydrous tetrahydrofuran (THF, Sigma-Aldrich) and 1,4-dioxane (Fisher Chemical) were used as solvents.

5.3.2 Synthesis of vitrified, HABI-containing, cross-linked polymer networks

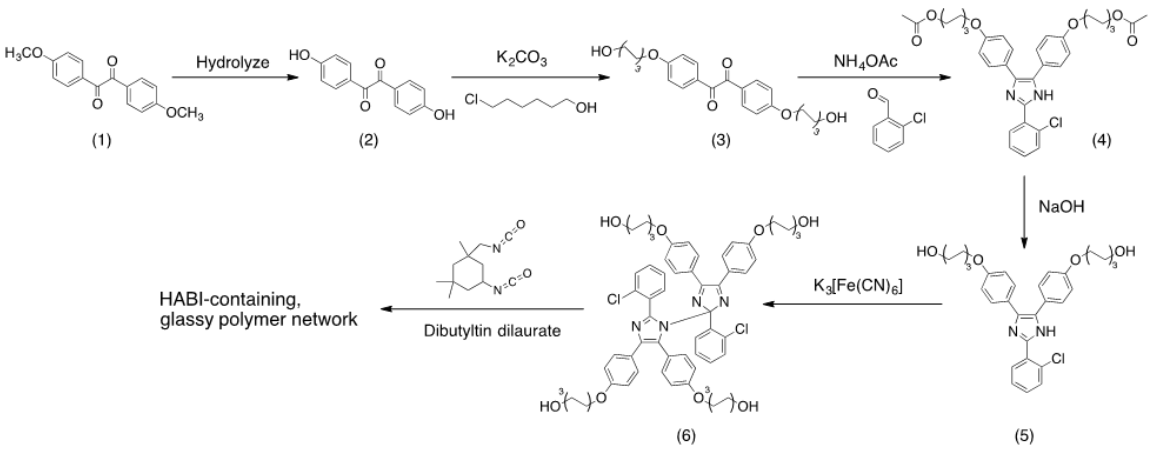

Scheme 5.1. *Synthesis of tetrakis(hydroxy)-substituted HABI (6), and its subsequent polymerization to yield a HABI-containing glassy, cross-linked polymer network via the alcohol-isocyanate reaction.*

5.3.2.1 Synthesis of 1,2-bis(4-hydroxyphenyl)ethane-1,2-dione (2)

In a 100-mL three-necked flask, 4,4′-dimethoxy benzil **1** (10.0 g, 37.0 mmol) was added into 30 mL acetic acid, followed by heating to 85°C for 30 minutes. Hydrobromic acid (40%, 20.0 mL, 0.10 mol) was added into the mixture and refluxed at 120°C for 5 days. After the reaction, the solution was distilled to remove acetic acid and excessive hydrobromic acid. The residue was dissolved in 50.0 mL ethyl acetate and washed with water. The solution was dried with anhydrous magnesium sulfate and the organic solvents were removed under reduced pressure. And then the crude product was purified by silica gel chromatography eluting with hexane/ethyl acetate (1/1, v/v) to afford 7.88 g of **2** (87.9% yield). ^{1}H NMR (400 MHz, DMSO-d6), δ: 6.91-6.94 (d, 4H), 7.72-7.75 (d, 4H), 10.82 (s, 2H).

5.3.2.2 Synthesis of 1,2-bis(4-((6-hydroxyhexyl)oxy)phenyl)ethane-1,2-dione (3)

2 (7.50 g, 31.0 mmol) and potassium carbonate (12.8 g, 92.9 mmol) were added to 100 mL of DMF and the mixture stirred. 6-Chlorohexanol (11.0 g, 80.5 mmol) was added and the mixture heated at 120°C for 16 hours under nitrogen. After cooling to room temperature, the mixture was filtered to remove potassium carbonate, DMF was evaporated under reduced pressure, and the residue was purified by silica gel chromatography eluting with hexane/ethyl acetate (1/3, v/v), yielding 11.4 g of **3** (83.2% yield). ^{1}H NMR (400 MHz, DMSO-d6), δ: 1.24-1.46 (m, 12H), 1.69-1.76 (m, 4H), 3.36-3.41 (q, 4H), 4.06-4.10 (q, 4H), 4.33-4.36 (t, 2H), 7.09-7.13 (d, 4H), 7.82-7.84 (d, 4H).

5.3.2.3 Synthesis of (((2-(2-chlorophenyl)-1H-imidazole-4,5-diyl)bis(4,1-phenylene))bis(oxy)) bis(hexane-6,1-diyl) diacetate (4)

A mixture of **3** (10.0 g, 22.6 mmol), 2-chlorobenzaldehyde (3.18 g, 22.6 mmol), ammonium acetate (14.8 g, 192 mmol), and acetic acid (150 mL) was refluxed for 16 hours under nitrogen. After cooling to room temperature, the solvent was partially removed under reduced pressure and poured into 10-fold water. The generated precipitate was filtered, washed with water, and dried. The precipitate was purified by silica gel chromatography eluting with hexane/ethyl acetate (1/2, v/v) to afford 12.6 g of **4** (86.0% yield). ^{1}H NMR (400 MHz, DMSO-d6), δ: 1.29-1.48 (m, 8H), 1.55-1.63 (m, 4H), 1.67-1.75 (m, 4H), 1.99-2.00 (t, 6H), 3.93-4.04 (m, 8H), 6.84-6.87 (d, 2H), 6.95-6.98 (d, 2H), 7.36-7.39 (d, 2H), 7.43-7.46 (t, 4H), 7.57-7.60 (t, 1H), 7.76-7.78 (t, 1H), 12.40 (s, 1H).

5.3.2.4 Synthesis of 6,6'-(((2-(2-chlorophenyl)-1H-imidazole-4,5-diyl(bis(4,1-phenylene)) bis(hexa-1-ol) (5)

A solution of **4** (10.0 g, 15.5 mmol) in tetrahydrofuran (THF) (100 mL) was mixed with 3 M NaOH aqueous solution (100 mL) and refluxed for 12 hours. After cooling to room temperature, solvent was partially removed under reduced pressure and extracted with dichloromethane. The organic layer was collected, washed with brine, and dried over anhydrous magnesium sulfate. The organic solvents were removed under reduced pressure to afford a yellow powder, yielding 7.87 g of **5** (90.5% yield). ^{1}H NMR (400 MHz, DMSO-d6), δ: 1.30-1.46 (m, 12H), 1.67-1.76 (m, 4H), 3.37-3.42 (m, 4H), 3.93-4.05 (m, 4H), 4.34-4.37 (m, 2H), 6.85-6.87 (d, 2H), 6.96-6.98 (d,2H), 7.37-7.39 (d, 2H), 7.43-7.46 (t, 4H), 7.57-7.60 (t, 1H), 7.76-7.78 (t, 1H), 12.41 (s, 1H).

5.3.2.5 Synthesis of tetrakis(hydroxy)-substituted HABI (6)

To a vigorously stirred solution of potassium ferricyanide (13.2 g, 40.0 mmol) and potassium hydroxide (24.0 g, 428 mmol) in water (200 mL), a solution of **5** (7.50 g, 13.3 mmol) in dichloromethane (100 mL) was added dropwise. The mixture was refluxed for 16 hours. After cooling to room temperature, the organic layer was collected, washed with water, dried over anhydrous magnesium sulfate, filtered, and the solvent removed under reduced pressure. The residue was purified by silica gel chromatography eluting with hexane/ethyl acetate (1/2, v/v) to afford 12.2 g of **6** (81.3% yield). ^{1}H NMR (400 MHz, DMSO-d6), δ: 1.28-1.48 (m, 24H), 1.59-1.77 (m, 8H), 3.36-3.44 (m, 8H), 3.83-4.07 (m, 8H), 4.31-4.39 (m, 4H), 6.67-6.71 (t, 4H), 6.77-6.79 (d, 2H),

6.86-6.89 (d, 2H), 7.06-7.11 (m, 4H), 7.15-7.28 (m, 8H), 7.39-7.43 (t, 1H), 7.52-7.54 (d, 2H), 7.68-7.70 (d, 1H).

5.3.2.6 Synthesis of HABI-containing, cross-linked polyurethane network

HABI-incorporating, cross-linked polyurethanes were synthesized *via* the alcohol-isocyanate reaction between tetrahydroxy HABI monomer and isophorone diisocyanate (IPDI) with a catalytic amount of dibutyltin dilaurate in anhydrous THF. For example, tetrahydroxy HABI monomer (500 mg, 0.44 mmol) and IPDI (197.7 mg, 0.89 mmol) were dissolved in chloroform (468.6 µL) and 10 µL of dibutyltin dilaurate solution in anhydrous THF (10%, v/v) were added. The liquid formulation was then injected between two glass microscope slides separated by 250 µm thick spacers. Cross-linked polymer films were polymerized overnight at ambient temperature and post-cured in a vacuum oven at 60°C for 24 hours. Samples of approximately 15 mm × 2.5 mm × 0.13 mm were cut from the cured films.

5.3.3 Light sources and intensity measurement

Violet light was provided by a collimated, LED-based illumination source (Thorlabs M405L2-C) with an emittance centered at 405 nm (FWHM 13 nm), used in combination with a current-adjustable LED driver (Thorlabs LEDD1B) for intensity control. Irradiation intensities were measured with an International Light IL1400A radiometer equipped with a broadband silicon detector (model SEL033), a 10× attenuation neutral density filter (model QNDS1), and a quartz diffuser (model W).

5.3.4 Fourier transform infrared (FTIR) spectroscopy

Resin formulations were introduced between glass microscope slides separated by 50 μm thick spacer to maintain constant sample thickness. Each sample was placed in a Thermo Scientific Nicolet 6700 FTIR spectrometer equipped with a horizontal transmission accessory, as described elsewhere,[20] and spectra were collected from 2000 to 4000 cm^{-1}. The residual functional group and solvent concentrations were determined from the peak area centered at 2275 cm^{-1} corresponding to the thiol group stretch, 3019 cm^{-1} corresponding to C-H stretch from chloroform, and 3300 cm^{-1} corresponding to the N-H stretch from urethane linkage formation. The sample thickness for the resin formulations was selected to ensure that the functional group peaks remained within the linear regime of the instrument detector while affording good signal to noise and maintaining optically thin and isothermal polymerization conditions. As the polymerization proceeded (after overnight reaction at ambient temperature and post-curing at 60°C for 1 day), the residual functional groups and solvent were again determined by monitoring the disappearance of the thiol group peak and the C-H stretch peak from chloroform and formation of the N-H stretch peak from urethane linkage (Figure 5.4a).

5.3.5 Dynamic mechanical analysis

Using the method described above, cross-linked polyurethane films were prepared. Samples of approximately 15 mm × 2.5 mm × 0.13 mm were cut from the cured films and mounted in a TA Instruments Q800 dynamic mechanical analyzer

(DMA) equipped with a film tension clamp. Experiments were performed at a strain and frequency of 0.1% and 1 Hz, respectively, scanning the temperature from -25°C to 180°C at 2°C·min^{-1}, and the elastic moduli (E′) and tan δ curves were recorded (Figure 5.4b).

Two strips of sample were healed upon irradiation, using the method described below, and then mounted in the DMA with a film tension clamp to measure the stress-strain curve. Samples were stretched out from 0.01 N of preload force to 18 N along with ramp force of 3.00 N·min^{-1}.

5.3.6 Ultraviolet-visible spectrophotometry

UV-vis spectrophotometry was performed using an Agilent Technologies Cary 60 UV-vis spectrophotometer. The same sample concentration (5 mM in DMF) was used for all HABI monomers used in this study (*o*-Cl-HABI, dihydroxy HABI, and tetrahydroxy HABI) and the absorbance spectra of these solutions were collected from 200 to 800 nm using 1 mm pathlength quartz cuvette both in the dark and under irradiation once the radical concentration had reached equilibrium. HABI photodissociation and subsequent recombination was examined by monitoring 557 nm, 606 nm, and 599 nm for *o*-Cl-HABI, dihydroxy HABI, and tetrahydroxy HABI, respectively, the wavelengths where visible light absorbance by the generated lophyl radicals were greatest (i.e., λ_{max}), while the sample solutions in the cuvette were irradiated with 405 nm at 10 mW·cm^{-2} for 5 minutes to ensure radical concentration equilibration, then for a further 32.5 minutes after the light was turned off.

Using the method described above, 130 μm thick HABI-based thermoset films were prepared and spectra were collected from 200 to 800 nm both in the dark and under irradiation. To collect spectra on samples after irradiation, HABI-based films were irradiated with 405 nm light at 10 $mW \cdot cm^{-2}$ for 70 minutes. HABI photodissociation and subsequent dark recombination within polymer network were also examined by monitoring λ_{max} of the HABI-based thermoset films, while the samples were irradiated with 405 nm at 10 $mW \cdot cm^{-2}$ for 70 minutes, then a further 17.5 minutes after the light cessation (see Figure 5.1).

5.3.7 Electron paramagnetic resonance spectroscopy

Electron paramagnetic resonance (EPR) spectroscopy was performed with a Bruker EMX spectrometer. The spectrometer was equipped with a TE102 cavity (Bruker model ER 4102ST), and a frequency of 9.712 GHz, 2.05 mW microwave power, 5.02×10^4 receiver gain, 100 kHz modulation frequency, and 1 G modulation amplitude were used for all experiments. Optical access to the cavity was afforded by a 10 mm × 23 mm grid providing 50% light transmittance to the sample. For the sample preparation, a 1.1 mm inner diameter glass capillary tube was filled with 20 μL of 5 mM HABI monomer solutions (*o*-Cl-HABI, dihydroxy HABI, and tetrahydroxy HABI) in DMF. For the HABI-based thermoset sample, 20 μL of resin formulations were prepared, as described above, and inserted into glass capillary tube. Glassy, HABI-containing polyurethane networks were polymerized within the glass capillary tube overnight reaction at room temperature and then post-cured in a vacuum oven at 60°C for 1 day. Each sample capillary tube was inserted into a 3.2 mm inner diameter quartz sample tube and inserted

again into the spectrometer cavity for analysis. The samples were irradiated in situ with 405 nm light at varying irradiation intensities and spectra were collected once the radical concentration reached steady state (90 seconds for HABI monomer solutions and 70 minutes for HABI-based thermoset polymers). Photodissociation and subsequent recombination of lophyl radicals was monitored at a 3468 G static field for HABI monomer solutions and a 3454 G static field for HABI-based thermoset polymers, the first derivative signal intensity maximum for the HABI species under irradiation, while the sample solutions were irradiated with 405 nm light for 5 minutes to ensure reaction equilibrium, then for a further 32.5 minutes in the dark. For HABI-based thermoset polymers, the samples were irradiated with 405 nm light for 70 minutes, then for a further 17.5 minutes in the dark. All experiments were performed at room temperature.

To measure the bond dissociation energies of HABI-based monomers, the spectrometer was equipped with a temperature-controlled cavity, and a frequency of 9.712 GHz, 2.05 mW microwave power, 5.02×10^4 receiver gain, 100 kHz modulation frequency, and 1 G modulation amplitude were used for all experiments. For the sample preparation, a 3.2 mm inner diameter quartz sample tube was filled with 190 μL of sample solutions and inserted into the spectrometer cavity for analysis. The spectra were collected at varying temperature from 50°C to 100°C with an increment of 5°C (Figure 5.3b and 3d). Radical concentrations were quantified by calibrating the EPR spectrum integral against known concentration solutions of DPPH in toluene using the same sample geometry, volume, and acquisition conditions employed for the HABI monomer solutions (Figure 5.3a).

5.3.8 Measurement of surface temperature on cross-linked polymer film incorporating HABI moiety

The surface temperature of glassy, HABI-containing polyurethane films during irradiation was measured using a FLIR TG165 spot thermal camera using an emissivity (ε) of 0.95. Surface temperature was recorded in every 15 seconds and the distance between the thermal camera and the sample was varied at 5, 12, and 30 cm. Sample strips were irradiated for 30 minutes, starting 2.5 minutes after data recording was begun, with 405 nm light at 40 $mW \cdot cm^{-2}$, and then left in the dark for a further 27.5 minutes.

5.3.9 Photo-mediated healing

Sample strips were cut from fully cured film to have dimensions of approximately 15 mm × 2.5 mm × 0.13 mm. Two sample strips were wet with DMF and immediately wiped to dry the surfaces but ensure intimate contact between samples, and then were assembled with each other to have 5 mm × 2.5 mm of overlapped region at the end of sample strips and mounted between glass microscope slides. Steel weights with masses varying from 10 g to 25 kg were placed on the top of glass microscope slide during the irradiation and dark recombination periods to determine the influence of weight on the photo-healing rate and efficiency. Sample strips were irradiated from underneath with 405 nm at 40 $mW \cdot cm^{-2}$ for 3, 10, and 30 minutes.

5.3.10 Surface profilometry

Samples for surface profilometry were prepared by soaking fully cured films in a mixture of acetonitrile and butyl 3-mercaptopropionate, then subjecting them to irradiation through a photomask with 405 nm light at 40 $mW \cdot cm^{-2}$ for different time periods (1, 5, and 15 minutes). After light cessation, the samples were rinsed with acetonitrile and dried prior to surface topography measurement.

Surface profilometry (Alphastep 500, Tencor Instruments) was used to measure the topography of photo-patterned surface of vitrified, HABI-thermosets. The letter 'I' from the 'Michigan' logo was scanned with 1 mm of scan length at a rate of 100 $\mu m \cdot s^{-1}$.

5.3.11 Measurement of bond dissociation energy

EPR data obtained from the temperature dependence of the dissociation equilibrium was used to determine the bond dissociation energy (BDE) for the C-N bond of each HABI monomer. The data was analyzed using a simplified form of the van 't Hoff equation,

$$\ln K_{eq} = \frac{\Delta S}{R} - \frac{\Delta H}{RT} \qquad (1)$$

where K_{eq} = $[R\cdot]^2/[HABI]$, and R· and HABI represent the lophyl radical and HABI monomer, respectively. The lophyl radical concentration at various temperatures was calculated using a standard DPPH calibration curve. Equation 1 shows that a plot of ln K_{eq} versus the reciprocal temperature yields a slope of $-\Delta H/R$. Slopes obtained from plots of ln K_{eq} against the reciprocal temperature and resultant ΔH (BDE) are summarized in Table 5.1 below (Note: the BDE of o-Cl-HABI has been reported as 17 kcal/mol).[21]

Table 5.1. *Bond dissociation energies of HABI monomers.*

	Slope	ΔH (BDE, kcal·mol^{-1})
Dihydroxy HABI	-7.75	15.40
Tetrahydroxy HABI	-9.20	18.29

5.4 Results and discussion

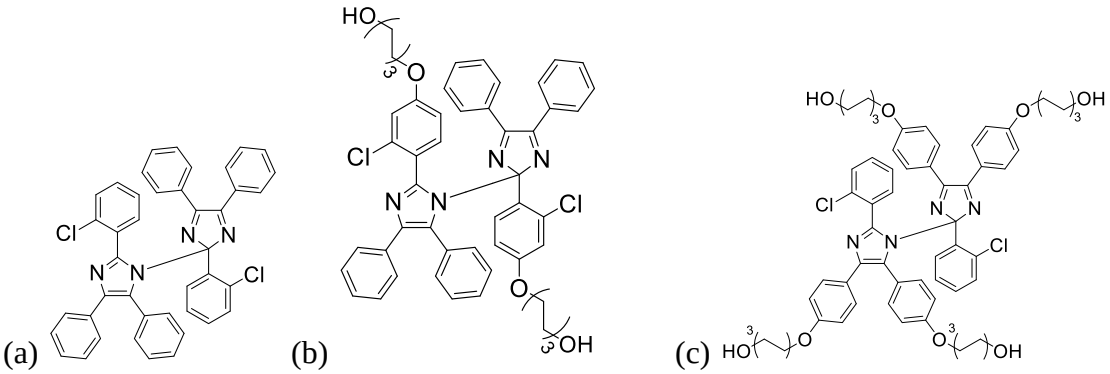

Scheme 5.2. *HABI monomers used in this study. (a) o-Cl-HABI (M.W.: 659.61 g·mol^{-1}). (b) Dihydroxy HABI (M.W.: 823.05 g·mol^{-1}). (c) Tetrahydroxy HABI (M.W.: 1124.25 g·mol^{-1}).*

The intrinsic healing capability of cross-linked polymer networks highly depends on the performancesof dynamic covalent bonds incorporated in the backbone of polymeric strands, such as how efficiently covalent bonds can be cleaved upon light irradiation, how many cleaved covalent bonds are able to participate in the bond exchange reaction, and how much time can be provided for the bond rearrangement

reaction. Three HABI monomers are examined here to compare the quantity of photo-cleaved lophyl radicals upon equivalent irradiation condition and lifetime of lophyl radicals to determine the HABI structure most capable of demonstrating superior healing capability upon incorporation in the backbone of cross-linked polymer networks (see Scheme 5.2). *o*-Cl-HABI is a commercially-available HABI photoinitiator, whereas dihydroxy HABI is a HABI photoinitiator synthesized for improved solubility and visible light absorbance, as described in Chapter 2. Tetrahydroxy HABI monomer was newly designed and synthesized here (Scheme 5.1).

The photo-mediated cleavage of HABI species were examined using UV-vis spectrophotometry. Prior to irradiation, these HABI monomers show weak absorption tails extending into the visible spectral region; however, irradiation at 405 nm yields a dramatic color change, as shown in Figure 5.1e, and the emergence of an absorption peak in the visible region (λ_{max} = 557, 606, and 599 nm for *o*-Cl-HABI, dihydroxy HABI, and tetrahydroxy HABI, respectively), originating from the generation of lophyl radicals. The area under the newly-generated absorbance curve was greatest for the tetrahydroxy HABI monomer, suggesting that this monomer exhibits superior lophyl radical capability under equivalent irradiation conditions. In order to examine the subsequent lophyl radical recombination after ceasing the light irradiation and their kinetic behavior, HABI monomer solutions were exposed to the visible light irradiation until their absorbance peak reached steady state, after which the light was turned off (Figure 5.1d). Tetrahydroxy HABI monomer-sourced lophyl radicals showed the longest lifetime among three HABI monomers examined here, and thus were expected to provide longest time for actual healing processes.

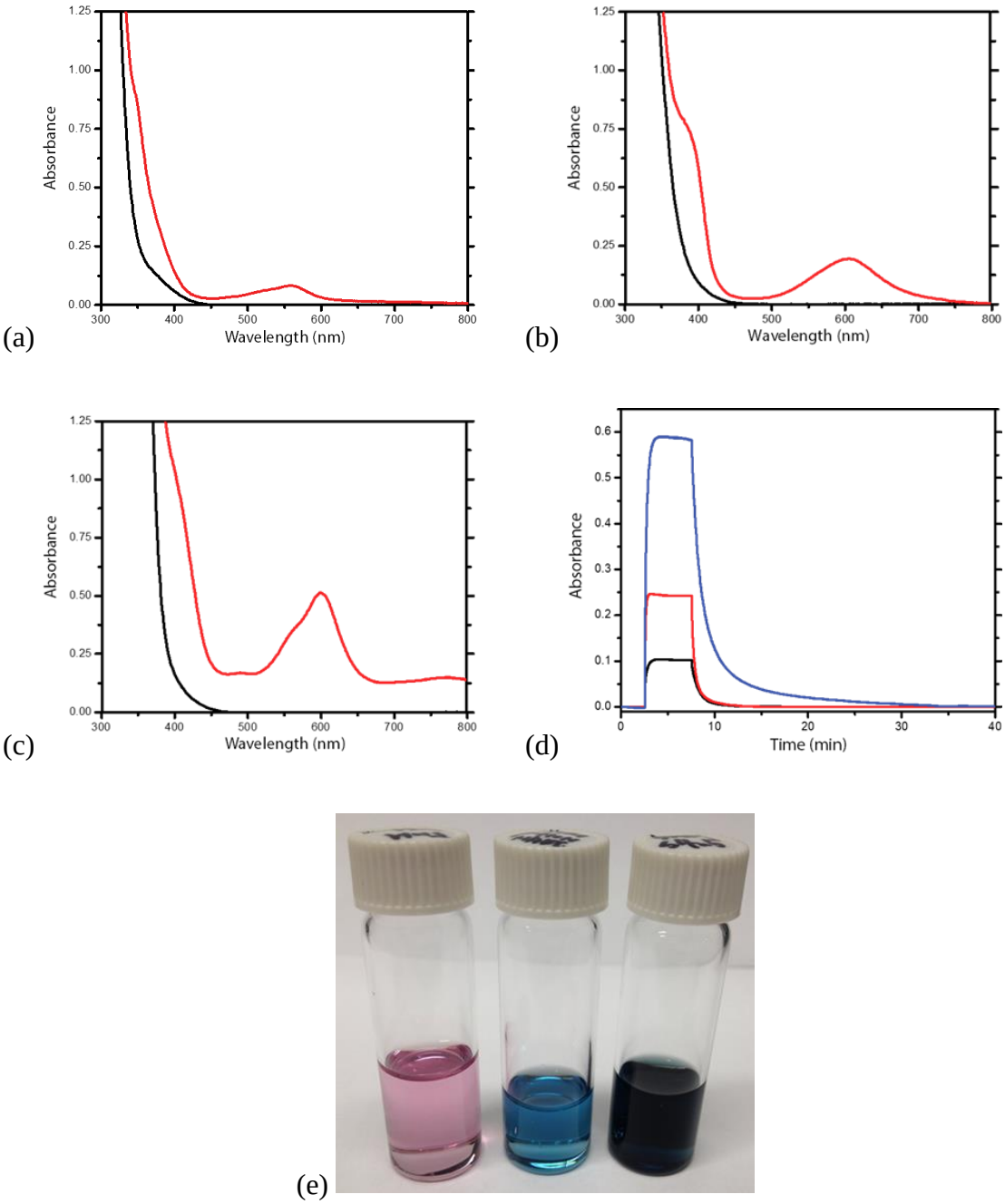

Figure 5.1. *UV-vis spectrophotometry with kinetics. UV-vis spectra of 5 mM (a) o-Cl-HABI, (b) dihydroxy HABI, (c) tetrahydroxy HABI monomer solution in DMF prior to irradiation (black) and at equilibrium under 405 nm irradiation at 10 mW·cm^{-2} for 90 seconds (red). (d) Absorbance at λ_{max} versus time for 5 mM o-Cl-HABI (black), dihydroxy HABI (red), and tetrahydroxy HABI (blue) monomer solutions in DMF, irradiated with 405 nm at 10 mW·cm^{-2} from 2.5-7.5 minutes. (e) Photographs of HABI monomer solutions showing the color change, attributable to the generation of lophyl radical upon visible light irradiation.*

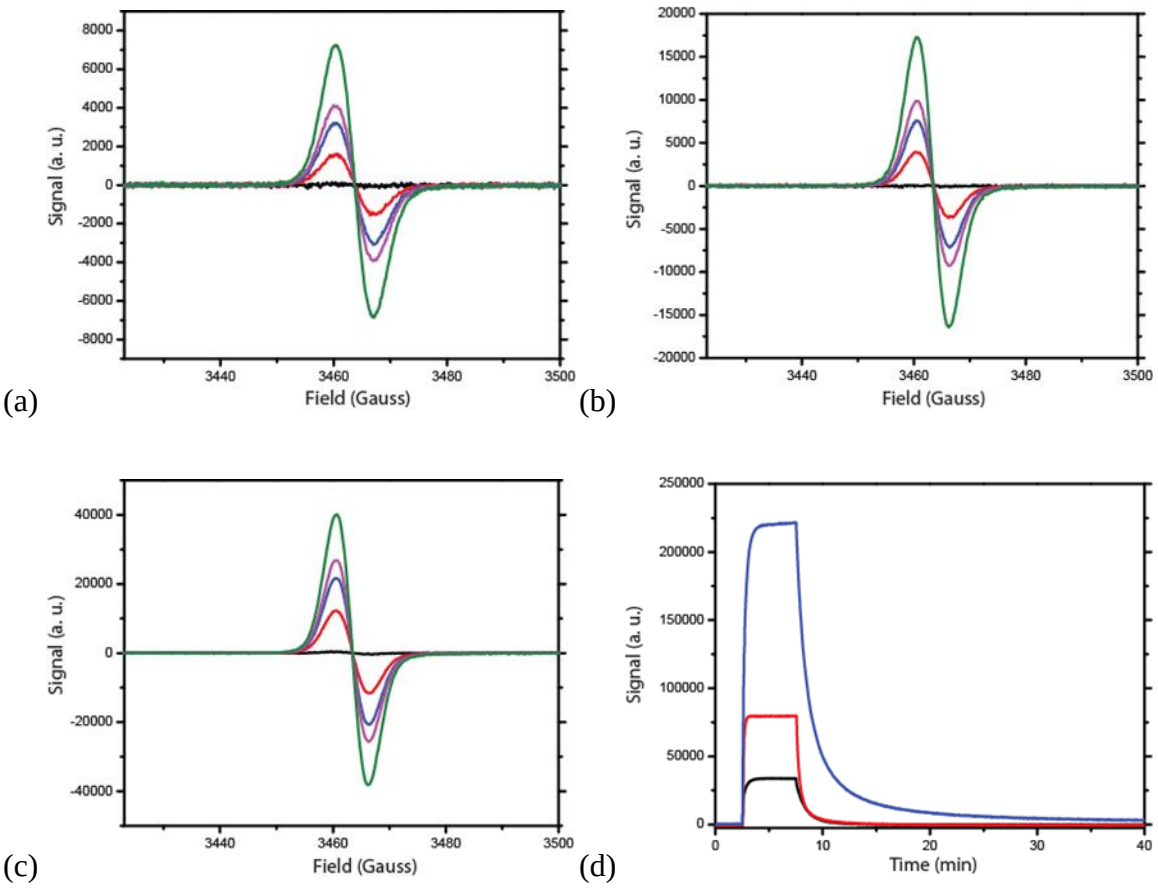

Figure 5.2. *Visible light-triggered lophyl radical generation and its recombination. EPR spectra of (a) o-Cl-HABI, (b) dihydroxy HABI, and (c) tetrahydroxy HABI monomer solutions (5 mM in DMF), prior to (black) and during irradiation of 405 nm with varying irradiation intensities of 1 mW·cm^{-2} (red), 5 mW·cm^{-2} (blue), 10 mW·cm^{-2} (magenta), and 40 mW·cm^{-2} (green), respectively. (d) Signal at field where maximum signal intensity exists, as determined by EPR spectroscopy, versus time for o-Cl-HABI (black), dihydroxy HABI (red), and tetrahydroxy HABI monomer solutions (blue).*

Electron paramagnetic resonance (EPR) spectroscopy was also used to compare the lophyl radical generating capability of HABI monomers and their lifetime during the recombination process. Whereas solutions of tetrahydroxy HABI showed no absorption peak in the dark, they demonstrated the greatest absorption peak of the HABI monomers examined here under equivalent irradiation conditions. Additionally, the generated

radicals displayed the longest lifetime, supporting results obtained by UV-vis spectrophotometry described above.

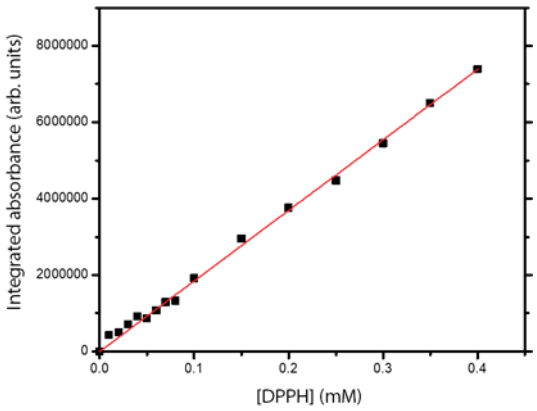

(a)

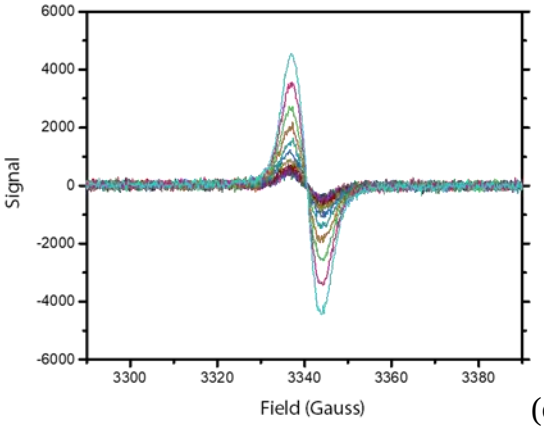

(b)

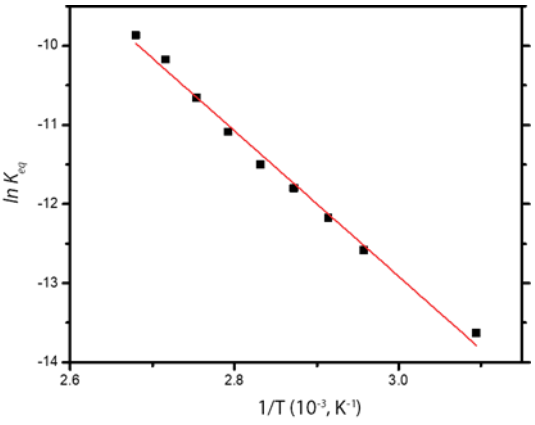

(c)

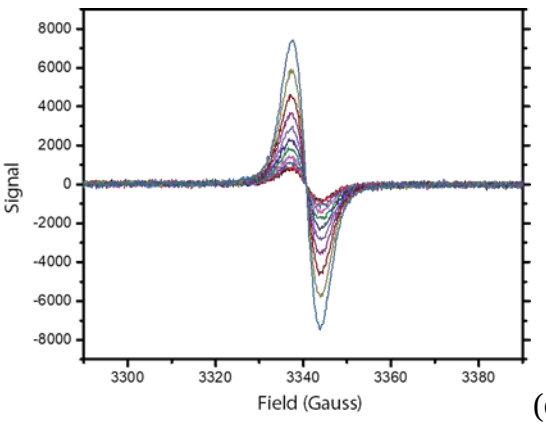

(d)

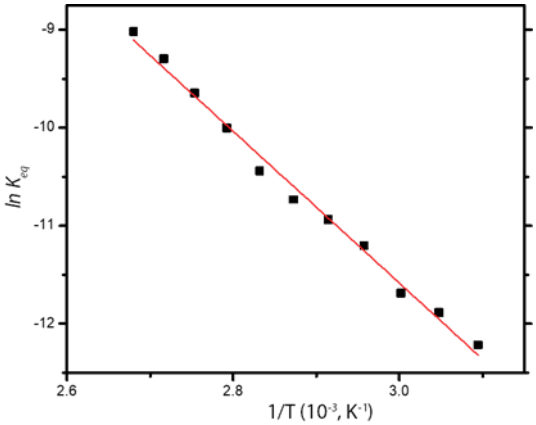

(e)

Figure 5.3. *Measurement of bond dissociation energies of HABI monomers. (a) Integrated absorbance, as determined by EPR spectroscopy, versus DPPH concentration in toluene and least squares linear fit (red line, y = 18473400x, r^2 = 0.999). (b) EPR scan of 5 mM tetrahydroxy HABI monomer solution in toluene at varying temperature, from 50°C to 100°C. (c) van 't Hoff plot according to equation 1 for 5 mM tetrahydroxy HABI monomer solution in toluene. (d) EPR scan of 5 mM dihydroxy HABI monomer solution in toluene at varying temperature, from 50°C to 100°C. (e) Van't Hoff plot according to equation 1 for 5 mM dihydroxy HABI monomer solution in toluene.*

Bond dissociation energies of three HABI monomers were examined to understand the difference of lophyl radical-forming capability and their lifetime. Radical concentrations were quantified by calibrating the EPR spectrum integral against known concentration solutions of DPPH using the same sample geometry, volume, and acquisition conditions employed for HABI monomer solutions (see Figure 5.3a). EPR spectra were at varying temperatures to determine the temperature-dependent dissociation equilibria, and the data were analyzed using a simplified form of the Van't Hoff equation (equation 1) for tetrahydroxy HABI and dihydroxy HABI monomer solutions (see Figure 5.3c and 3e). Equation 1 shows that a plot of ln K_{eq} against the reciprocal temperature will yield $-\Delta H/R$ from the slope. Slopes obtained from plots of ln K_{eq} against the reciprocal temperature and resultant ΔH values (BDE) are summarized in the table below (Note: BDE of *o*-Cl-HABI is known to 17 kcal·mol^{-1}).[21] As the BDEs of three HABI monomers do not demonstrate large differences, we anticipate that the difference of lophyl radical-forming capability of HABI monomers and their lifetime originates not from BDE differences but from other factors, such as steric hindrance.

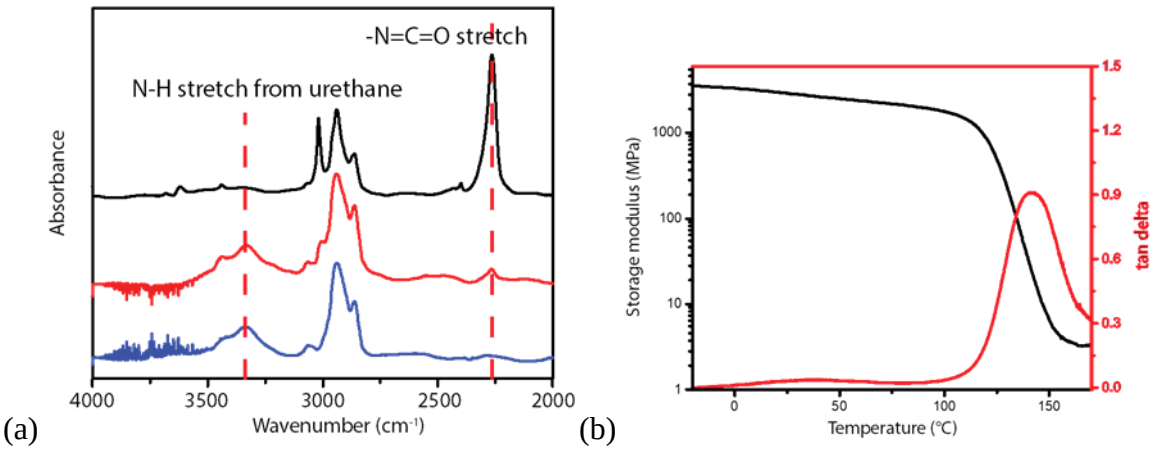

Figure 5.4. *(a) The alcohol-isocyanate polymerization between tetrahydroxy HABI and IPDI, monitored by FTIR. FTIR spectra of monomer solution before reaction starts (blue), after overnight reaction at room temperature (red), and after post-curing for 1 day (black). (b) Storage modulus versus (E', black) and tan δ (red) versus temperature for polymerized films.*

Sample HABI-based thermoset films were synthesized *via* the alcohol-isocyanate reaction between tetrahydroxy HABI and IPDI in the presence of a catalytic amount of dibutyltin dilaurate catalyst. The complete conversion of this polymerization was monitored by FTIR (Figure 5.4a). The strong absorption peak around 2270 cm^{-1}, corresponding to -NCO stretch, dramatically decreased after reaction overnight at room temperature and completely disappeared after post-curing for 1 day at raised temperature. Additionally, a new peak around 3330 cm^{-1}, corresponding to an -NH stretch from the generated urethane functional group, arose after the polymerization, implying the completion of the alcohol-isocyanate reaction and successful network formation. DMA was subsequently used to determine the viscoelastic properties of the resultant glassy, HABI-incorporating cross-linked polymer networks. Here, the storage modulus of the polymerized film at room temperature was approximately 3 GPa and the T_g was ~140°C, showing that the resultant sample is the vitrified and glassy. A single broad peak in the

tan δ curve demonstrated homogeneous mixing of the tetrahydroxy HABI and IPDI species throughout the cross-linked material.

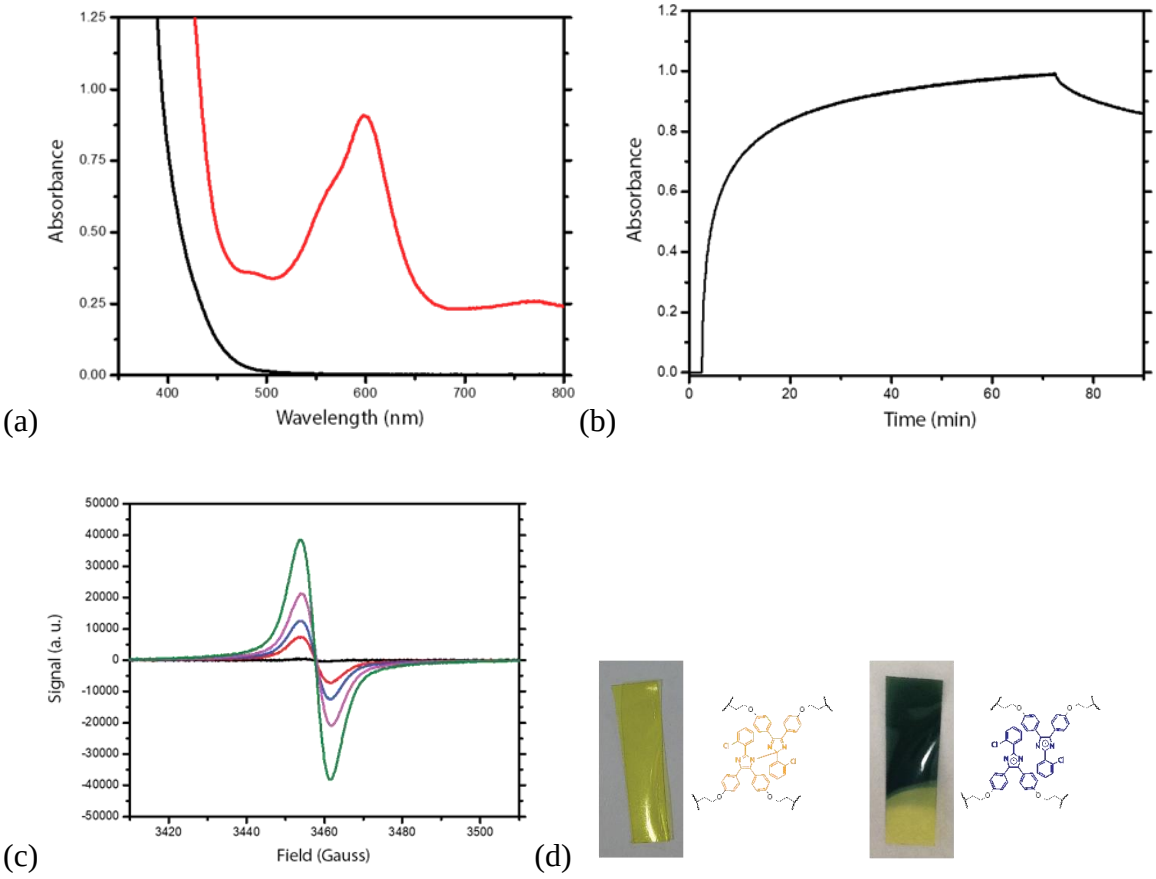

Figure 5.5. *(a) UV-vis spectra of vitrified, HABI-containing cross-linked polymer network prior to (black) and during irradiation (red) with 405 nm at 10 mW·cm^{-2}. (b) UV-vis kinetics of vitrified, HABI-containing cross-linked polymer network, irradiated with 405 nm at 10 mW·cm^{-2} from 2.5 to 72.5 minutes. (c) EPR spectra of vitrified, HABI-containing cross-linked polymer network, prior to irradiation (black) and irradiated with 405 nm at 1 mW·cm^{-2} (red), 5 mW·cm^{-2} (blue), 10 mW·cm^{-2} (magenta), and 40 mW·cm^{-2} (green). (d) Photographs of vitrified, HABI-containing cross-linked polymer network showing color change upon visible light irradiation and schematics of molecular structures of HABI moiety within networks.*

After network formation, the HABI-based thermoset samples were exposed again to the visible light irradiation to confirm the lophyl radical-forming capability within glassy networks. Prior to light irradiation, these samples showed a weak absorption peak in the visible region; however, a newly-generated, strong peak around 600 nm arose upon irradiation, confirming the lophyl radical-forming capability within glassy network. The rate of photo-mediated HABI dissociation and subsequent dark recombination was also examined using UV-vis spectrophotometry (see Figure 5.5b). Relative to the result of HABI monomer solutions, the rates of the photodissociation upon light irradiation and the subsequent dark recombination were sluggish. These differences likely arise from the different mobility environments the respective HABI species. In solution, individual HABI molecules are able to freely diffuse such that they can readily dissociate and associate. In contrast, the mobility of HABI functional groups when they are incorporated in the glassy networks is significantly more restricted. Nevertheless, photographs in Figure 5.5d show that HABI functionalities, despite limited chain mobility, can still generate lophyls radical upon irradiation and the transition between HABI and lophyl radicals remains reversible.

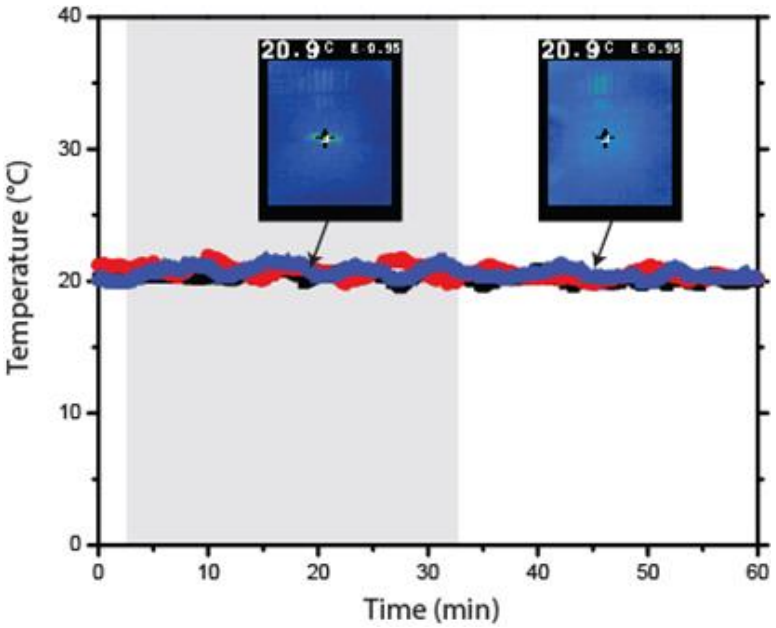

Figure 5.6. *Temperature change on the surface of glassy, HABI-containing polyurethane film, as determined by FLIR camera, during the irradiation by 405 nm at an intensity of 40 mW·cm^{-2} (grey area) and after incident light cessation. Distances between the lamp and the HABI-based thermosets were varied at 5 cm (blue triangle), 12 cm (red circle), and 30 cm (black square).*

To examine the influence of temperature on the photo-mediated healing capability of vitrified, HABI-based thermoset polymers, the temperature change on the sample surface upon irradiation were measured using an FLIR camera (see Figure 5.6). Here, the irradiation conditions employed were identical to those utilized for the actual photo-mediated healing process as described in the experimental section above. Upon irradiation and subsequent light cessation, there was no observable temperature change. Thus, any influence of the temperature on the photo-mediated healing of vitrified, HABI-based thermoset polymers can be excluded.

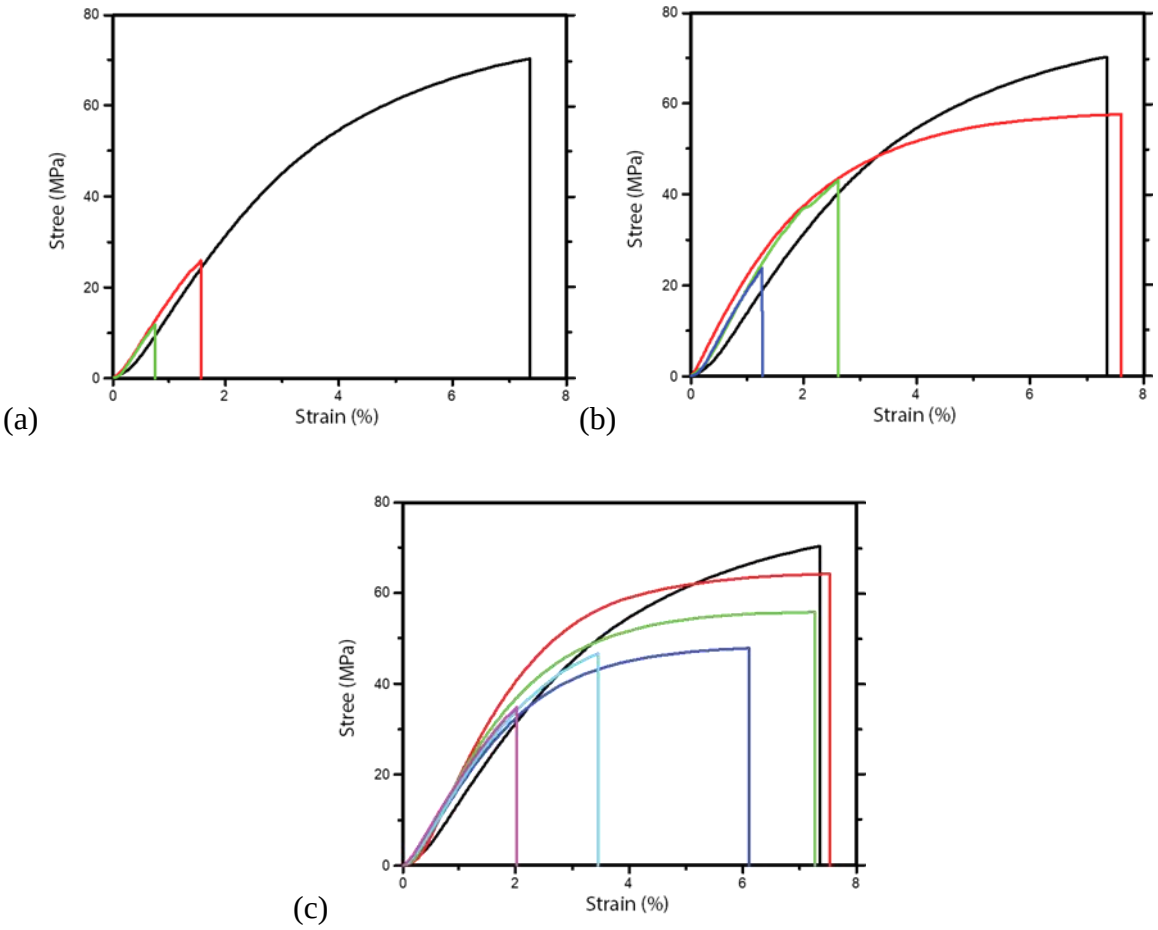

Figure 5.7. *Mechanical testing of photo-mediated healed HABI-based thermoset polymer. Samples were wiped with DMF and then irradiated with 405 nm at 40 mW·cm^{-2}. (a) Stress-strain curves of pristine (black) and healed samples, irradiated for 3 minutes having 5 kg (red) and 500 g (green) of calibration weight on the top of the samples. (b) Stress-strain curves of un-healed (black) and healed samples, irradiated for 10 minutes having 5 kg (red), 500 g (green), and 200 g (blue) of calibration weight on the top of the samples during irradiation. (c) Stress-strain curves of pristine (black) and healed samples, irradiated for 30 minutes having 5 kg (red), 500 g (green), 200 g (blue), 100 g (magenta), and 50 g (purple) of calibration weight on the top of the samples during irradiation.*

The photo-mediated healing capability of HABI-incorporating, cross-linked polymer networks was investigated at room temperature and under aerobic conditions. To demonstrate this, two samples strips were wiped with DMF and immediately dried to ensure intimate contact between the sample strips and afford some chain mobility at the

overlapped interface. The overlapped region of the two sample strips was then exposed to the visible light irradiation for 3, 10, or 30 minutes while various calibration weights were placed on the top of the sample during the light irradiation until the completion of recombination process, to examine the influence of weights for the photo-mediated healing capability. Sample strips, irradiated for 3 minutes, didn't exhibit acceptable healing capability even when 5 kg were placed on the top of the sample strips (Figure 5.7a); however, the healing efficiency improved significantly as the irradiation time was increased. Sample strips, irradiated for 30 minutes, showed almost complete restoration of their mechanical integrity with the aid of 5 kg and 500 g calibration weights. Mechanical pressure also assisted the photo-mediated healing process, likely owing to ensuring better contact at the overlapped area of two sample strips.

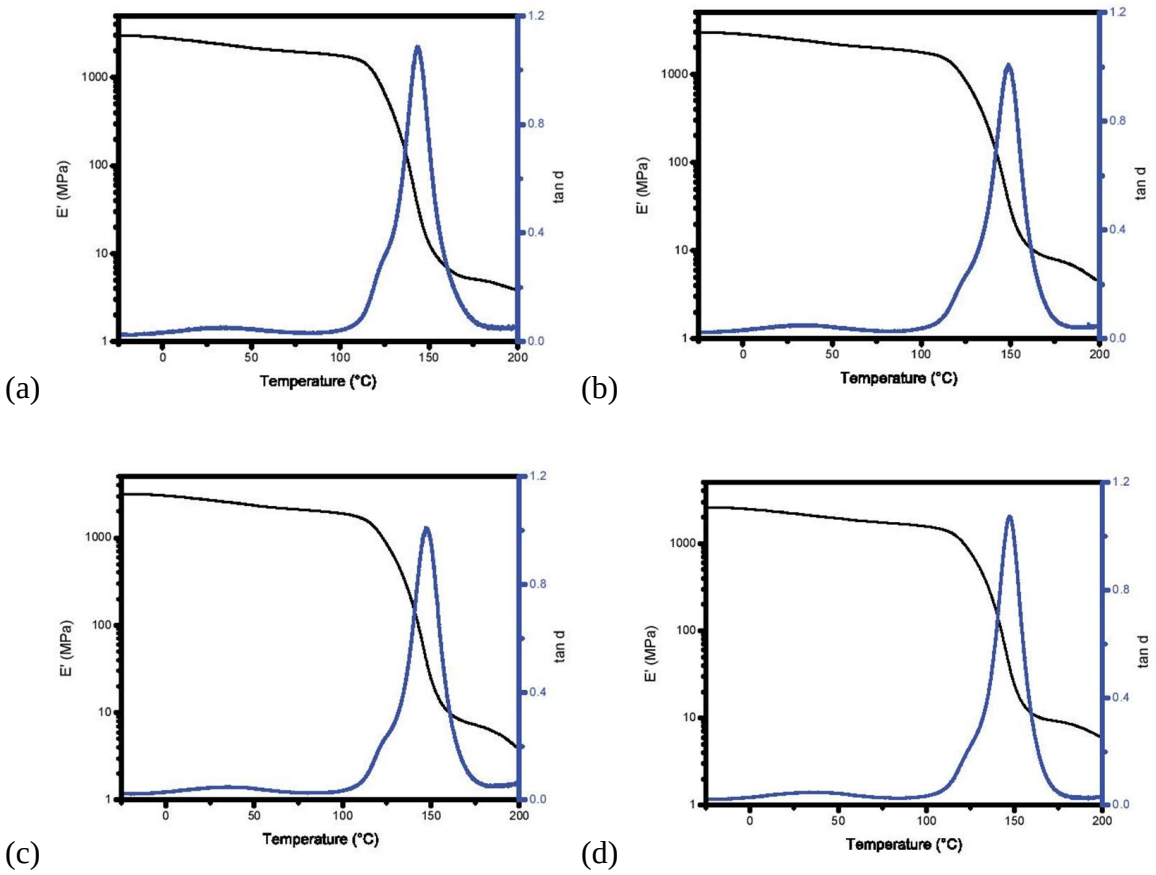

Figure 5.8. *Storage modulus (blue) and tan δ (black) versus temperature for vitrified, HABI-incorporating thermoset polymer, swollen with methanol for (a) 0 hour, (b) 6 hours, (c) 24 hours, and (d) 48 hours.*

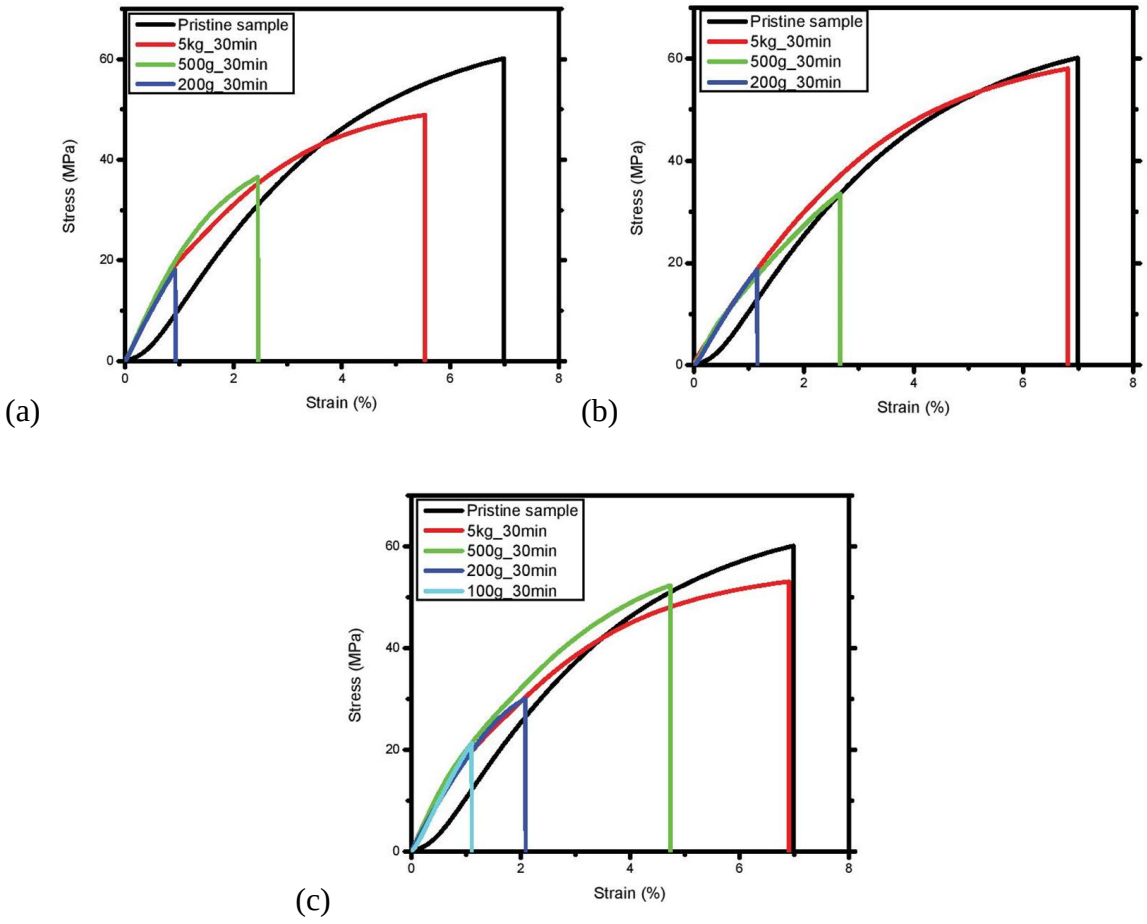

Figure 5.9. *Mechanical testing of photo-triggered healed, vitrified HABI-based thermoset polymer. Samples were soaked in methanol for (a) 6 hours, (b) 24 hours, and (c) 48 hours and irradiated with 405 nm at 40 mW·cm^{-2} for 30 minutes.*

Samples examined in Figure 5.7 was lightly swollen with DMF. Although the results of photo-mediated healing experiment were satisfactory, those can be attributable to the presence of organic solvent, DMF, and subsequent enhancement of chain mobility on irradiated and healed area. In order to exclude the solvent effect, DMA was used to examine the viscoelastic properties of samples, which were soaked in methanol for varying periods of time (6, 24, and 48 hours) prior to photo-mediated healing experiments (see Figure 5.8). Notably, the swelling degree for samples in methanol was

relatively low at 12.6%. As a result, the HABI-incorporating thermoset polymers swollen with methanol remained vitrified even after being soaked in methanol for 48 hours.

The mechanical properties of the samples soaked in methanol, prior to and after photo-mediated healing experiment, were examined and are shown in Figure 5.9. Varying calibration weights were placed on the top of the overlapped samples during light exposure to ascertain the effect of pressure on photo-mediated healing. Similar to the results reported in Figure 5.7, HABI-incorporating thermoset polymers exhibited exceptional photo-mediated healing capability within glassy networks, where the mechanical integrity of the samples was fully restored after visible light irradiation with moderate intensity (40 $mW \cdot cm^{-2}$) for 30 minutes. As the pressure or weights on the samples were increased, the healing efficiency improved, likely attributable to the pressure affording better contact at the interface of the samples, leading to more HABIs participating in bond rearrangement reaction. Despite restricted chain mobility within these glassy networks, the HABI-containing thermoset polymers exhibited superior healing capability, which could be attributable to several factors, including 1) the transient reduction in T_g at the overlapped and healed area owing to photo-mediated backbone cleavage upon irradiation, and 2) the presence of methanol within the glassy network acting as a plasticizer, enhancing the chain mobility during photo-mediated healing process.

(a)

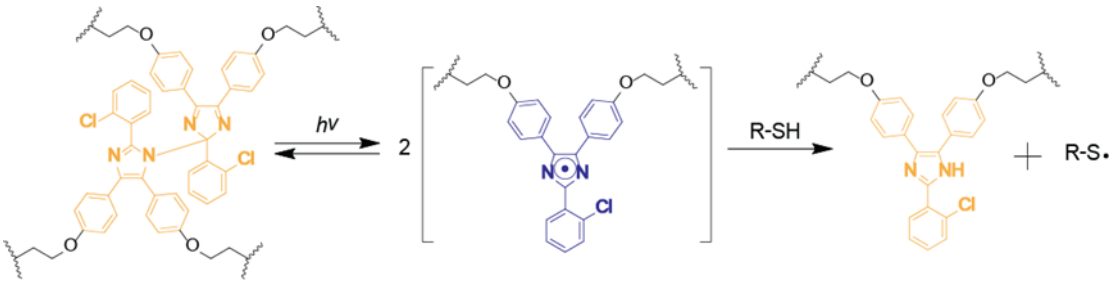
hv
2
R-SH
R-S•
Cl
N
O
NH

(b)

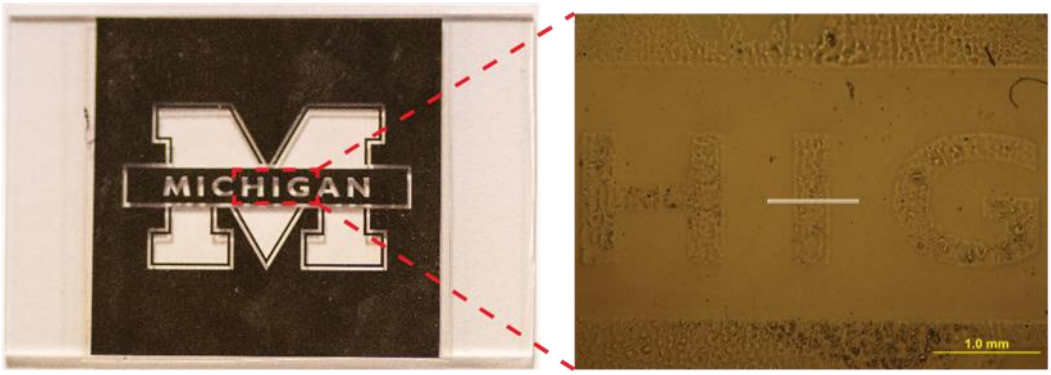
MICHIGAN
1.0 mm

(c)

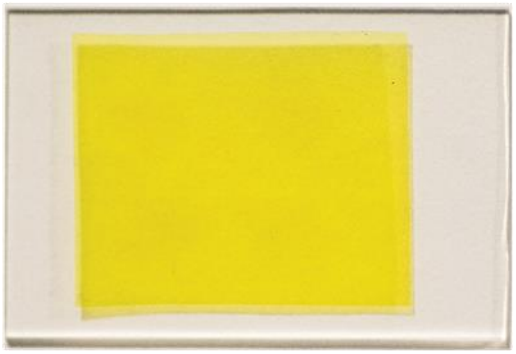

(d)


MICHIGAN

(e)

(f)

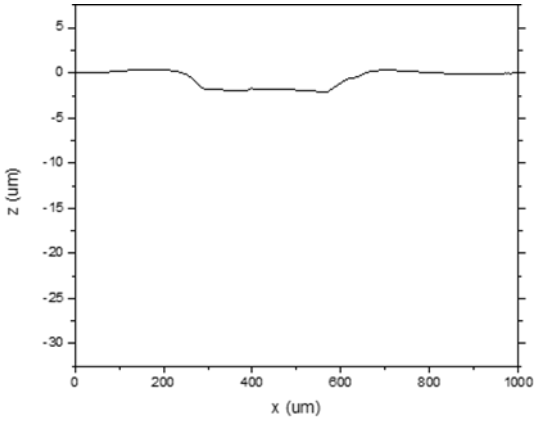
z (um)
x (um)
5
0
-5
-10
-15
-20
-25
-30
0
200
400
600
800
1000

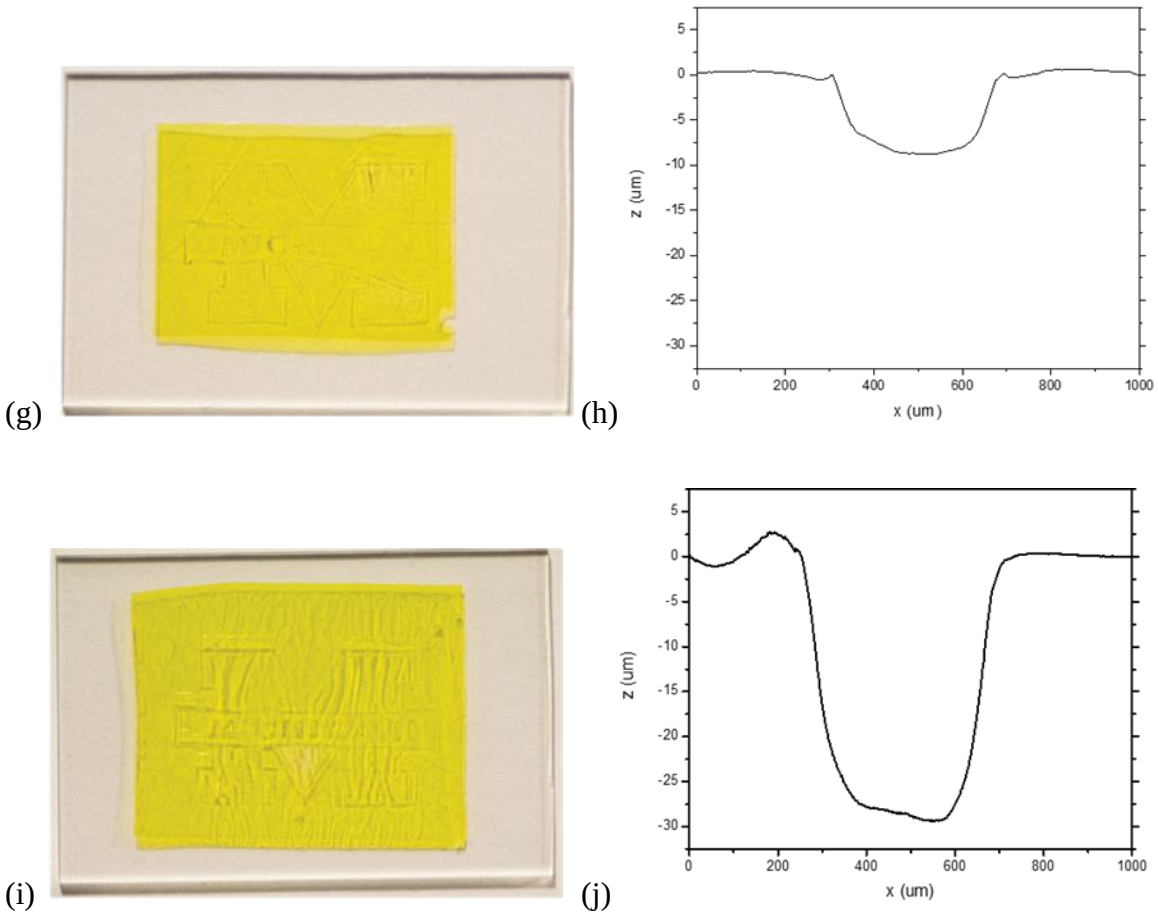

Figure 5.10. *Photopatterning of glassy, HABI-based thermoset sample, attributable to the irreversible characteristics of HABI moiety in the presence of hydrogen donating molecules. (a) Selective reversibility during the transition between HABI and lophyl radical in the presence of H-donor. (b) Photomask used in this study and optical microscopic image of photopatterned surface of glassy, HABI-based thermoset (bar represents the scanned area for the measurement of depth of the trench, as shown in figure 5.9(f), (h), (j)). (c) Photograph of HABI-based film upon visible light irradiation. Photographs of photopatterned, vitrified HABI-based thermoset sample, irradiated with 405 nm at 40 mW·cm^{-2} for (e) 1 minute, (g) 5 minutes, and (i) 15 minutes. The depth of trench, measured using surface profilometry, for the sample irradiated with 405 nm at 40 mW·cm^{-2} for (f) 1 minute, (h) 5 minutes, and (j) 15 minutes.*

Introducing enhanced molecular mobility and chemical dynamics into cross-linked polymer network affords the capability for intrinsic healing; however, once set, chemical dynamics in the polymeric strands ceases and is only turned on and off by light

irradiation and light cessation, although the reversible nature of HABIs can be permanently turned off on demand by adding hydrogen-donating species. In the presence of a hydrogen donor, such as aromatic alcohols or thiols, HABI-derived lophyl radicals abstract hydrogen from the H-donor and irreversibly convert into imidazole groups (see Figure 5.9a). Inspired by the selective reversibility of HABI functionalities, a photopatterning experiment was conducted here where fully-cured, HABI-containing thermoset samples were prepared and soaked in a mixture of acetonitrile and a mono-functional thiol, butyl 3-mercaptopropionate. The samples were then irradiated with 405 nm for different time periods, during which the HABI cross-links were converted into irreversible imidazole functionalities, resulting in the loss cross-link density at the irradiated area. As a result, de-cross-linked polymeric strands in the irradiated regions could be washed away when the samples were rinsed with acetonitrile; however, cross-linked polymeric strands at the shaded area remain intact, resulting in topographical featured patterned throughout the cross-linked polymer samples. The depths of the trenches in the irradiated areas were measured using the surface profilometry. Upon 1 minute of light irradiation, the depth of trench was about 2 μm, and increased from 2 μm to 30 μm as the irradiation time increased from 1 minute to 15 minutes.

5.5 Conclusion

In summary, HABI-incorporating, covalently cross-linked thermoset polymers developed here were able to undergo photomediated backbone cleavage under visible light irradiation, temporarily affording reduced cross-link density and dynamic connectivity rearrangement, and revert back to stable, static networks upon irradiation

cessation. The slow recombination of lophyl radicals provided sufficient time for effective healing of these vitrified thermosets and the reduction in cross-link density temporarily decreased the T_g of materials in the irradiated area, enabling sub-glass transition temperature healing of vitrified thermosets to be achieved.

5.6 References

(1) Burnworth, M.; Tang, L. M.; Kumpfer, J. R.; Duncan, A. J.; Beyer, F. L.; Fiore, G. L.; Rowan, S. J.; Weder, C. Optically healable supramolecular polymers. *Nature* **2011**, *472*, 334-U230.

(2) Balkenende, D. W. R.; Monnier, C. A.; Fiore, G. L.; Weder, C. Optically responsive supramolecular polymer glasses. *Nat. Commun.* **2016**, *7*, 9.

(3) Scott, T. F.; Schneider, A. D.; Cook, W. D.; Bowman, C. N. Photoinduced plasticity in cross-linked polymers. *Science* **2005**, *308*, 1615-1617.

(4) Amamoto, Y.; Kamada, J.; Otsuka, H.; Takahara, A.; Matyjaszewski, K. Repeatable Photoinduced Self-Healing of Covalently Cross-Linked Polymers through Reshuffling of Trithiocarbonate Units. *Angew. Chem.-Int. Edit.* **2011**, *50*, 1660-1663.

(5) Amamoto, Y.; Otsuka, H.; Takahara, A.; Matyjaszewski, K. Self-Healing of Covalently Cross-Linked Polymers by Reshuffling Thiuram Disulfide Moieties in Air under Visible Light. *Advanced Materials* **2012**, *24*, 3975-3980.

(6) White, S. R.; Sottos, N. R.; Geubelle, P. H.; Moore, J. S.; Kessler, M. R.; Sriram, S. R.; Brown, E. N.; Viswanathan, S. Autonomic healing of polymer composites. *Nature* **2001**, *409*, 794-797.

(7) Toohey, K. S.; Sottos, N. R.; Lewis, J. A.; Moore, J. S.; White, S. R. Self-healing materials with microvascular networks. *Nat. Mater.* **2007**, *6*, 581-585.

(8) Hoogenboom, R. Hard Autonomous Self-Healing Supramolecular Materials-A Contradiction in Terms? *Angew. Chem.-Int. Edit.* **2012**, *51*, 11942-11944.

(9) Chen, Y. L.; Kushner, A. M.; Williams, G. A.; Guan, Z. B. Multiphase design of autonomic self-healing thermoplastic elastomers. *Nat. Chem.* **2012**, *4*, 467-472.

(10) Garcia, J. M. Recyclable, strong thermosets, and organogels via paraformaldehyde condensation with diamines. *Abstr. Pap. Am. Chem. Soc.* **2014**, *248*, 1.

(11) Garcia, J. M.; Jones, G. O.; Virwani, K.; McCloskey, B. D.; Boday, D. J.; ter Huurne, G. M.; Horn, H. W.; Coady, D. J.; Bintaleb, A. M.; Alabdulrahman, A. M. S.; Alsewailem, F.; Almegren, H. A. A.; Hedrick, J. L. Recyclable, Strong Thermosets and Organogels via Paraformaldehyde Condensation with Diamines. *Science* **2014**, *344*, 732-735.

(12) Hayashi, T.; Maeda, K. Preparation of a new phototropic substance. *Bull. Chem. Soc. Jpn.* **1960**, *33*.

(13) White, D. M.; Sonnenberg, J. Oxidation of triarylimidazoles. Structures of photochromic and piezochromic dimers of triarylimidazyl radicals. *Journal of the American Chemical Society* **1966**, *88*, 3825-+.

(14) Hayashi, T.; Maeda, K.; Morinaga, M. The mechanism of the photochromism and thermochromism of 2,2',4,4',5,5'-hexaphenyl-1,1'-biimidazolyl. *Bulletin of the Chemical Society of Japan* **1964**, *37*, 1563-1564.

(15) Qin, X. Z.; Liu, A.; Trifunac, A. D.; Krongauz, V. V. Photodissociation of hexaarylbiimidazole. 1. Triplet-state formation. *Journal of Physical Chemistry* **1991**, *95*, 5822-5826.

(16) Ahn, D. Z., S. R. Scott, T. F. Rapid, photomediated healing of hexaarylbiimidazole-based covalently cross-linked gels. *Chem. Mater.* **2017**, *29*, 7023-7031.

(17) Wojtecki, R. J.; Meador, M. A.; Rowan, S. J. Using the dynamic bond to access macroscopically responsive structurally dynamic polymers. *Nat. Mater.* **2011**, *10*, 14-27.

(18) Zou, W. K.; Dong, J. T.; Luo, Y. W.; Zhao, Q.; Xie, T. Dynamic Covalent Polymer Networks: from Old Chemistry to Modern Day Innovations. *Advanced Materials* **2017**, *29*, 1606100.

(19) An, S. Y.; Arunbabu, D.; Noh, S. M.; Song, Y. K.; Oh, J. K. Recent strategies to develop self-healable crosslinked polymeric networks. *Chemical Communications* **2015**, *51*, 13058-13070.

(20) Lovell, L. G.; Berchtold, K. A.; Elliott, J. E.; Lu, H.; Bowman, C. N. Understanding the kinetics and network formation of dimethacrylate dental resins. *Polymers for Advanced Technologies* **2001**, *12*, 335-345.

(21) Tanaseichuk, B. S. Triarylimidazole radicals and their dimers. *Khim. Geterotsiklicheskikh Soedin.* **1972**, 1299-+.

Chapter 6

Conclusion

6.1 Summary of research

Hexaarylbiimidazoles (HABIs) were first synthesized more than five decades ago.[1] Their unique properties, including a coloration upon visible light irradiation and slow recombination kinetics of the lophyl radicals generated by HABI photolysis, attracted much attention immediately after the synthesis of this class of compounds.[2-5] DuPont in particular was instrumental in the development of this functional group and, after extensive research, commercialized HABIs for proofing paper, photoimaging and photoinitiators. After its release, this product line, named DYLUX®, showed steady growth until the early 2000s; however, the line has since been discontinued owing to financial difficulties, resulting from corporate overexpansion. Consequently, this class of photo- and thermo-chromic compounds is well known and the chemistry of HABIs has been intensively studied both in academia and industry.[6-8] Nevertheless, many attributes of HABIs remain under-examined. For example, although the recombination kinetics and mechanisms of HABIs have been studied for more than five decades, there is still apparent disagreement between reported reaction orders.[9-11] Moreover, as new applications are found for these existing compounds, contemporary research continues to HABIs back into the spotlight (e.g., the mechanophoric nature of HABIs has been recently used for the development of stress-sensing materials[12]). Thus, in this dissertation, we designed and synthesized a novel HABI photoinitiator for improved solubility and

visible light absorbance[6] (Chapter 2) and re-examined the reaction kinetics of HABI photodissociation and subsequent lophyl radical recombination in an attempt to better understand and resolve the apparent disagreement between reported reaction orders (Chapter 3).[7] Additionally, we utilized the HABI functional group as a new class of dynamic covalent bond and demonstrated novel, HABI-containing photo-healable materials (Chapter 4 and 5).[8]

In Chapter 2, we designed and synthesized a novel HABI photoinitiator.[6] Conventional dental resin formulations are primarily composed of (di)methacrylate based monomers. Unfortunately, the radical-mediated chain growth polymerization of these dimethacrylate formulations has some drawbacks, including strong polymerization inhibition by oxygen, high concentrations of extractable monomers after polymerization cessation, and the development of high shrinkage stress in the polymerized materials. In order to address these shortcomings of conventional resins, several polymerization mechanisms, including the radical-mediated thiol–ene step growth mechanism, have emerged as potential alternatives for composite dental restorative materials. We proposed a newly-synthesized HABI photoinitiator as a visible light-active candidate to initiate thiol–ene polymerization and yield vitrified, cross-linked polymer networks with good polymerization rates. As a result, blue light irradiation of thiol–ene resin formulations incorporating this HABI photoinitiator yielded vitrified, cross-linked polymer matrices that were significantly more homogeneous than methacrylate-based polymer networks photopolymerized while polymerizatiunder equivalent irradiation conditions.

Chapter 3 details the examination of the reaction kinetics of HABI photodissociation and subsequent lophyl radical recombination. Free radicals are common reactive species in many chemical reactions and biological processes. Although there have been efforts to explain the complex recombination behavior of HABI-derived lophyl radicals, their mechanism is still unclear. Thus, by carrying out extensive study using UV-vis spectrophotometry and EPR spectroscopy, we tried to elucidate the mechanism of HABIs in solution. We examined two model HABI photoinitiators, *o*-Cl-HABI and *p*-HOH-HABI in this study, and revealed that they are well fit as 3/2- and second-order reactions for the two respective parent species.

The study on the development of new classes of dynamic covalent bonds has recently received much attention, in part owing to the potential for intrinsic self-healing or external stimuli-triggered healable materials development when these special types of covalent bonds are incorporated into cross-linked polymer networks. In Chapter 4 and 5, we utilized HABI-based functional groups as a new class of dynamic covalent bond to demonstrate the photo-mediated healable polymeric materials. HABIs have never been used for the application of self-healing materials. Lophyl radicals generated by HABI homolysis are insensitive to atmospheric oxygen and show extraordinary slow recombination rates, attributable to their unique chemical structure affording stabilization by steric hindrance and electron delocalization.[13] Thus, owing to the low reactivity and long lifetime of the lophyl radicals originating from HABI photolysis, cross-linked polymers bearing HABI-containing network strands offer a unique mechanism for intrinsically healable materials.

To demonstrate the photo-mediated healing capability of HABI-incorporating, cross-linked polymer networks, we synthesized two novel HABI monomers bearing polymerizable functional groups at their termini and polymerized them to obtain HABI-containing, intrinsically-healable cross-linked polymer networks as polymeric gels[8] (shown in Chapter 4) and vitrified cross-linked polymer (described in Chapter 5). The HABI-containing polymeric gel showed photo-mediated healing and rapid restoration of mechanical integrity only after 1 to 3 minutes of visible light exposure. Although many backbone-borne, dynamic functional groups have been employed to achieve intrinsically-healable polymeric gels and elastomers, effective restoration of mechanical properties upon contacting fracture surfaces typically takes several hours or days.[14,15] In contrast, exceptionally fast healing rate was achieved by the incorporation of HABIs into the cross-linked polymeric gels.

Covalently cross-linked, vitrified polymer networks find utility as structural materials across a wide variety of applications where *in situ* polymerization, dimensional stability, environmental resistance, and permanence are required. However, hard autonomous self-healing materials have been considered a contradiction in terms because dynamic intermolecular interactions necessitate sufficient chain dynamics and mobility attainable only at temperatures in excess of the T_g. To address this intractable problem, we incorporated HABI moieties into the vitrified, polyurethane networks. Owing to the slow recombination of lophyl radicals and photo-mediated backbone cleavage upon irradiation with visible light, temporarily affording reduced cross-link density and dynamic connectivity rearrangement, exceptional, sub-glass transition temperature healing of vitrified thermosets was achieved.

To conclude, we designed and synthesized HABI-based photoinitiators and monomers to afford HABI-incorporating, cross-linked polymer networks. Within these networks, HABI moieties undergo homolytic cleavage, yielding lophyl radicals which slowly recombine with each other, recovering the parent HABI groups. Owing to the photo-mediated backbone cleavage of HABIs and slow recombination rates of lophyl radicals, rapid healing rates in gels and sub-T_g cold welding of cross-linked polymer networks were achieved. We anticipate that the described approach will find broad applications including the development of other dynamic functionalities, enabling the healing of vitrified polymeric materials or materials which respond to their physical environment, impacting their composition and, consequently, physical properties.

6.2 Future work

The work described in this thesis opens the door to several new research avenues in self-healing, self-reporting, and self-reinforcing polymeric materials. This section briefly discusses potential future directions.

At the macroscopic scale, mechanical loads induce familiar bulk changes – such as bending, compression, twisting and stretching – in the shapes of materials, but the material response extends across many orders of magnitude in length and time. In the past, chemists have focused almost exclusively on the use of light or heat to effect chemical reactions; however, they have been increasingly interested in exploring, understanding and even exploiting the changes that mechanical stresses can induce in the chemical reactivities of polymer chain. In fact, almost as soon as the nature of polymers

had been recognized, certain simple manipulations of polymer solids, melts or solutions were shown to result in fragmentation of their backbones without the high temperatures that are normally required for strong covalent bonds to break at detectable rates. This phenomenon is often referred to as mechanochemistry, a burgeoning field that has garnered significant interest in recent years for a wide range of applications, including mechanically-activated catalysts,[16] self-strengthening polymer networks,[17] and polymer actuators.[18]

HABIs are also well known as piezo-chromic materials, whereby they efficiently produce indigo-colored 2,4,5-triarylimidazolyl radicals upon mechanical stress, such as grinding; indeed, the mechanophoric nature of HABIs has been of increasing research interest in recent years.[12] One of the distinctive features of HABIs is their strong coloration of lophyl radicals upon mechanical stresses. Nevertheless, the HABI functionality itself is not of practical use until it has been incorporated into the cross-linked polymer network. Thus, one future potential research direction would be the fabrication of polymeric films incorporating HABI functionalities to utilize HABIs as stress-indicating sensor. Upon application of a mechanical load, HABIs can generate strong indigo-colored lophyl radical, providing a readily-observed visual cue to indicate the fatigue or stress state within the polymer network (see Figure 6.1).

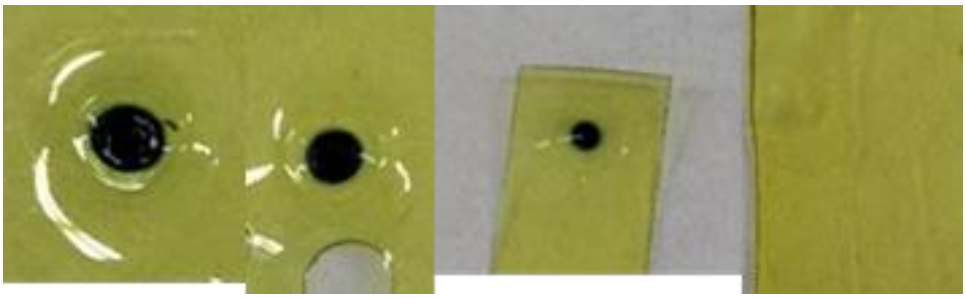

Figure 6.1. *Photographs of compressed, HABI-containing cross-linked polymer network. Samples were pressed for 1 minute under constant force (from left to right: 10 kN, 3 kN, 500 N, and 100 N).*

Although repeated cycles of mechanical load are known to trigger destructive bond scission reaction in polymers, reducing the lifespan of these synthetic materials, mechanical stresses can be also used to effect non-destructive reactions in mechanophores incorporated in polymer backbones to strengthen the material's integrity. Given that HABIs can produce reactive lophyl radicals upon mechanical load which can be used to trigger the secondary polymerization within polymer networks, they are promising candidate functionalities to yield such self-reinforcing behavior in polymer matrices. Preliminary attempts to implement self-reinforcing polymers have focused on a two-stage polymerization approach using a resin formulated from tetrathiol, triallyl, and HABI-based diacrylate monomers (see Figure 6.2) with an overall stoichiometric ratio of thiol to carbon-carbon double bond groups of 1:1. The first stage of this polymerization proceeds *via* a Michael addition between the multi-functional thiol and acrylate monomers, a reaction step that is self-limited by complete consumption of the acrylate functional groups. Upon completion of this reaction, the resultant polymer network is a loosely cross-linked, low modulus material with properties that are ideally tailored for intermediate polymer processing. The stage 2 reaction is triggered by mechanical force

to cleave the polymer backbone-borne HABI groups to generate lophyl radicals that abstract hydrogens from the residual thiol groups, yielding thiyl radicals which initiate a radical-mediated thiol–ene polymerization to afford a highly cross-linked, high modulus polymer (see Figure 6.3). Although preliminary, this demonstration of molecular-level mechanical response and impact on polymer properties will lead to the design of synthetic materials that, like biological counterparts, actively remodel locally in response to their physical environment.

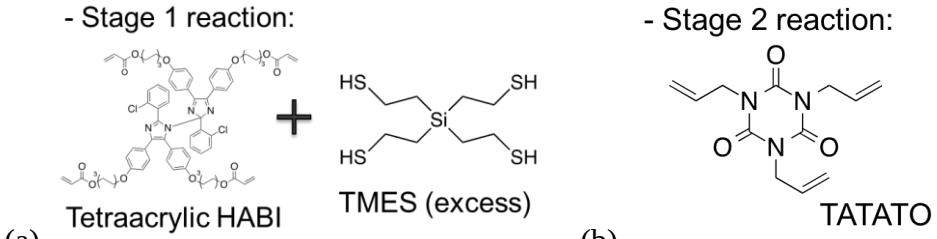

Figure 6.2. *Monomers for dual-network forming thiol–acrylate/thiol–ene resin systems.*

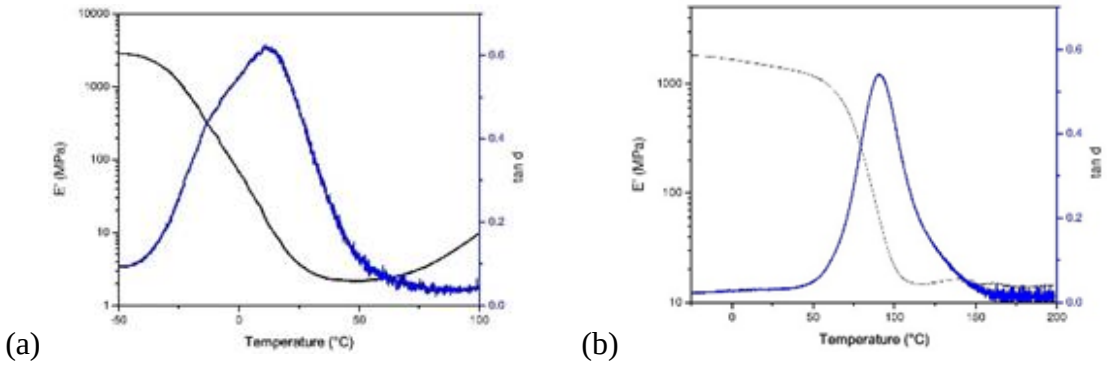

Figure 6.3. *DMA traces of HABI-based thermoset polymer (a) before and (b) after the application of ultrasound. The polymer T_g of polymer increases from 12°C to 90°C and storage modulus at room temperature increases from 2 MPa to 1.5 GPa.*

6.3 References

(1) Hayashi, T.; Maeda, K. Preparation of a new phototropic substance. *Bull. Chem. Soc. Jpn.* **1960**, *33*.

(2) Qin, X. Z.; Liu, A.; Trifunac, A. D.; Krongauz, V. V. Photodissociation of hexaarylbiimidazole. 1. Triplet-state formation. *Journal of Physical Chemistry* **1991**, *95*, 5822-5826.

(3) Liu, A. D.; Trifunac, A. D.; Krongauz, V. V. Photodissociation of hexaarylbiimidazole. 2. Direct and sensitized dissociation. *Journal of Physical Chemistry* **1992**, *96*, 207-211.

(4) Monroe, B. M.; Weed, G. C. Photoinitiators for Free-Radical-Initiated Photoimaging Systems. *Chemical Reviews* **1993**, *93*, 435-448.

(5) Caspar, J. V.; Khudyakov, I. V.; Turro, N. J.; Weed, G. C. ESR Study of Lophyl Free Radicals in Dry Films. *Macromolecules* **1995**, *28*, 636-641.

(6) Ahn, D.; Sathe, S. S.; Clarkson, B. H.; Scott, T. F. Hexaarylbiimidazoles as visible light thiol-ene photoinitiators. *Dental Materials* **2015**, *31*, 1075-1089.

(7) Sathe, S. S.; Ahn, D.; Scott, T. F. Re-examining the photomediated dissociation and recombination kinetics of hexaarylbiimidazoles. *Industrial and Engineering Chemistry Research* **2015**, *54*, 4203-4212.

(8) Ahn, D.; Zavada, S. R.; Scott, T. F. Rapid, Photomediated Healing of Hexaarylbiimidazole-Based Covalently Cross-Linked Gels. *Chem. Mater.* **2017**, *29*, 7023-7031.

(9) Hayashi, T.; Maeda, K.; Takeuchi, M. A Kinetic Study of the Photochromism of 2,2′,4,4′,5,5′-Hexaphenyl-1,1′-biimidazolyl with Electron Spin Resonance. *Bull. Chem. Soc. Jpn.* **1964**, *37*, 1717-1718.

(10) Wilks, M. A. J.; Willis, M. R. Kinetics of the photochromic decay reaction of solutions of 2,2′,4,4′,5,5′-hexaphenyl bi-imidazolyl [11]. *Nature* **1966**, *212*, 500-502.

(11) Strehmel, V.; Wishart, J. F.; Polyansky, D. E.; Strehmel, B. Recombination of photogenerated lophyl radicals in imidazolium-based ionic liquids. *ChemPhysChem* **2009**, *10*, 3112-3118.

(12) Verstraeten, F.; Göstl, R.; Sijbesma, R. P. Stress-induced colouration and crosslinking of polymeric materials by mechanochemical formation of triphenylimidazolyl radicals. *Chemical Communications* **2016**, *52*, 8608-8611.

(13) Kawano, M.; Sano, T.; Abe, J.; Ohashi, Y. The first in situ direct observation of the light-induced radical pair from a hexaarylbiimidazolyl derivative by X-ray crystallography. *Journal of the American Chemical Society* **1999**, *121*, 8106-8107.

(14) Amamoto, Y.; Kamada, J.; Otsuka, H.; Takahara, A.; Matyjaszewski, K. Repeatable Photoinduced Self-Healing of Covalently Cross-Linked Polymers through Reshuffling of Trithiocarbonate Units. *Angew. Chem.-Int. Edit.* **2011**, *50*, 1660-1663.

(15) Amamoto, Y.; Otsuka, H.; Takahara, A.; Matyjaszewski, K. Self-Healing of Covalently Cross-Linked Polymers by Reshuffling Thiuram Disulfide Moieties in Air under Visible Light. *Advanced Materials* **2012**, *24*, 3975-3980.

(16) Piermattei, A.; Karthikeyan, S.; Sijbesma, R. P. Activating catalysts with mechanical force. *Nat. Chem.* **2009**, *1*, 133-137.

(17) Ramirez, A. L. B.; Kean, Z. S.; Orlicki, J. A.; Champhekar, M.; Elsakr, S. M.; Krause, W. E.; Craig, S. L. Mechanochemical strengthening of a synthetic polymer in response to typically destructive shear forces. *Nat. Chem.* **2013**, *5*, 757-761.

(18) Beyer, M. K.; Clausen-Schaumann, H. Mechanochemistry: The mechanical activation of covalent bonds. *Chemical Reviews* **2005**, *105*, 2921-2948.